Electronic Raman Spectroscopy on Semiconductor Quantum Dots

Dissertation
zur Erlangung des Doktorgrades
des Departements Physik
der Universität Hamburg

vorgelegt von
Thomas Brocke
aus Hamburg

Hamburg
2007

Gutachterin/Gutachter der Dissertation:	Prof. Dr. Detlef Heitmann Prof. Dr. Daniela Pfannkuche
Gutachter der Disputation:	Prof. Dr. Detlef Heitmann Prof. Dr. Wolfgang Hansen
Datum der Disputation:	14. September 2007
Vorsitzender des Prüfungsausschusses:	PD Dr. Alexander Chudnovskiy
Vorsitzender des Promotionsausschusses:	Prof. Dr. Günter Huber
Dekan der Fakultät für Mathematik, Informatik und Naturwissenschaften:	Prof. Dr. Arno Frühwald

Abstract

We present Raman and photoluminescence experiments on low-dimensional electron systems based on the compound III-V semiconductors GaAs, AlAs and InAs. A detailed analysis of electronic Raman spectra measured on an ensemble of self-assembled InAs quantum dots on GaAs, excited resonantly at the $E_0 + \Delta$ gap is shown. The highly asymmetric double quantum well system consisting of the backgate and the wetting layer is also studied by resonant Raman spectroscopy. Apart from the single-well single-particle, charge and spin density excitations the measurements show electronic Raman signals that can be explained by a weak tunnel coupling between the two quantum wells. A comparison of the single particle excitations to the results of self-consistent calculations of the Schrödinger and Poisson equations of the system shows a good agreement. Capacitance and photoluminescence spectroscopy was performed on samples with two close layers of self-assembled InAs quantum dots on GaAs. We further present results of photoluminescence excitation (PLE) spectroscopy on InAs/GaAs quantum dots measured at the $E_0 + \Delta$ gap illustrating the possibilities and limitations of the PLE method when applied on a large ensemble.

Raman and photoluminescence spectroscopy was performed exciting resonantly at the E_0 gap transitions on InAs dots grown on AlAs, grown on GaAs and grown on GaAs with the so-called In-flush technique. Macroscopic ensemble measurements on the InAs/AlAs dots did not exhibit any distinguishable electronic Raman signals but featured what in retrospective may be assumed to be photoluminescence peaks of few resonantly excited quantum dots as well as excitations that shift with half the laser energy, for which a physical model is proposed. Measurements on the InAs/GaAs systems are shown ranging from macroscopic ensemble measurements to measurements on single quantum dots. We examine the resonance behavior of the dots and establish and apply methods to distinguish between single dot Raman and single dot photoluminescence signals.

Inhaltsangabe

In dieser Arbeit präsentieren wir Raman- und Photolumineszenz-Experimente an niedrig-dimensionalen Elektronensystemen basierend auf den III-V-Verbindungshalbleitern GaAs, AlAs und InAs. Wir zeigen eine detaillierte Analyse elektronischer Raman-Messungen an einem Ensemble von selbstorganisiert gewachsenen InAs-Quantenpunkten auf GaAs, die resonant am $E_0 + \Delta$-Gap angeregt wurden. Ebenso untersuchen wir ein hoch asymmetrisches Doppelquantumwell-System, das durch das Backgate und die so genannte Wetting Layer in unseren Proben entsteht, mittles resonanter Raman-Streuung. Neben den Einteilchen-, Ladungs- und Spindichteanregungen aus einzelnen Quantum Wells konnten wir auch Ramansignale beobachten, die durch eine schwache Kopplung der beiden Systeme erklärt werden können. Ein Vergleich zwischen den gemessenen Einteilchenanregungen und selbstkonsistenten Berechnungen der Schrödinger- und Poisson-Gleichungen zeigt eine gute Übereinstimmung. Weiterhin führten wir Kapazitäts- und Photolumineszenz-Spektroskopie an einer Probe mit zwei Lagen von Quantenpunkten durch. Ferner zeigen wir Ergebnisse von Photolumineszenz-Anregungs-Spektroskopie am $E_0 + \Delta$-Gap von InAs/GaAs-Quantenpunkten um die Möglichkeiten und Grenzen der Methode, angewandt auf ein großes Ensemble, aufzuzeigen.

Raman- und Photolumineszenz-Spektrokopie, resonant angeregt am E_0-Gap, wurden durchgeführt an Proben, die auf herkömmliche Art auf AlAs oder GaAs, bzw. mit der In-Flush-Technik auf GaAs gewachsen wurden. Makroskopische Ensemble-Messungen an den InAs/AlAs-Quantenpunkten zeigten keine eindeutigen elektronischen Raman-Signale, enthielten aber schmale Anregungen, die im Nachhinein als Photolumineszenz-Signale weniger Quantenpunkte gedeutet werden könnten sowie Anregungen, die mit halber Laserenergie auf absoluter und relativer Energieskala schieben. Messungen an den InAs/GaAs-System werden gezeigt, die von makroskopischen Ensemble-Messungen bis zu Messungen an einzelnen Quantenpunkten reichen. Wir untersuchen das Resonanz-Verhalten der Quantenpunkte und etablieren Methoden um zwischen Einzelpunkt-Raman- und Photolumineszenzsignalen zu unterscheiden.

Contents

1 Introduction **1**

2 Theory **4**
2.1 Low-dimensional electron systems 4
2.1.1 Two-dimensional electron systems 4
2.1.2 Zero-dimensional electron systems 9
2.2 Self-consistent band structure calculations for *2DES*s 12
2.3 Capacitance spectroscopy 14
2.4 Photoluminescence 15
2.4.1 Photoluminescence excitation spectroscopy 17
2.5 Raman Spectroscopy 17
2.5.1 Raman scattering 18
2.5.2 Scattering processes and cross sections 21
2.5.3 Raman selection rules 24

3 Sample design and preparation **25**
3.1 Material properties 25
3.2 Growth of low-dimensional systems 25
3.2.1 Self-assembled quantum dots 26
3.2.2 Double quantum dots 28
3.2.3 Changing the energy gap in *SAQD*s 28
3.3 *MIS* structures 31
3.4 Nanoapertures 32

4 Experimental setups **34**

5 Experimental results and discussion **38**
5.1 Resonant Raman spectroscopy of *SAQD*s at the $E_0 + \Delta$ gap . 38
5.2 The backgate wetting–layer system 46
5.2.1 Voltage-dependent Raman measurements 46
5.2.2 Comparison with simulations 58

5.2.3 q-vector dependent Raman measurements 63
5.2.4 Summary and comparison to the quantum dot system . 63
5.3 Measurements on self-assembled InAs double quantum dots . . 65
5.4 PLE spectroscopy on InAs quantum dots at the $E_0 + \Delta$ gap . 70
5.5 Spectroscopy on InAs/AlAs quantum dots 76
5.6 Raman Spectroscopy on InAs/GaAs quantum dots at the E_0 gap 80
5.7 Spectroscopy on $SAQD$s grown with the In-flush technique . . 84
5.7.1 Macroscopic photoluminescence experiments 84
5.7.2 Resonant Raman experiments 86
5.8 Measurements with the microscope setup 92
5.8.1 Measurements on the unstructured part of the sample with the 20× objective 93
5.8.2 Measurements on the unstructured part of the sample with the 80× objective 95
5.8.3 Measurements with the 80× objective through nanoapertures 98

6 Summary **103**

Bibliography **107**

Chapter 1

Introduction

Many of today's everyday appliances would not be conceivable were it not for the rapid advances that the semiconductor industry has made in the last decades. Mobile phones with the computing power of a ten year old personal computer are just one example of what the massive increase in component density on computer chips has made possible. This increase in density does of course go along with a size reduction of the basic elements that the electronic components consist of — the next generation of processors (to go into serial production as of 2007/2008) has been announced to contain structures as small as 45 nm. As the structures reach the limit where the number of atoms to a structure becomes countable it is not only the realization of these «nanoscopic» structures that poses a challenge — the physics of electrons and holes on this scale is quite different. Therefore, a detailed analysis and knowledge of low-dimensional systems, where electrons are contained in one or even all three dimensions within a few nanometers, is crucial for the development of future electronic components. Whether these will be similar to those that we know (but smaller), or whether at some point the new properties of the low-dimensional systems will be used to create the famed quantum computer, only time will show.

The focus of this work are the electronic properties of quantum dots, i.e. structures where the electrons are contained within few nanometers in all three dimensions by a potential barrier. Because of the three-dimensional enclosure the optical properties of quantum dots are not unlike those of atoms — although on a different energy scale — which is why they are also referred to as *artificial atoms*. Changing the size and material composition of the quantum dots enables us to change the energies of the electrons within the dots. A lot of research has been done on quantum dots in recent years due to the fundamental interest in adjustable atoms as well as possible new applications such as single photon sources or quantum bits.

There is a variety of different quantum dot structures that have received varying attention over the years. This work concentrates on different self-assembled quantum dots. Other notable quantum dot systems include deep-mesa etched systems, gate-defined systems and chemically synthesized nano-structures. Similarly, the material used for structure growth can be anything from Si and Ge to III-V compound semiconductors such as GaAs or II-VI semiconductors such as CdTe and ZnS. We used structures based on the semiconductors InAs, GaAs and AlAs because of their favorable optical properties and the well understood growth mechanisms.

Electronic Raman spectroscopy has been used to study the many-particle excitations of low-dimensional electron systems as early as the late 1970's [Pin79, Abs79]. First Raman measurements on quantum dots were performed on etched GaAs/AlGaAs quantum dots in 1994 by Strenz *et al.* [Str94]. The self-assembled quantum dots have the advantage of containing only very few electrons as compared to the hundreds of electrons that etched quantum dots usually contain (although recently García *et al.* have shown Raman experiments on etched GaAs/AlGaAs quantum dots with only few electrons [Gar05]). The first publication on Raman scattering on self-assembled InAs quantum dots on GaAs was by Chu *et al.* [Chu00] and reported on measurements on a sample with fifteen layers of quantum dots separated by GaAs and doping layers. By using a highly sensitive *CCD* camera and exciting resonantly we have succeeded in enhancing the Raman signal enough to be able to measure Raman signals of a single layer of quantum dots that we could charge with single electrons [Bro03a].

The ultimate goal would be the detection of the Raman signals of a single quantum dot, thus eliminating the inhomogeneous broadening effects of an ensemble measurement. For photoluminescence experiments this has been accomplished several years ago, see e.g. [Bay00]. To separate the single dot Raman signal from any other signal that the sample may exhibit, a profound understanding of the quantum dot luminescence properties as well as the Raman properties of all electronic systems in the sample is necessary.

This thesis tries to contribute to this understanding and establishes methods for the distinction of the different optical signals as well as showing first Raman measurements on few self-assembled quantum dots. It is organized as follows.

Chapter 2 outlines the basic theoretical concepts necessary for the understanding of this work. In Chapter 3 and 4 we show details of the sample preparation and the experimental setups. In Chapter 5 we discuss the experimental results, which are divided into several parts. Starting with results on self-assembled InAs/GaAs quantum dots obtained by exciting resonantly at the $E_0+\Delta$ gap, we move on to Raman measurements on the double quantum

well system backgate-wetting layer. The third section shows results of capacitance and photoluminescence spectroscopy on double quantum dots and the fourth section evaluates the possibilities of photoluminescence excitation spectroscopy at the $E_0 + \Delta$ gap on large ensembles of quantum dots. The following sections show the results of resonant Raman spectroscopy at the E_0 gap on InAs/AlAs dots, InAs/GaAs dots and InAs/GaAs dots grown with the In-flush technique before we gradually decrease the number of observed dots in the last part by using a microscope Raman setup and nanoapertures in an Al mask on top of the sample. Chapter 6 summarizes this work.

Chapter 2

Theory

2.1 Low-dimensional electron systems

2.1.1 Two-dimensional electron systems

In a bulk semiconductor, electrons in the conduction band can move freely through the crystal in every dimension. They can occupy a quasi-continuum of energies and momentums, experiencing a quadratic energy dispersion near the Γ-point in the reciprocal lattice which can be written as

$$E = \frac{\hbar^2 |\vec{k}|^2}{2m^*}, \tag{2.1}$$

where m^* is the effective mass of the electron and $\vec{k}$ is the wave vector. Confining the electrons in one direction leads to a so-called two-dimensional electron system (*2DES*) or quantum well. We will call the directions where the electrons can still move freely x and y while z will be the direction of the confinement. In our experimental systems this is also the growth direction. While the focus of this work will be on zero-dimensional systems, our samples contain at least one quantum well (the so-called wetting layer) and often a second one which serves as a back contact. We will use these systems as examples to further discuss the physics and the possible collective excitations of electrons in *2DES*s.

The wetting layer is a thin layer of InAs that forms during the growth of the self-assembled quantum dots used in this work (see Chapter 3.2 for details). This layer is surrounded by GaAs or AlAs, which have a much larger band gap. The resulting band structure is depicted for GaAs in Fig. 2.1 (a). The shape of the confinement potential is in first approximation rectangular and symmetric, unless doping layers are introduced. Fig. 2.1 (b) shows a

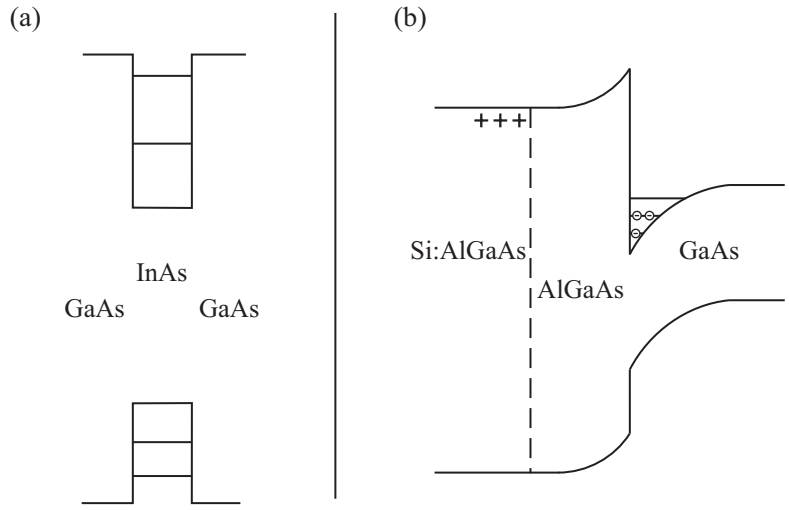

Figure 2.1: Band structures of (a) an InAs wetting layer surrounded by GaAs and (b) a *2DES* created by modulation doping as used in this work as a back contact.

2DES grown with a different approach. An AlGaAs layer highly n-doped with Si is overgrown by a thin layer of undoped AlGaAs — called the spacer layer — and a thick layer of GaAs. The excess electrons from the doping layer travel through the spacer layer and into the GaAs, losing energy mainly to phonons in the process. This leaves the Si donor atoms with a positive charge, attracting the free electrons that are now in the GaAs layer. Therefore, the electrons accumulate near the AlGaAs/GaAs heterojunction, changing the band structure. The potential for the electrons can be calculated self-consistently by solving the Poisson and Schrödinger equations alternately (see Chapter 2.2). The resulting quantum well structure is rather triangular than rectangular in shape. Usually, the structure is grown with the doping layer on top and applied in High Electron Mobility Transistors (*HEMT*s). The way the structure is grown here, it is called an *inverted HEMT* structure.

Both systems still have parabolic energy dispersions in k_x and k_y with a series of subbands because of the confinement. They can be written as

$$E_i = E_i^z + \hbar^2 \frac{(k_x^2 + k_y^2)}{2m^*}, \tag{2.2}$$

where i is the index of the subbands. E_i^z depends strongly on the confinement potential.

In a simple single particle picture, an excitation of an electron is represented by lifting the electron to a higher state which can be either on another subband (intersubband excitation) or, with the need of a momentum

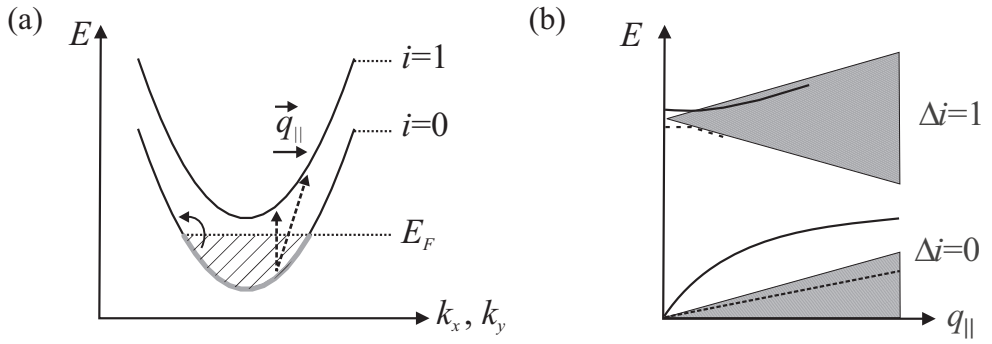

Figure 2.2: (a) Possible intersubband (dashed lines) and intrasubband (solid line) excitations in a quantum well with one subband filled with electrons. The horizontal line marks the Fermi energy E_F. (b) Dispersions of different intersubband ($\Delta i = 1$) and intrasubband ($\Delta i = 0$) excitations. The gray areas show the single-particle continua, the solid lines the *CDE*s and the dashed lines the *SDE*s.

transfer, the same subband (intrasubband excitation). These excitations are depicted in Fig. 2.2 (a). Without momentum transfer only intersubband excitations are possible. Due to the Coulomb and exchange interactions between the electrons all excitations in the quantum wells are *collective* excitations. There are, however, some excitations which have all the characteristics of a single particle excitation (*SPE*) and are only very slightly shifted in energy which shall therefore be called *SPE*s. The other collective excitations are divided into charge density excitations (*CDE*) and spin density excitations (*SDE*) depending on whether the center of charge oscillates (*CDE*s) or not (*SDE*s). *SDE*s are usually shifted to lower energies because of the exchange interaction. Since the center of charge moves in the *CDE*s, the Coulomb interaction becomes more important and the *CDE*s are shifted to higher energies with respect to the corresponding *SPE* and *SDE*. The difference between the energies of the *CDE* and the *SDE* is called depolarization shift. Pinczuk *et al.* have calculated the energies of the collective excitations in a modulation doped quantum well to be [Pin89]:

$$\omega_{SDE}^2 = E_{ij}^2 - 2n_i E_{ij}\beta_{ij} \tag{2.3}$$

$$\omega_{CDE}^2 = E_{ij}^2 + 2n_i E_{ij}\left(\frac{\alpha_{ij}}{\epsilon(\omega_{CDE})} - \beta_{ij}\right), \tag{2.4}$$

where E_{ij} is the difference between the two subbands i and j and n_i is the two-dimensional electron density. α_{ij} and β_{ij} are Coulomb matrix elements, where α_{ij} describes the depolarization shift. The dielectric function $\epsilon(\omega_{CDE})$ also takes into account the interaction of *CDE*s with optical phonons. GaAs is a

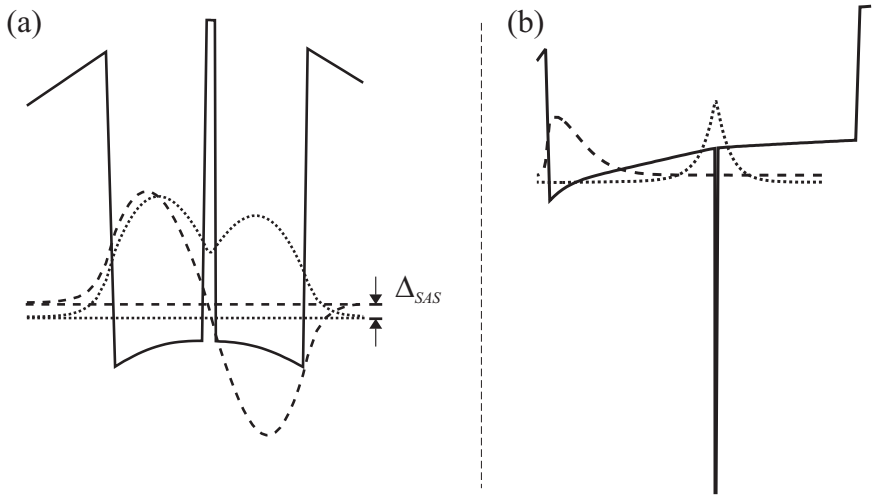

Figure 2.3: Band structures and electron wave functions for (a) a strongly coupled nearly symmetric system and (b) the highly asymmetric system embedded in our structures. The dotted and dashed horizontal lines represent the energy of the respective electronic states. The band structures and wave functions are calculated with G. Snider's 1D Poisson solver, which is explained in Chapter 2.2.

polar crystal, which is why charge density fluctuations can couple to lattice oscillations via the Coulomb interaction. The dielectric function $\epsilon(\omega_{CDE})$ can be written as [Pin82]:

$$\epsilon(\omega_{CDE}) = \epsilon_\infty \frac{\omega_{LO}^2 - \omega_{CDE}^2}{\omega_{LO}^2 - \omega_{CDE}^2}, \tag{2.5}$$

with the high frequency dielectric constant $\epsilon_\infty = 10.8$. Only the longitudinal optical phonons couple to the charge density excitations, because transverse optical phonons have a different polarization. Macroscopically, however, a coupling to the *TO* phonons is possible (see [Zie87, Bit04] for details).

By looking at Fig. 2.2 (b) it is clear that excitations will exhibit a k-vector dispersion that will be different for inter- and intrasubband excitations. By using Raman spectroscopy all of these excitations can be measured and identified by their different polarization behavior and energy dispersions.

Bringing two *2DES*s close together, they start influencing each other via the Coulomb interaction. This means that excitations in the two systems can no longer be studied separately but have to be treated as a coupled system. The strength and type of coupling depends strongly on the distance between the two systems and the height of the barrier. If the two systems are very close to one another (of the order of a few nanometers), there will

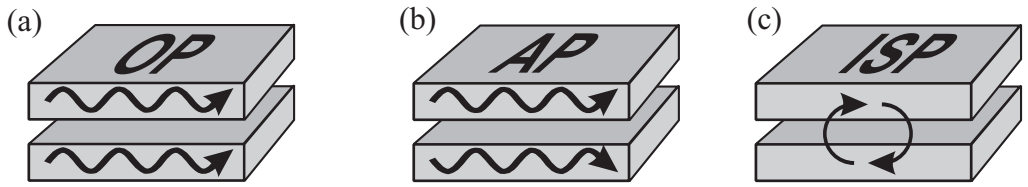

Figure 2.4: The three possibilities for charge density excitations in strongly coupled bilayer systems. (a) Optical plasmon, the charges oscillate in phase. (b) Acoustical plasmon, the charges oscillate with opposite phase. (c) Intersubband plasmon, the charges oscillate between the two layers.

not only be strong Coulomb interaction but electrons will also have a certain probability of tunneling through the barrier and into the other *2DES*. For a perfectly symmetric quantum well, the wave functions separate into a symmetric and an antisymmetric part where the antisymmetric state has the higher energy. The energy difference between the two states is called Δ_{SAS}. Most real systems are, of course, not perfectly symmetric but slightly asymmetric as in Fig. 2.3 (a). It can be shown that this asymmetry leads to a larger energy separation between the two lowest states, which are still called symmetric and antisymmetric in analogy to the perfectly symmetric system. The energy difference between the two states is then simply called Δ in most publications. In a system with strong coupling, i.e. where there is a high probability for the electrons to tunnel from one well to the other, and for the case that only the lowest subbands are occupied, there are three different charge density excitations (*plasmons*), as described by Hu *et al.* in [Hu01]. The macroscopical model for these excitations is illustrated in Fig. 2.4.

- Optical plasmons (*OP*, Fig. 2.4 (a)): these are excitations where the charge carriers of both subbands oscillate in phase. Their energy dispersion goes with the square root of the wave vector.

- Acoustical plasmons (*AP*, Fig. 2.4 (b)): here the charge carriers oscillate in opposite phase. Acoustical plasmons have a linear wave vector dispersion at small wave vectors q. Both optical and acoustical plasmons can be understood as waves traveling in the plane of the coupled *2DES* in a macroscopical picture.

- Intersubband plasmons (*ISP*, Fig. 2.4 (c)): if the charges oscillate perpendicular to the *2DES* plane rather than parallel to it, we call the excitation an intersubband plasmon. Bootsmann [Boo03] calculated

their energy after [Dec94] to be:

$$E_{ISP} = \sqrt{\Delta^2 - 2\Delta(n_0 - n_1)\left(\frac{\alpha}{\epsilon(\omega_{ISP})} - \beta\right)}. \tag{2.6}$$

It should be noted that in this calculation the difference between the two densities n_0 and n_1 enters, not the sum.

For a weakly coupled system, where only the Coulomb interaction between the two quantum wells plays an important role, there can be optical and acoustical plasmons as well. Das Sarma and Madhukar show in [Sar81] that their energies are given by

$$\omega_+ = \sqrt{\frac{e^2}{2\epsilon\epsilon_0 m^*}(n_1 + n_2)q} \tag{2.7}$$

$$\omega_- = \sqrt{2d\frac{n_1 n_2}{(n_1 + n_2)^2}q} \cdot \omega_+. \tag{2.8}$$

Here ω_+ is the frequency of the optical and ω_- that of the acoustical plasmon. n_1 and n_2 are the electron densities of the two quantum wells and d is the width of the layer between the two wells.

The system that we have to deal with in our experiments is shown in Fig. 2.3 (b). It is a highly asymmetric double quantum well consisting of an inverted *HEMT* and the InAs wetting layer. The two quantum wells are different on nearly all levels: the shape of the confinement potentials, the material of the quantum wells and the energies of the ground and excited states. Furthermore, the coupling of the electrons depends on the energy level they occupy, i.e. the coupling becomes stronger for the higher subbands. We will discuss the excitations of this extremely asymmetric system in more detail in Chapter 5.2 from an empirical point of view.

2.1.2 Zero-dimensional electron systems

The focus of this work are zero-dimensional electron systems. These are also called quantum dots or artificial atoms, because like natural atoms they have a discrete energy spectrum. However, unlike real atoms it is a challenging task to produce two or more artificial atoms that have the exact same physical properties. This implies that whenever more than one quantum dot is measured, e.g. in photoluminescence or Raman spectroscopy, several sets of peaks are observed simultaneously, which can result in one broad peak if several thousands of quantum dots are measured at once. To be able to resolve

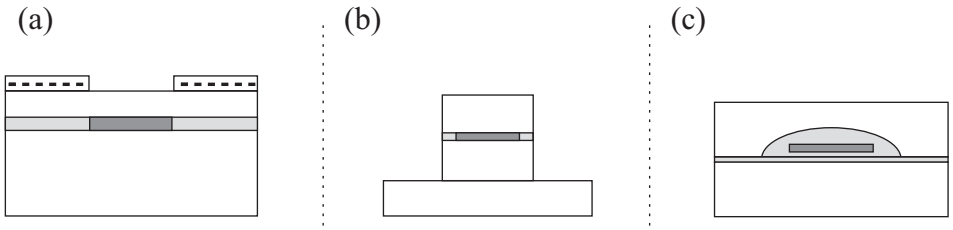

Figure 2.5: Schematic representations of three different methods to fabricate zero-dimensional electron systems: (a) by depletion of a *2DES* near the surface with two electrodes on top of the sample; (b) by lithographic methods, etching small pillars out of a *2DES*-sample; (c) by self-assembled Stranski-Krastanov growth. The actual *0DES* is sketched in dark gray, the light gray regions are to distinguish the different materials.

all the different peaks that a single dot can produce, it is necessary to have either perfectly homogeneous quantum dot ensembles or the prerequisites to measure one single quantum dot at a time. We shall now briefly discuss different methods (shown in Fig. 2.5) for the fabrication of quantum dots in order to motivate our choice.

The first method (Fig. 2.5 (a)) is to grow a *2DES* near the surface of a sample and then define a small gate structure on top of it. By applying a negative voltage to the gate, the *2DES* underneath can be depleted so that by choosing a suitable gate configuration the *2DES* can be depleted completely but for a small area which defines the quantum dot. This method is often used for transport measurements on quantum dots, because it is a comparably simple task to choose the gate configuration in such a way that single electrons can be transferred to and from the quantum dot. Meurer *et al.* have shown in [Meu92] that it is possible to create arrays of these gate-defined quantum dots and charge them simultaneously with single electrons. The quantization energies in these dots are rather small (about 2 meV) which is unfavorable for Raman experiments. The second method is to take a *2DES* and use lithographic methods and deep-mesa etching to reduce the system to pillars of e.g. 200 nm containing the electron system (see Fig. 2.5 (b)). The third method, represented in Fig. 2.5 (c), uses the difference in the lattice constants of GaAs and InAs to form self-assembled quantum dots (*SAQD*s). This method and its advantages and disadvantages are described in more detail in Chapter 3.2.1. For now we want to concentrate on the theoretical properties of these quantum dot systems. Both lithographically processed quantum dots and self-assembled quantum dots are not symmetric in all three dimensions. As Fig. 2.5 suggests the electronic systems are larger in

the lateral directions ($20 - 40$ nm for self-assembled dots) than in growth direction ($4 - 8$ nm for self-assembled dots) which is why they are called *two-dimensional quantum dots*.

In order to solve the Schrödinger equation for such a system, the lateral and growth directions can be separated. Wojs *et al.* show in [Woj96] that for a lens-shaped quantum dot the resulting band structure is nearly parabolic so that the energy levels in the dots can be calculated by using a two-dimensional harmonic oscillator model. This results in equally spaced energy levels with the eigenenergies [Foc28]

$$E_{nm} = \hbar\Omega_0(2n + |m| + 1), \tag{2.9}$$

where $n = 0, 1, 2, \ldots$ is the radial and $m = 0, \pm 1, \pm 2, \ldots$ the azimuthal or angular momentum quantum number of the circularly symmetric structure, and $\hbar\Omega_0$ is the quantization energy. The degeneracy of the energy levels, including spin, is $2N$, where N is defined as $N = 2n + |m| + 1$. In analogy to real atoms, these levels are denominated $s, p, d, f, ...$ for $N = 1, 2, 3, 4, ...$ Neglecting for a moment all interaction between the electrons in the quantum dot, all excitations would be of the energy $\hbar\Omega_0$ or a multiple of it. As discussed for a *2DES* the interactions between the electrons lead to different collective excitations. These are basically the same in quantum dots with a large number of electrons (≈ 100) and quantum wells, although in quantum dots we do not expect to find any energy dispersion for different q vectors as the energies are fully quantized. Looking at a quantum dot with only few electrons ($2 \ldots 6$), the different excitations can be calculated exactly by solving the many-particle Schrödinger equation with the model Hamiltonian:

$$H = \sum_{i=1}^{N} \left[\frac{p_i^2}{2m^*} + \frac{m^*}{2}\Omega_0^2 \vec{r}_i^{\,2} \right] + \frac{e^2}{4\pi\epsilon\epsilon_0} \sum_{i \neq j}^{N} \frac{1}{|\vec{r}_i - \vec{r}_j|} \tag{2.10}$$

with $\vec{r} = (r_x, r_y)$ since the dot is assumed to be two-dimensional with a strong confinement in z-direction. Calculating the eigenenergies for the different excited states in a dot with a certain number of electrons and comparing them to the ground state energies we obtain the possible excitation energies for the given electron configuration. In this model, excitations where the total spin is preserved correspond to *CDE*s and those where the total spin changes correspond to *SDE*s in the macroscopic model. For every electron configuration there can also be found an excitation with the energy $\hbar\Omega_0$, which would correspond to a *SPE*. This is a consequence of the generalized Kohn theorem which states that in a quantum dot with parabolic potential the energy of the center of mass motion is independent of the number of electrons in the dot [Mak90].

In analogy to the coupled *2DES*s, two quantum dots can be brought in close proximity to one another to form a double quantum dot. If the tunneling barrier between the two dots is very small we get a symmetric and an antisymmetric wave function with an energy spacing Δ just like described in the previous chapter for double quantum wells.

2.2 Self-consistent band structure calculations for *2DES*s

To calculate the band structure of our systems the Schrödinger and Poisson equations have to be solved simultaneously and self-consistently. Tan *et al.* present in [Tan90] a flexible method that has been implemented by Greg Snider in his program *1D Poisson Solver*. The program assumes that the growth direction z can be separated from the lateral direction and that movement in the xy plane is free (hence *1D*). So it works very well for 2D systems but is not applicable to the 0D systems.

In the first step, the one-dimensional Schrödinger equation

$$-\frac{\hbar^2}{2}\frac{d}{dz}\left(\frac{1}{m^*(z)}\frac{d}{dz}\right)\psi(z) + V(z)\psi(z) = E\psi(z) \tag{2.11}$$

has to be solved, where ψ is the wave function, m^* is the effective mass of the electrons or holes, and V is the potential energy, for which a trial potential V^{in} is assumed in the first iteration. The one-dimensional Poisson equation is of the form

$$\frac{d}{dz}\left(\epsilon_s(z)\frac{d}{dz}\right)\phi(z) = \frac{-q[N_D(z) - n(x)]}{\epsilon_0}, \tag{2.12}$$

where ϵ_s is the dielectric constant, ϕ is the electrostatic potential, N_D is the ionized donor concentration, and n is the electron density distribution. So, for our next step in the process, the solution of the Poisson equation, we need the density distribution n. This is related to the electron wave function from 2.11 by

$$n(z) = \sum_{k=1}^{m} \psi_k^*(z)\psi_k(z)n_k, \tag{2.13}$$

where m is the number of bound states, and n_k is the electron occupation for each state. The electron concentration for each state can be expressed by

$$n_k = \frac{m^*}{\pi\hbar^2}\int_{E_k}^{\infty}\frac{1}{1+e^{(E-E_F)/kT}}dE. \tag{2.14}$$

Now, by solving the Poisson equation 2.12, we get the electrostatic potential ϕ, which is related to the potential energy V by

$$V(z) = -q\phi(z) + \Delta E_c(z), \tag{2.15}$$

where ΔE_c is a pseudopotential energy due to the band offset at the heterointerface. If the difference between V^{out} obtained by equation 2.15 and V^{in} is greater than a given δ, the procedure is restarted from the first step with the new potential energy $V^{in} := V^{out}$. The procedure is successful if the condition $|V^{in} - V^{out}| \leq \delta$ is achieved after a few iterations.

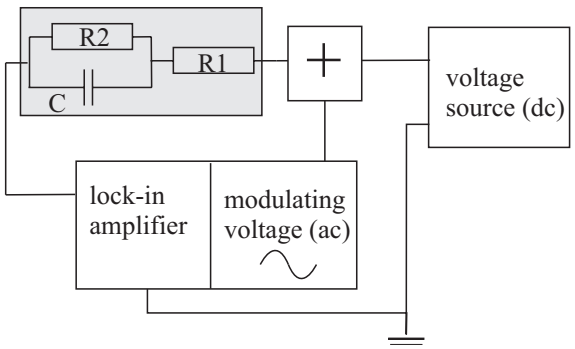

Figure 2.6: Sketch of a setup for C-V capacitance spectroscopy. A modulated dc voltage is applied to the sample (represented in the gray box by a capacitance and two resistances) and the response is measured phase dependent by a lock-in amplifier.

2.3 Capacitance spectroscopy

An important part of this work has been performed on quantum dot systems (this includes implicitly the wetting layer) embedded in a *MIS* (metal-insulator-semiconductor) structure. This sample design allowed us to charge the quantum dots with single electrons by applying a gate voltage (see Chapter 3.3). In order to identify the gate voltages at which each of the quantum dots is charged with $N = 1..6$ electrons we used C-V capacitance spectroscopy.

In general, capacitance spectroscopy means any measurement of the differential capacitance when another parameter is gradually changed (e.g. magnetic field or gate voltage). In our case, only C-V capacitance spectroscopy was used where the differential capacitance of the sample is measured against the gate voltage.

Figure 2.6 sketches the experimental setup. The sample is represented within the gray box by a capacitance C and two resistances R_1 and R_2. R_1 is given by the contacts to the gate and backgate. R_2 is the resistance of the sample itself and should therefore ideally be infinite, as the sample is supposed to be insulating at low temperature. The dc and ac voltages are added via a little circuit, designated by the + sign, and contacted to the gate of the sample. The ac voltage is supplied by the lock-in amplifier, the dc voltage by an external source. The in and out of phase response of the sample is measured. In the following we shall discuss the physical meaning of the measured in and out of phase currents.

Neglecting R_2 in the calculations, we have two impedances, R_1 and $\frac{1}{i\omega C}$,

in the sample, where $\omega = 2\pi f$ is the angular frequency of the ac voltage. The second impedance is imaginary so that a phase shift is introduced by the capacitance. The lock-in amplifier measures both the real (in phase) and the imaginary (out of phase) part of the current I through the sample. If we now look at the change δI in the current, we find that

$$\delta I = \frac{1}{Z}\delta U, \tag{2.16}$$

where $Z = R_1 + \frac{1}{i\omega C}$ is the total impedance of the sample and δU is the change in the voltage. Separated into real and imaginary parts we get:

$$\delta I = Re(\delta I) + iIm(\delta I) = \frac{R_1 \delta U}{R_1^2 + \frac{1}{\omega^2 C^2}} + i\frac{\frac{1}{\omega C}\delta U}{R_1^2 + \frac{1}{\omega^2 C^2}}. \tag{2.17}$$

It can be seen from Eq. 2.17 that both the in phase and the out of phase current depend on both impedances. It is only when the condition

$$R_1 \ll \frac{1}{\omega C} \tag{2.18}$$

is fulfilled that the imaginary part of the current can be approximated to $Im(\delta I) = \omega C \delta U$ and thus the capacitance of the sample can be deduced from the measurement.

2.4 Photoluminescence

Among the optical methods to characterize epitaxially grown quantum dots, photoluminescence is probably the most common. It has been used in this work to find out where the electron and hole ground states lie and how far the first excited states are separated energetically. This information is crucial for resonant Raman measurements and their interpretation. In this section we will describe the underlying processes of photoluminescence and point out a few peculiarities about photoluminescence of quantum dots.

The basic principle of photoluminescence spectroscopy is shown in Fig. 2.7 for quantum dots. In the first step, the excitation, an electron-hole pair is created in the sample. This can be done in the quantum dots themselves or in the surrounding material, depending on the energy of the incoming light. For quantum dots it is advantageous to excite within the surrounding material, because the quantum dots form only a very small part of the sample volume and thus have a very weak absorption compared to the bulk material.

In the second step, called relaxation, the electrons and holes move (individually or as electron-hole pairs) in the crystal and lose energy in non-radiative processes, e.g. to phonons. The relaxation process in the bulk

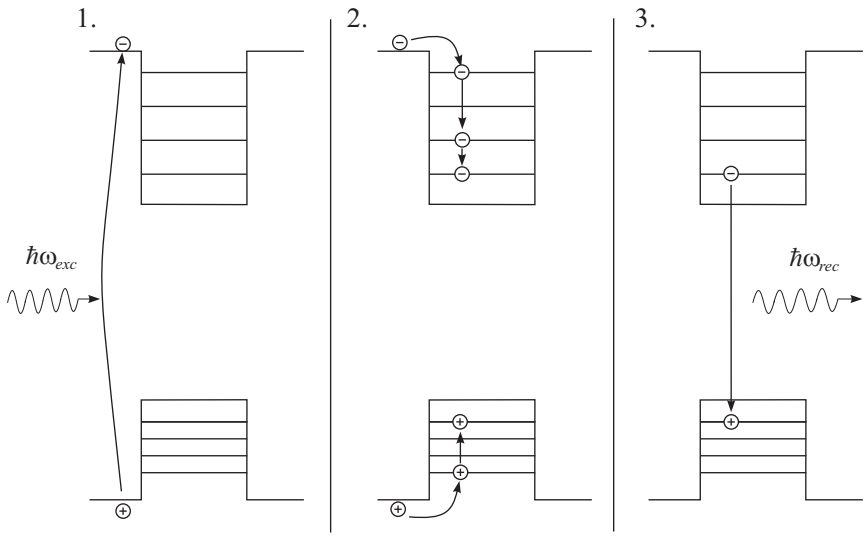

Figure 2.7: Schematic representation of the photoluminescence processes in a quantum dot: 1. A photon with the energy $\hbar\omega_{exc}$ is absorbed in the quantum dot or (as shown) in the surrounding material, creating an electron-hole pair (excitation). 2. Electron and hole move to the energetically lowest state in the quantum dot (relaxation). 3. The electron-hole pair recombines, emitting a photon with energy $\hbar\omega_{rec}$ (recombination).

material is easily understood as there is a continuum of states for the electrons and holes to occupy so that energy and momentum conservation is not a problem. In the quantum dots however, this is not the case because there are only few and discrete states. The only known process of relaxation for the electrons is via the creation of phonons, which have quantized energies as well. This fact is known as the *phonon bottleneck* and is still a subject to discussion in the literature (see, for example, [Ura01, Nar06]).

Having reached the lowest unoccupied states, the electron and the hole recombine in the last step, emitting the photon that is detected as photoluminescence light. Although the relaxation time is much smaller than the life time of the electron-hole pairs, it is possible that an electron-hole pair recombines before it has reached the absolute minimum energy possible. If the energy of the emitted photon is above the band gap of the bulk material, it can (and most probably will) then be reabsorbed and a new electron-hole pair will thus be formed, relaxing further in energy. As a result the transitions with the lowest energies are always the strongest observed in photoluminescence spectroscopy. This usually results in an energetic difference between the maxima of photoluminescence and absorption spectra which is called

Stokes shift[1].

In quantum dots it is possible to observe excited states by enhancing the power density of the exciting laser, hence creating more electrons and holes that fill up the lowest states in the quantum dots. When there are more than two electrons and holes in the quantum dot at a given time, the probability that an electron from the first excited state will recombine with a hole from the first excited hole state increases. With further enhancement of the laser intensity, more excited states become visible. Because of the parity conservation rules, only transitions with $\Delta N = 0, 2, 4, ...$ are possible. The most prominent excitations are those with $\Delta N = 0$, i. e. s-s, p-p, d-d etc.

2.4.1 Photoluminescence excitation spectroscopy

Photoluminescence excitation (*PLE*) spectroscopy uses the same principles of excitation, relaxation and recombination as photoluminescence spectroscopy. The difference is in the method of detection. While in photoluminescence the energy of the exciting laser is fixed and the whole spectrum of the emitted light is detected, in *PLE* spectroscopy a single wavelength is chosen for detection[2] and the intensity at this wavelength is measured against the energy of the exciting laser. The most common choice for the detection wavelength is in the region of the photoluminescence peak. This way, we get information about the first step of the process (excitation) rather than the last step (recombination). The higher the density of states at the energy of the exciting laser, the more electron-hole pairs are created and hence the photoluminescence intensity increases. From this notion it is clear that the *PLE* signal will be proportional to absorption spectra if the recombination energy is independent of the excitation energy.

In our case we measured the whole photoluminescence spectrum as a function of the excitation energy with our experimental setup. In this context we will refer to the method as *multichannel PLE*.

2.5 Raman Spectroscopy

The main part of this thesis is about electronic Raman spectroscopy on quantum dot structures so we will discuss this method in more detail than the

[1] There is another meaning of the term "Stokes shift" in the field of Raman spectroscopy which will be described in chapter 2.5.1.

[2] In the actual experiment this is of course a small spectral window whose width is given by the spectral resolution of the spectrometer.

preceding ones. We will first give a general overview over the method and its terminology before we discuss the scattering processes in more detail.

2.5.1 Raman scattering

Raman scattering is named after the Indian physicist Chandrasekhara Venkata Raman (1888 – 1970) who received the Nobel prize in physics for "his work on the scattering of light and for the discovery of the effect named after him" in 1930. Inelastic light scattering had been predicted by Smekal in 1923 [Sme23] before Raman (and nearly at the same time Landsberg and Mandelstam) was able to measure the effect. It was at first used to study excitations of molecules and molecular structure. The very small intensities of the scattered light made the first experiments very challenging, because strong monochromatic light sources were not available at the time. With the advent of the laser in 1960 Raman scattering became a very popular method for the structural analysis of the excitations in gases, fluids and crystals (i.e. phonons).

Due to the historical background, Raman spectroscopy on solids is nowadays widely known as a means of studying phonons, while it is also a very apt method to study electronic collective excitations in nanostructured semiconductors. To emphasize that we concentrate on this aspect of the phenomenon, we often use the term *electronic* Raman spectroscopy. The term «inelastic light scattering on electronic excitations» is also a synonym for the same processes, which is sometimes used to avoid any ambiguity.

The principle of Raman scattering is sketched in Fig. 2.8. There are two possible processes for the inelastic scattering of light named Stokes and Anti-Stokes processes. The former is sketched in Fig. 2.8 (a): A photon with the energy $\hbar\omega_0$ and the momentum $\hbar\vec{k}_0$ is scattered in the sample by the production of an excitation with energy $\hbar\Omega$ and momentum $\hbar\vec{q}$. The Anti-Stokes process shown in Fig. 2.8 (b) is principally the same with the only difference that an excitation is eliminated rather than created during the process. For both processes energy and momentum conservation have to be fulfilled so that we get

$$\hbar\omega_s = \hbar\omega_0 \mp \hbar\Omega \tag{2.19}$$

$$\hbar\vec{k}_s = \hbar\vec{k}_0 \mp \hbar\vec{q} \tag{2.20}$$

for the energy and the momentum of the scattered light. All our measurements are performed at low temperatures (4 to 10 K). Without illumination there is only thermal excitation which is very low at these temperatures. The observed signals therefore appear only in the Stokes regime. It can be easily

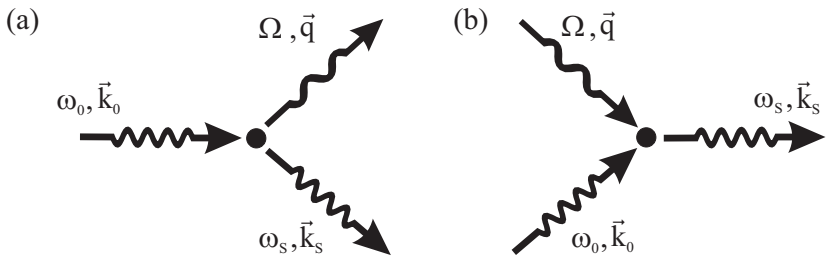

Figure 2.8: Principle processes of Raman scattering: (a) During the process an excitation is created, the scattered light is lower in energy than the incoming light (Stokes). (b) During the process an excitation is eliminated, the scattered light has a higher energy than the incoming light (Anti-Stokes).

seen that the difference between the incident and the scattered light is the energy of the excitation created in the sample. It is commonly called *Raman* or *Stokes shift*. It should be noted that the latter denomination can be easily confounded with the Stokes shift observed between photoluminescence and absorption spectra. Another ambiguity arises from the term *excitation energy* which can be understood as the energy of the excitation created by Raman scattering (which is of course identical to the Raman shift) or the energy of the laser, i.e. the energy of the incident photon. In this case it will not always be possible to avoid this term because evidently Raman shift can only be used when discussing the Raman experiment but not when discussing the energetic structure of the system independent of the spectroscopical method. We will avoid the term excitation energy for the energy of the laser, as it is misleading. In a photoluminescence experiment the term would be appropriate, because the energy of the absorbed photon is the energy by which the electron is actually excited. In Raman spectroscopy, the energy of the laser is important only for resonance effects. We shall get back to this point later in this chapter.

So far we have only discussed the information we get from the energy of the scattered photon. However, as stated above, conservation of momentum can also be applied, which allows us to study the q-vector dispersion of the excitations. In this work all Raman measurements were performed in the back-scattering configuration depicted in Fig. 2.9, where the incident and scattered light are antiparallel to one another. The incident photon has the momentum $\hbar\vec{k}_0$, where $|\vec{k}_0| = \frac{2\pi}{\lambda_0}$, the scattered photon has a momentum $\hbar\vec{k}_s$ with $|\vec{k}_s| = \frac{2\pi}{\lambda_s}$. It is common to divide the momentum transferred to the excitations into the momentum $\vec{q}_\perp$ in growth direction and the momentum $\vec{q}_\parallel$ in the lateral directions. The denomination stems from Raman scattering

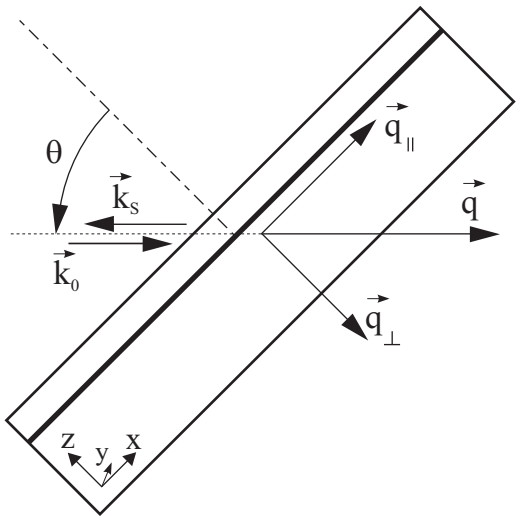

Figure 2.9: Back-scattering configuration in Raman processes. Incident and scattered light are antiparallel to each other and form an angle θ with the surface normal of the sample.

on two-dimensional electron systems (*2DES*), where these momentums are perpendicular and parallel to the *2DES* respectively. If we consider that the energy of the incident laser is usually much higher than the energy of the excitation created, we can state that the incoming and scattered wavelengths are approximately equal and thus $\vec{k}_s \approx -\vec{k}_0$, so that the total momentum transfer to the excitations is $\vec{q} = \vec{q}_\perp + \vec{q}_\parallel = 2\vec{k}_0$. The absolute values of $\vec{q}_\perp$ and $\vec{q}_\parallel$ depend on the angle of the incident light to the sample θ. In general, only the absolute value of $\vec{q}_\parallel$ is of interest, because in a *2DES* only the parallel momentum can be changed continuously. It is given by

$$\left|\vec{q}_\parallel\right| = 2\left|\vec{k}_0\right| \sin\theta. \tag{2.21}$$

A priori, momentum transfer is not of such a high interest in a quantum dot because the energy spectrum in k space is discrete if interaction between the dots is neglected. This means that excitations in quantum dots are not expected to change in energy when the momentum transfer is increased or decreased. On the other hand, an excitation which does exhibit a q-vector dispersion cannot originate from a quantum dot, so this property can be used to identify excitations. It is also important to note that a momentum transfer to the sample can be helpful for breaking selection rules (see Chapter 2.5.3).

2.5.2 Scattering processes and cross sections

We will now discuss the scattering processes in more detail, in particular resonant scattering processes. These are not as present in literature as the normal scattering processes, but we find them to be the main contributions to our signals. To describe the coupling of the incident light with the electrons in the nanostructure, we use a perturbation approach where the momentum $\vec{p}$ of the electron is replaced by $\vec{p}+e\vec{A}$ in the Hamiltonian H_0 of the unperturbed system:

$$\begin{aligned} H &= \frac{1}{2m}\sum_i \left[\left(\vec{p}_i + e\vec{A}(\vec{r}_i)\right)^2 + U(\vec{r}_i)\right] + \hat{V}_{e-e} + \hat{V}_{e-ph} \\ &= H_0 + \frac{1}{2m}\sum_i \left[\left(\vec{A}(\vec{r}_i)\right)^2 + \vec{p}_i\vec{A}(\vec{r}_i) + \vec{A}(\vec{r}_i)\vec{p}_i\right] \end{aligned} \tag{2.22}$$

$\vec{A}$ is the vector potential of the electromagnetic field, $\hat{V}_{e-e}$ and $\hat{V}_{e-ph}$ are the Coulomb and the electron-phonon interaction respectively. The potential energy U contains the lattice-periodic potential as well as all external potentials. The last three terms in the second line of 2.22 are the perturbations of the system. The term $(\vec{A}(\vec{r}_i))^2$ introduces the perturbation of the first order. There is no interaction with the electronic system in this term, so it does not describe any *resonant* scattering mechanisms and can be ignored in our further considerations. The other two terms describe the second order perturbation (SOP) and, when taking into account the electron and phonon interactions, the third order perturbation (TOP), which show a characteristic resonance behavior. To understand the origin of these resonances, Burstein *et al.* (for SOP, [Bur80]) and Danan *et al.* (for TOP, [Dan89]) have developed a model for light scattering on *2DES* that can be adopted for *0DES* as well. The scattering mechanisms are represented in Fig. 2.10. The figure can be understood to represent scattering on quantum dots, where the vertical lines are the energies of the quantized system, or scattering on a quantum well, where the vertical lines represent the lowest subband states. Fig. 2.10 (a) shows a two-step scattering mechanism. In the first step an electron is lifted from a valence band state to an empty state in the conduction band by absorption of an incident laser photon. Another electron of lower energy and either the opposite or the same spin as the first combines with the created hole in the second step, leaving the system in a state where effectively an excitation with or without spin flip has taken place. The third step in the scattering mechanism shown in Fig. 2.10 (b) represents the screening of the excitation by the other electrons in the system via the creation of another excitation. While the first mechanism describes a single particle excitation,

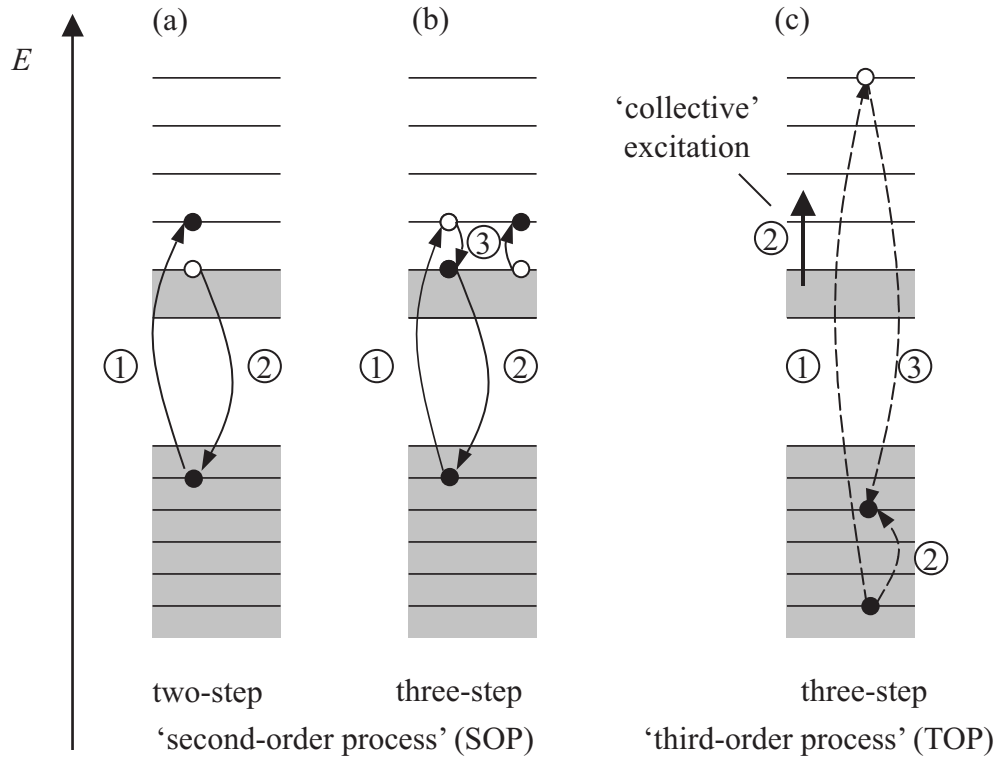

Figure 2.10: Schematic pictures of the scattering mechanisms for electronic excitations in a quantum dot. (a) Two-step and (b) three-step scattering processes from second-order perturbation theory. (c) The three-step scattering process described by third-order perturbation theory. Filled and empty circles represent occupied and unoccupied states after the scattering process. The gray shaded area marks the energy region below the Fermi energy, where electronic states are occupied.

the screening can be used to explain many-particle excitations, i.e. *CDE*s and *SDE*s.

The third mechanism can explain scattering processes where the energy of the incident light is well above the band gap of the system. The incident photon creates an electron-hole pair in the system which somehow relaxes to a lower energy state, e.g. by the relaxation of the hole as shown in Fig. 2.10 (c). In this step, a collective excitation of the electrons can be produced by Coulomb interaction of the relaxing hole with the Fermi sea. In the third step the electron-hole pair recombines, emitting the scattered photon.

Before carrying on to the scattering cross sections of the described mechanisms, we want to stress the differences between Raman scattering and photo-

luminescence experiments. It is tempting to regard the processes in Fig. 2.10 as luminescence processes, especially the three-step mechanisms shown in Fig. 2.10 (b) and (c). This is furthered by the existence of *hot luminescence*, where the electron-hole pair does not relax completely before recombination. Formally, the difference between hot luminescence and Raman scattering manifests itself in the different matrix elements of the two processes as described by Shen [She74]. Experimentally, it is not easy to measure Raman scattering without measuring hot luminescence. The difference is mainly in different line widths which may lead to a broad luminescence background underneath the Raman signal.

For the discussed scattering mechanisms, the scattering cross section is given by [Ham69]

$$\frac{d^2\sigma}{d\Omega d\omega} = \frac{\omega_S}{\omega_I}\frac{e^4}{c^4 m^4} S(\omega), \tag{2.23}$$

where the structure factor $S(\omega)$ is defined as

$$S(\omega) = \sum_f \left| \langle f | \hat{V}_{eff} | i \rangle \right|^2 \delta(E_f - E_i - \omega). \tag{2.24}$$

$\omega_I(\omega_S)$ is the energy of the incident (scattered) photon, $\omega = \omega_I - \omega_S$ is the energy transfer. The effective operator $\hat{V}_{eff}$ describes the transition from the initial state $\langle i|$ with energy E_i to the final state $\langle f|$ with the energy E_f. Govorov describes in [Gov97] how the effective operator can be expanded to

$$\hat{V}_{eff} = \sum_{\alpha,\beta} \gamma_{\alpha\beta} \hat{c}^\dagger_\beta \hat{c}_\alpha \tag{2.25}$$

in a many-particle system in terms of creation ($\hat{c}^\dagger$) and annihilation ($\hat{c}$) operators of single-electron states. α and β represent sets of quantum numbers (n, m, σ), for the radial, azimuthal and spin quantum numbers of the corresponding states. Neglecting the interaction between electrons and holes, the scattering amplitudes can be written as

$$\begin{aligned} \gamma_{\alpha\beta} \sim \langle \alpha | e^{i\vec{q}\vec{r}} | \beta \rangle \, \vec{e}_I \vec{e}_S + \frac{1}{m} \sum_{\beta'} \frac{\langle \beta | \vec{p}\vec{A}_S | \beta' \rangle \langle \beta' | \vec{p}\vec{A}_I | \alpha \rangle}{E_\alpha - E_{\beta'} + \hbar\omega_I} \\ + \sum_{\nu\nu'} \frac{\langle \beta | \vec{p}\vec{A}_S | \nu' \rangle \langle \nu' | \hat{V}_{e-e} | \nu \rangle \langle \nu | \vec{p}\vec{A}_I | \alpha \rangle}{(E_\beta - E_{\nu'} + \hbar\omega_S)(E_\alpha - E_\nu + \hbar\omega_I)}, \end{aligned} \tag{2.26}$$

where in the last two terms only the strongest resonant terms are written. The first term in Eq. 2.26 represents nonresonant processes from the $\vec{A}^2$ terms

in first order perturbation theory. The resonant second and third terms describe second and third order processes as shown in Fig. 2.10 (a) and (c).

Schüller gives an overview of Raman experiments on quantum dots etched with holographic lithography in [Sch99]. He finds that the second- and third-order processes are the dominant contributions when the laser energy is tuned to resonance. Resonance energies can be any energies that coincide with a real transition in the structure. The third-order processes as described in [Dan89] rely on the existence of a hole transition in the valence band that has the same energy as the electronic excitation created in the third step. This process is therefore strongly enhanced when exciting resonantly at the E_0 gap, as compared to excitation at the $E_0 + \Delta$ gap from the split-off band, because the light and heavy hole bands furnish a quasi-continuum of states. The split-off band is created by the interaction of the spin and the angular momentum of the electrons in the valence band and consists of only one hole band. In InAs quantum dots it lies 0.6 eV below the light and heavy hole bands at the Γ point [Pus97].

2.5.3 Raman selection rules

Another consequence of the calculation of the scattering cross sections by Hamilton and McWorther in [Ham69] are the polarization selection rules. These allow for the separation of spinflip and non-spinflip or charge- and spin-density excitations. The former appear only in *polarized* spectra where the polarization of the incident and scattered light are parallel to each other. The latter can be observed in *depolarized* spectra where the polarizations are perpendicular to one another. If the difference between spinflip and non-spinflip single particle excitations is too small to be resolved, they may appear at the same energy and in both polarization configurations.

Calculating the matrix elements responsible for inelastic light scattering also yields the result that only excitations with even parity can be observed, which is due to the fact that Raman processes are two-photon processes. This parity selection rule makes Raman spectroscopy the ideal counterpart to (far) infrared absorption spectroscopy, where excitations with odd parity are observed. In Raman spectroscopy, this selection rule can be broken when a large q-vector is transferred in the light scattering process.

Chapter 3

Sample design and preparation

3.1 Material properties

The semiconductors used in this work are GaAs, AlAs, $Al_xGa_{1-x}As$ and InAs, which all grow in the zincblende structure. The lattice constants of GaAs, AlAs and InAs are displayed in Tab. 3.1 along with their energy gaps at room temperature. GaAs and InAs are direct semiconductors, AlAs has an indirect band gap. The ternary compound $Al_xGa_{1-x}As$ has a direct band gap for an aluminum concentration of up to $x \approx 0.4$ and an indirect band gap for larger x. In the literature it is often called AlGaAs for simplicity, which we will adopt here. In most cases, the aluminum concentration in our samples is between $x = 0.3$ and $x = 0.35$.

3.2 Growth of low-dimensional systems

We have briefly discussed several possibilities to form two-dimensional electron systems and quantum dots in Chapter 2.1. We will now discuss the technical particularities of the growth of low-dimensional systems, especially of self-assembled quantum dots.

Material	Lattice constant(Å)	Energy gap (eV)
GaAs	5.6533	1.42
AlAs	5.6605	2.17
InAs	6.0584	0.36

Table 3.1: Lattice constants and energy gaps at room temperature of the semiconductors used in this work. The properties of AlGaAs can be deduced by linear interpolation between pure GaAs and pure AlAs values.

All samples have been grown by molecular beam epitaxy (MBE) in the group of Prof. Wolfgang Hansen at the Institut für Angewandte Physik in Hamburg. This method allows for a very clean heterostructure growth with the precision of a monolayer[1]. The structures are grown on a GaAs substrate oriented along the (100) axis. Because the lattice constants of GaAs and AlAs are nearly identical, the two semiconductors (as well as AlGaAs) can be grown on top of each other without notable lattice mismatch. The growth of quantum wells using GaAs and AlGaAs with MBE is a standard procedure nowadays that we will not discuss further at this point.

3.2.1 Self-assembled quantum dots

Of the three different methods to confine electrons into a quantum dot, we use only self-assembled growth in this work, because it enables us to produce charge-tunable quantum dot ensembles of a very good homogeneity with very few electrons ($N = 1..6$). A remarkable amount of research has been dedicated to this type of quantum dots in recent years which lead to a profound understanding of the growth mechanisms involved, allowing for more sophisticated methods like the In-flush technique described below.

As can be seen in Tab. 3.1, the lattice constant of InAs is $\sim$7% larger than that of GaAs. Growing InAs on top of GaAs leads to Stranski-Krastanov growth as shown in Fig. 3.1. The first $1-2$ monolayers of InAs form the so-called wetting layer. This layer grows with the same lattice constant as the GaAs substrate so that a certain amount of strain builds up. The strain is released by the formation of small InAs islands when more InAs is deposited [Leo93, Leo94]. If the growth conditions are chosen appropriately, these islands can build up to small quantum dots of a few nanometer in height and about 20 nm in width. The InAs islands are overgrown with GaAs so that the electrons within the dots are confined by the higher band gap material in every direction. The wetting layer remains as a very thin quantum well throughout the process. In growth direction the quantum dots have been reported to be of lens shape after overgrowth, although it is not uncommon to represent them as pyramids, which is the shape they have before overgrowth. As Fig. 3.1 suggests, there is a certain amount of intermixing between the InAs layers and the GaAs substrate. Hence, the composition of the dots is not pure InAs but InGaAs with a Ga content that depends strongly on growth parameters like temperature and In flow because of intermixing processes. For a detailed discussion of these processes, see [Hey07].

[1] All materials used here grow in the zincblende structure, so here a monolayer has the thickness of half a lattice constant.

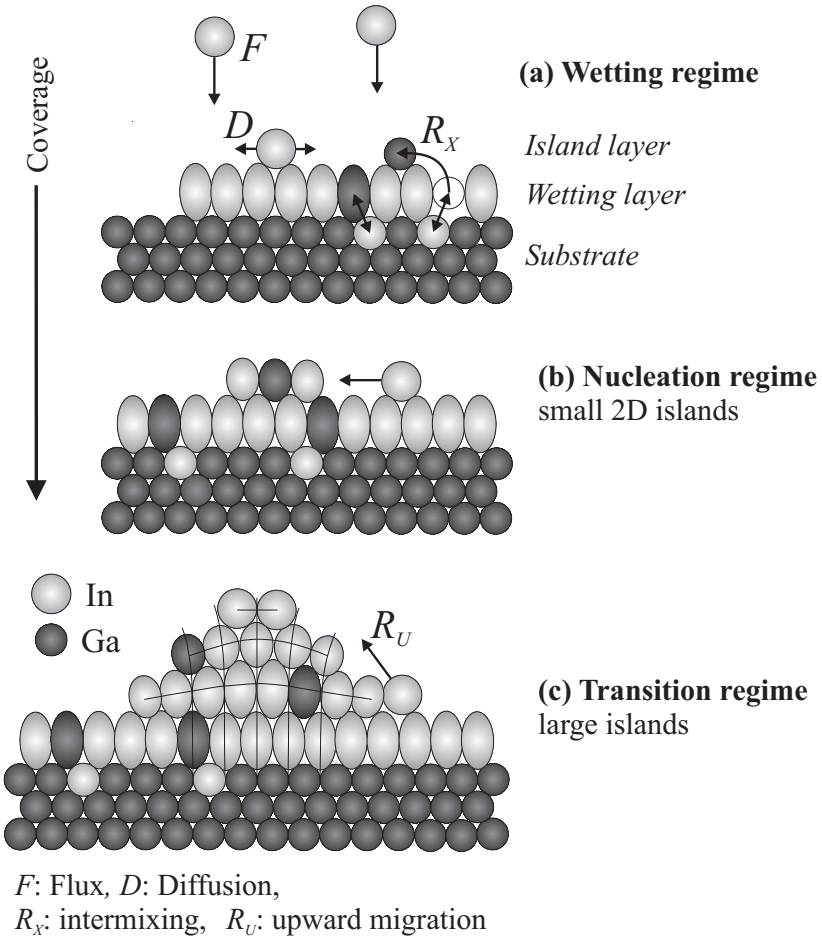

Figure 3.1: Stranski-Krastanov growth of InAs quantum dots after [Hey07] (used with kind permission from Ch. Heyn). In the wetting regime (a), $1-2$ monolayers of InAs form the wetting layer, grown with an inherent strain on the substrate because of the different lattice constants. With further deposition of material, small 2D islands start to form (b). Further InAs deposition leads to the formation of 3D quantum dots (c).

3.2.2 Double quantum dots

Because of the statistical distribution of the self-assembled dots over the sample it seems a difficult task to produce self-assembled double quantum dots (either vertically or horizontally). Nevertheless, Xie *et al.* [Xie95] have shown that a vertical alignment of multiple layers of quantum dots is in fact easily accomplished because the dots do not only self-assemble but also self-align. This is attributed to the strain field that remains in the vicinity of the dots after overgrowth. Just as the InAs wetting layer is growing with the «wrong» lattice constant, the GaAs growing on top of the quantum dots can not immediately grow with the «right» crystal structure. This favors the formation of the new quantum dots on top of the dots of the first layer. By growing a layer of GaAs on top of the quantum dots that is only slightly thicker than the quantum dot height, we can thus obtain ensembles of vertically coupled quantum dots.

3.2.3 Changing the energy gap in *SAQD*s

In this section we would like to give an overview — without claiming completeness — of some methods to engineer the energies in self-assembled quantum dot systems that have been developed over the years. We have shown in the previous chapters that there are two different energy scales that have to be discussed for a full comprehension of resonant Raman scattering:

- the recombination energy which is responsible for resonant Raman processes, measured in photoluminescence experiments (of the order of $1-2$ eV),
- the energy difference between the electronic states which can be measured in Raman and *FIR* absorption spectroscopy (of the order of 50 meV).

Tuning these energies is of high interest, e.g. for quantum dot lasers that emit in the technologically important 1.3 µm band or to adjust them to the range of maximum sensitivity of the available laboratory instruments. The energies can be tuned by changing one or more of the following parameters:

- the composition of the quantum dot — changing this will affect the ground state energy as well as the energy difference between electronic states,
- the composition of the barrier material — this affects the height of the confinement potential and thus also both energies,

- the height of the dots in growth direction — this has no effect on the energy difference between excited states but a huge effect on the ground state and therefore the recombination energy,

- the lateral size of the dots — while this also affects both energies, the impact on the ground state energy is rather small compared to the influence of the dot height.

Changing the quantum dot composition

It has already been mentioned that according to various publications the quantum dots do not consist of pure InAs due to intermixing processes during the island growth and during overgrowth. In fact, it appears that the composition of the dots is not even uniform throughout the dot. The amount of intermixing can be controlled to some extent by the growth temperature and In flow. Malik *et al.* present in [Mal97] a method called *rapid thermal annealing* which enforces the intermixing process by ramping the temperature up after the growth of the sample. It should be noted that a stronger intermixing also leads to larger dots. These two processes have opposite effects — the intermixing leading to a larger energy gap and the enlargement of the dots leading to a smaller energy gap. The effect of the intermixing is found to be the stronger one so that a shift to higher energies is observed after the process.

Changing the barrier composition

Changing the composition of the substrate and the surrounding material of the dots is a simple method to change the confinement potential of the dots. Instead of GaAs, AlGaAs or even pure AlAs is used as substrate. These have a larger energy gap than GaAs so that the confinement potential is enlarged. As a side effect, the dots growing on AlAs are smaller than dots grown on GaAs, which leads to a further enlargement of the eigenstate energies. Besides the change in the confinement potential, the energy gap of the dot material is also raised because of the intermixing effects discussed in the last paragraph. Complications may arise for optical experiments because for Al concentrations larger than 0.4 the AlGaAs becomes an indirect semiconductor. Leon *et al.* and Polimeni *et al.*, among others, have studied the energetic structure of quantum dots grown on AlGaAs with varying Al content [Leo95, Pol99].

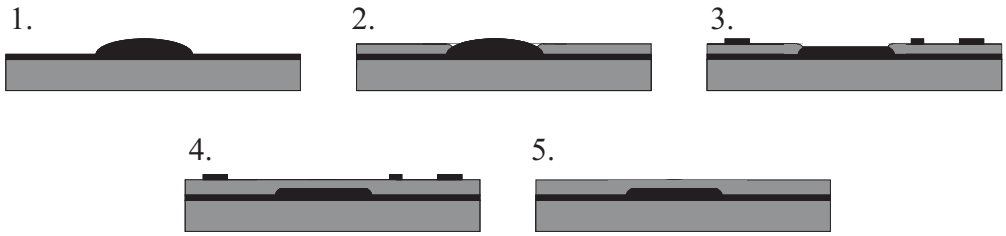

Figure 3.2: In-flush technique after [Was99]. In the first step, self-assembled InAs (black) quantum dots are grown on GaAs (gray). After the deposition of a few nanometers of GaAs (2.), the uncovered InAs forms a second wetting-layer on the new GaAs layer (3.). In the next step, the GaAs closes the energetically costly crater (4.) and the remaining InAs is removed by rapid heating, the In-flush step (5.).

Changing the size of the dots

The size of the self-assembled quantum dots depends heavily on the growth parameters [Chu99, Gar98] and the substrate [Bal01]. The dots can thus be varied in size within a limited range. Most of the parameters change the lateral size of the dots and the height of the dots simultaneously. Wasilewski *et al.* present in [Was99] and [Faf99] a method that ideally changes only the height of the dots. The method is illustrated in Fig. 3.2. First, normal self-assembled InAs quantum dots are grown on GaAs. These have the usual statistical distribution in height and lateral size. In the second step, a thin layer of GaAs — thinner than the dot height — is grown. In this situation the free-standing InAs is not in an energetically favorable position so that it can move on top of the «clean» GaAs layer to form a new partial wetting-layer (3.). The InAs that is now at the top of the islands still has an important lattice mismatch so that the surrounding GaAs can cover the disk, closing the energetically costly dips without further deposition of GaAs (4.). In the last step, the sample is rapidly heated to remove the remaining InAs. This so-called In-flush technique results in flat disks that have a higher energy gap but nearly the same energy differences within the conduction band as dots produced without the flush technique. It is conceivable, however, that during the third step, where the temperature of the sample is raised, intermixing effects are enhanced, changing the eigenenergies of the lateral confinement.

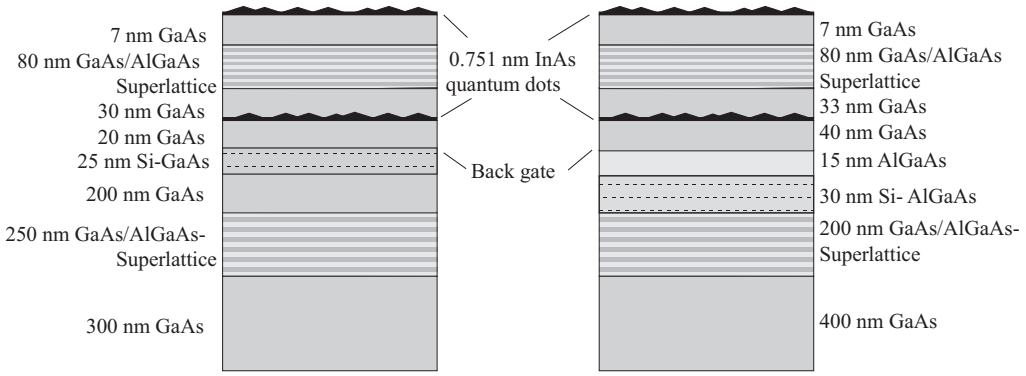

Figure 3.3: Schematic representation of two typical sample layouts (left: sample #931, right: sample #1005). InAs quantum dots are grown in a *MIS* structure with a highly doped GaAs layer (left sample) or an inverted *HEMT* (right sample) as a back contact. The dots on top of the sample are grown for *AFM* measurements.

3.3 *MIS* structures

Most of the low-dimensional systems we examine in this work are embedded in a Metal-Insulator-Semiconductor (*MIS*) structure that allows us to change the electron density in the *2DES* or, in the case of the zero-dimensional systems, the number of electrons in the dots by applying a voltage between the metal front gate and a highly doped layer or inverted *HEMT* within the sample. The back gate is connected by alloyed contacts on the sample, fabricated by deposition of a AuGe/Ni/AuGe layer sequence[2] with thicknesses of 25/5/25 nm and subsequent heating to 300 °C for 2 min. The GaAs layer between the back gate and the front gate acts as an insulator at low temperatures. A superlattice of GaAs and AlAs is grown within this layer as a blocking layer to allow for capacitance spectroscopy at higher voltages. A typical sample layout is sketched in Fig. 3.3. On top of the sample, another layer of quantum dots is grown with the same parameters as the first but without overgrowth. These can be examined with atomic force microscopy (*AFM*) before the deposition of the metallic gate and thus give us an idea of the dot size and distribution of the in-grown layer. The deposition of the Ti front gate and the AuGe for the backgate contacts is carried out with copper shadow masks by metallic vapor deposition in a high vacuum oven.

[2] AuGe is deposited in the eutectic composition 88:12.

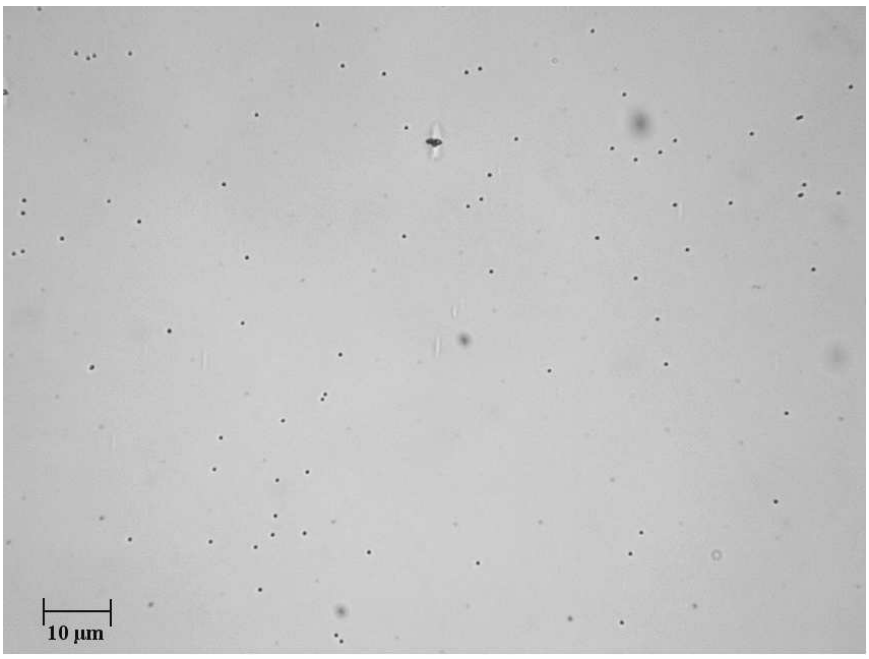

Figure 3.4: Optical microscope picture of the sample surface after the nanoaperture process. The little black dots in the picture are the small holes that remain in the Al mask after the removal of the latex spheres.

3.4 Nanoapertures

We have mentioned earlier that it is desirable to measure on few or even single quantum dots instead of ensembles. To achieve this in our optical experiments, Tim Köppen in his diploma thesis prepared aluminum masks with nanoapertures on the samples by applying latex spheres of a well defined diameter (230 nm) in a highly diluted solution onto the sample surface and scattering them by spin-coating. In the next step, a 80 nm thick layer of aluminum was deposited on the surface. Subsequently, the latex spheres were removed with tetrahydrofuran and an ultrasonic bath, leaving holes in the aluminum layer, the so-called nanoapertures, where the spheres had been. Fig. 3.4 demonstrates that the holes in the Al mask are distributed fairly homogeneously over the sample surface, and only very few locations with two or more holes touching each other are formed. The density and size of the holes are prepared such that it is possible to focus the laser on one hole at a time in the microscope Raman setup and that on average there are only five dots underneath a hole (depending also on the dot density). In Fig. 3.5 a typical cross section of such a hole is shown. The profile was taken with an

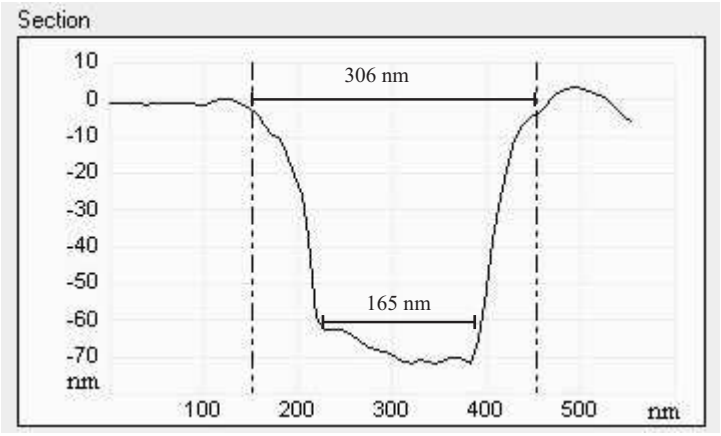

Figure 3.5: Typical cross section of a hole in the Al mask taken via atomic force microscopy (*AFM*).

atomic force microscope. The hole is (235 ± 70) nm in size, reproducing the size of the latex spheres, and about 70 nm deep with a nearly rectangular profile. The rather large errors can be explained by a flattened or dirty *AFM* tip.

Chapter 4

Experimental setups

We used two different laboratories for our experiments. One was used for photoluminescence (PL) and photoluminescence excitation (PLE) experiments and the other for the Raman experiments and the measurements on samples with nanoapertures.

The PL measurements were performed with the setup shown in Fig. 4.1. We used an Ar^+ laser emitting at 514 nm for excitation with intensities of the order of 1 W. For the PLE experiments a Ti:Sapphire laser was introduced into the setup, pumped by the Ar^+ laser emitting in multiline mode for higher pump power. The Ti:Sa laser was tunable within a range between 700 and 850 nm and delivered intensities up to 50 mW. The samples were mounted in an Oxford helium-flow cryostat with glass windows for optical experiments. The luminescence light was collected and coupled into the spectrometer by two lenses. We used a Fourier transform spectrometer with optionally a Si or a Ge detector for measurement. The collected data was transferred to a computer where the spectra were calculated from the measured interferograms by fast Fourier transformation.

The Raman setup is shown in Fig. 4.2. The Ti:Sa laser used for the light scattering experiments was pumped by a diode-pumped solid state laser emitting at 532 nm. Two different mirror sets were used in the Ti:Sa laser that allowed for the emission ranges between 700 and 850 nm ($1.46 - 1.77$ eV) and between 850 and 990 nm ($1.25 - 1.46$ eV). The maximum intensity of the laser varied between 5 and 100 mW depending on the efficiency of the lasing process. For some wavelengths a prism monochromator was necessary to remove weak laser modes beside the main mode in the spectra. The polarization of the laser light could be rotated by a Fresnel rhombus ($\lambda/2$ plate) in order to obtain polarized and depolarized Raman spectra. The intensity of the laser could be adjusted by introducing gray filters into the optical path for a strong and defined reduction and by a set of a $\lambda/2$ plate

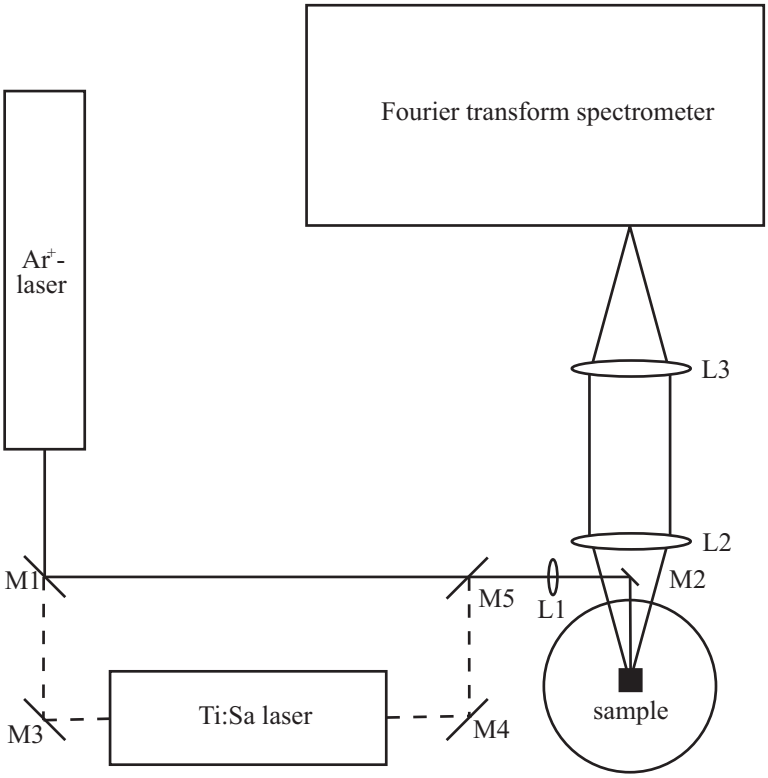

Figure 4.1: Schematic representation of the *PL* and *PLE* setup. The solid line shows the optical path for the *PL* measurement. For the *PLE* experiments, mirror M1 was removed and M3, M4, M5 and the Ti:Sa laser were introduced.

and a polarizer for a continuous change in intensity. A Si diode could be introduced into the optical path to measure the laser intensity.

There were two different cryostats available in the Raman setup. For macroscopic measurements a He-flow cryostat was employed in which the samples could be cooled down to 3 K. The samples were fixated on a sample mount that could be rotated along an axis perpendicular to the laser beam. The thermal contact between the sample and the liquid helium was ensured by helium gas surrounding the sample. The laser light was focused on the sample by a cylindrical (spherical) lens for a line (point) focus and the scattered light was collected and aligned by an achromat and coupled into the triple Raman spectrometer. In Fig. 4.2 the optical path for the macroscopic measurements is shown by the solid lines. The dashed lines represent the optical path for the microscope measurements. In this setup the laser light was guided downwards by a semi-transparent mirror within the microscope and was focused onto the sample by the objective. The size of the focal point

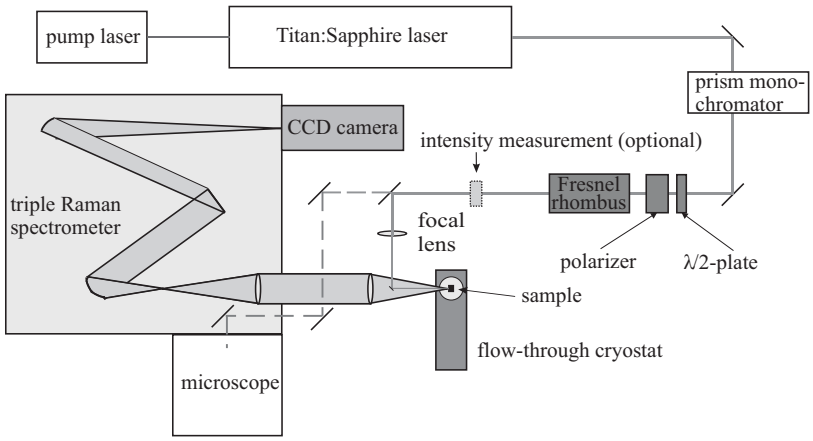

Figure 4.2: Schematic representation of the Raman setup. The solid line shows the optical path for the macroscopic measurement. The dashed line show the path of the laser for microscope measurements.

could thus be down to 2 µm, using the objective with the largest magnification. The sample was mounted in another He-flow cryostat on a copper block that was cooled directly by the liquid helium. The scattered light was collected by the same objective, passed through the semi-transparent mirror and was then coupled into the triple Raman spectrometer by a set of mirrors and lenses (not shown). The microscope could also be used to examine the surface of the sample by sliding a mirror above the beam splitter out of the optical path.

The spectrometer consists mainly of three gratings that have been set to subtractive mode for the spectra. In this mode the stray light reduction is very high (of the order of 10^{-8}) which is necessary to detect the extremely weak Raman signals near the laser frequency. The gratings have different reflectivities for linearly polarized light parallel or perpendicular to their axis. A separate analyzer is hence not needed to distinguish between polarized and depolarized spectra. The spectrally resolved light is imaged by a highly sensitive charged coupled device (*CCD*) camera that is cooled down by a Peltier element in order to reduce electrical noise. The camera had a quantum efficiency of up to 90 % in the visible range and was sensitive for photons with energies down to 1.27 eV with a quantum efficiency of over 20 %. The spectra were obtained taking three accumulations if not noted otherwise which were then compared so that spikes that appeared in only one of the accumulations could be eliminated[1]. The data was analyzed on a computer which also

[1]Spikes can appear in single accumulations when a cosmic particle hits the *CCD* array,

enabled the control of the lasers, the Fresnel rhombus, the tipping angle of the sample, the gate voltage and the spectrometer. This high degree of automization made extensive studies of the Raman signal in dependence of any of those parameters possible.

creating local charges. The longer the accumulation time the higher is the probability of spikes in the spectrum.

Chapter 5

Experimental results and discussion

We will now present the results of our experiments and discuss them in detail. In all experiments the samples were cooled down to $4 - 10\,\mathrm{K}$ to minimize thermal effects unless stated otherwise.

5.1 Resonant Raman spectroscopy of *SAQD*s at the $E_0 + \Delta$ gap

It has been stated before that the Raman signal from electronic excitations in quantum dots is expected to be very small unless we can take advantage of some resonance mechanism. For our first experiments on self-assembled quantum dots we used the electronic transitions near the $E_0 + \Delta$ gap of the dots for a resonant enhancement of the signal. This gap had the advantage of being within the range of maximum sensitivity of our *CCD* camera and within the scope of our Ti:Sapphire laser with the mirror set we used for the GaAs experiments. From an experimentalist's point of view this also had the advantage that the laser light we used for the scattering was within the visible range, making for an easier beam alignment compared to infrared light.

To our knowledge, there had only been one publication on the subject of light scattering experiments on electronic excitations in self-assembled quantum dots when we started our experiments [Chu00]. In their work, Chu *et al.* present Raman experiments on 15 layers of quantum dots without coupling between the layers and six electrons in each dot. The experimental setup was very similar to ours and they also used the $E_0 + \Delta$ gap for resonance effects. They observed a broad signal (25 meV FWHM) at about 50 meV in

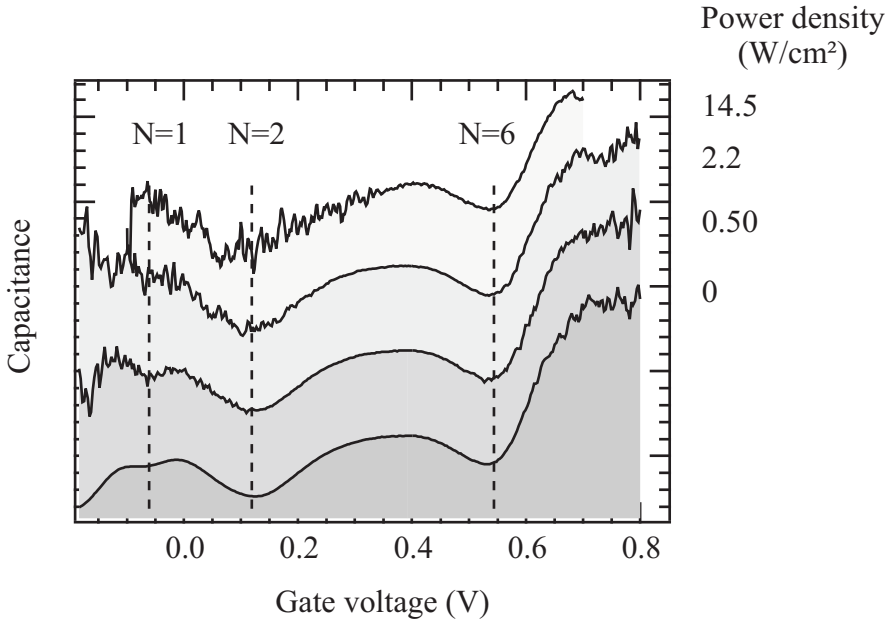

Figure 5.1: CV spectroscopy on InAs quantum dots without illumination (lowest curve) and under the same conditions as in the Raman experiments. The dashed lines mark the voltages where all quantum dots are charged with $N = 1, 2, 6$ electrons. On the right hand side, laser power densities are given.

the depolarized spectra. They interpreted the signal as a spin density excitation with a transition between the p and d level in the quantum dots. In the author's diploma thesis [Bro03b] we presented very similar measurements on samples with just one layer of nominally uncharged quantum dots. Interestingly, in our experiments the signal only appears in the polarized spectrum in contrast to the work by Chu *et al.*

This encouraged us to continue our experiments with quantum dots embedded in a *MIS* structure as described in Chapter 3.3. By applying a voltage between the front and the back gate we were able to charge the dots with one to six electrons. This has been demonstrated by capacitance measurements as shown in Fig. 5.1. The lowest spectrum shows a capacitance measurement without illumination. The first peak at -0.2 V marks the charging of the first electron into the s shell of the dots. The injection of the second electron takes slightly more energy because of the Coulomb blockade and can thus be found at a higher voltage (0.0 V). The four electrons of the p shell tunnel into the dots between 0.2 and 0.5 V. These peaks cannot be resolved individually because of the inhomogeneous broadening due to the size distribution of the dots. The last increase in capacitance is attributed to the charging

of the wetting layer. This assignment was made in analogy to [Mil97]. The other three spectra shown with an offset in Fig. 5.1 were taken while the sample was illuminated with the Ti:Sapphire laser at a typical wavelength and power densities that correspond to the illumination during our Raman experiments. While the signal is disturbed massively by the light in the region below 0.2 V and above 0.6 V the broad peak that is assigned to the charging of the p shell remains smooth and does not shift, contrary to what one might have expected. This shows that we can control the number of electrons in the dots between two and six even while the sample is illuminated. However, this behavior could not be observed in a sample where the backgate consisted of a highly doped GaAs layer. Here, even the smallest illumination lead to a heavily disturbed signal. The reason for this is not definitely clear yet but it is probably due to the creation of electron-hole pairs in the doped region. As a consequence, the above measurements as well as all other experiments in this section were performed on samples with an inverted *HEMT* as a back gate.

A typical Raman spectrum of an ensemble of quantum dots is shown in Fig. 5.2. The two curves show the polarized and depolarized spectrum of quantum dots charged with two electrons per dot at a laser energy of 1.679 eV. As in all subsequent Raman spectra, the energy axis indicates the Raman shift, i.e. the energy difference between the incident laser and the scattered light. All spectra are taken in the Stokes regime so that a higher Raman shift corresponds to lower absolute energies. In the displayed spectra, two sharp edges can be seen at 4 meV and 85 meV. These edges originate from the foremonochromator in the spectrometer and a slit for stray light reduction. Although the triple Raman spectrometer has a very strong reduction of stray light, the laser line is still clearly visible as a sharp peak at 0 meV in most of the spectra that are taken close to the laser energy. At 36.7 meV the bulk-like LO phonon of GaAs is visible in both spectra. With a 100 % polarization selectivity the phonon would not be present in the depolarized spectrum because of the Raman selection rules. Our selectivity is slightly less than 100 % so that the strong signals in the polarized spectrum also appear with less intensity in the depolarized spectrum. At twice the energy (73.4 meV) another peak is found that can be assigned to the creation of two LO phonons in the GaAs bulk material. The GaAs TO phonon at 33.9 meV in the polarized spectrum is a forbidden excitation that is only visible if the selection rules are indeed broken, e.g. by a momentum transfer to the sample or by a disturbance in the crystal. In our experiment such a disturbance is given by the quantum dots. Also, the sample is tilted to 70° so that the selection rules are broken. Between the two GaAs phonons there is another sharp line at 35.3 meV. Pusep *et al.* have shown that there are GaAs-

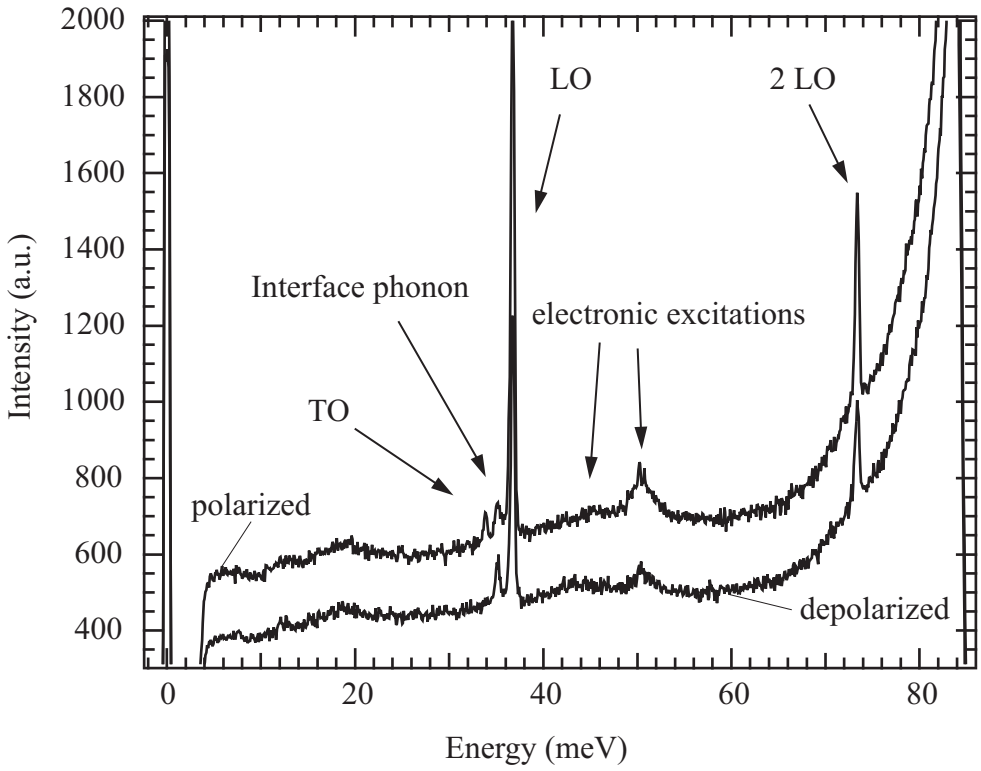

Figure 5.2: Polarized (upper curve) and depolarized (lower curve) Raman signal of sample with self-organized quantum dots. The energy axis indicates the energy of the excitation. At 0 meV a sharp peak can be seen that originates from elastic scattering of the laser light. The GaAs bulk *LO*, *2LO* and *TO* phonons can be seen as well as a small peak that is attributed to an interface phonon. Two broader peaks between 40 and 50 meV can be attributed to electronic excitations in the quantum dots. The polarized is displayed with a vertical offset for clarity.

like interface phonon modes in this energy range that can be detected via Raman spectroscopy and which arise from the interface between the dots and the GaAs material [Pus98]. It is nevertheless astounding that in our spectra this sharp peak is equally strong in polarized and depolarized configuration. As for the other phonons it should only be present in the polarized spectrum because the momentum quantum number would not be conserved otherwise. On the right hand side of the spectrum we see an increase in intensity before it drops suddenly because of the stray light reduction (the nearly vertical line near the right axis). This increase is due to the photoluminescence of the GaAs bulk material which is very strong, compared to the Raman intensities — the peak would appear at approximately 140 meV in our Raman

representation. A small signal at 20 meV is an experimental relict from the laser as can be easily shown by moving the sample out of the laser spot.

Finally, two peaks with widths of about 5 meV appear at about 42 and 45 meV. These can be attributed to electronic excitations as we will discuss on the following measurements. The main points of this discussion have been published in [Bro03a] and the basic measurements were also part of the author's diploma thesis [Bro03b]. In Fig. 5.3 we show Raman measurements on the same sample as in the previous measurement but for different gate voltages and thus different occupation of the electronic states. By comparison with the capacitance spectroscopy we can deduce the number of electrons in the dots at a given voltage. As in Fig. 5.2, there are two electronic excitations that we have labeled A and B. The band A is stronger for lower gate voltages (fewer electrons) and the band B is the stronger one for higher gate voltages (more electrons). Furthermore, band A shifts to lower energies and gets broader when electrons are loaded into the dot. Assuming that A is an excitation of an electron from the s shell into the p shell and that B is the excitation of an electron from the p shell to the d shell, we can infer a few properties of these excitations that we will then analyze in our experiments.

In a simple single-particle model the two excitations would have the same energy of about 45 meV regardless of the number of electrons and the electronic states involved because of the parabolic confinement. The energy can be estimated e.g. from photoluminescence experiments where the difference between the first and the second electron-hole transition is $\sim$60 meV [1]. However, the maximum of excitation B is at a slightly smaller energy than that of excitation A. This can be explained by the fact that our approximation of a fully parabolic confinement potential is not strictly correct. The edges of the potential flatten out due to the wetting layer so that the energy difference between the upper levels is smaller than 45 meV. This can also be seen in photoluminescence experiments at high excitation intensities where the difference between the s-s transition and the p-p transition is slightly larger than the difference between the p-p and the d-d transition. Comparing photoluminescence and Raman measurements (Fig. 5.4) it is striking that the peak widths of our Raman signal are much smaller than the peak widths of 30 meV in *PL* measurements. Both widths are due to the size distribution of the dots, but the Raman excitation is only dependent on the lateral confinement and therefore the energy width is affected only by the lateral size distribution of the dots. The reason for this is that the electrons are excited within the conduction band while in photoluminescence experiments the ob-

[1] The quantization energy of the holes in the quantum dots is estimated to be about 15 meV.

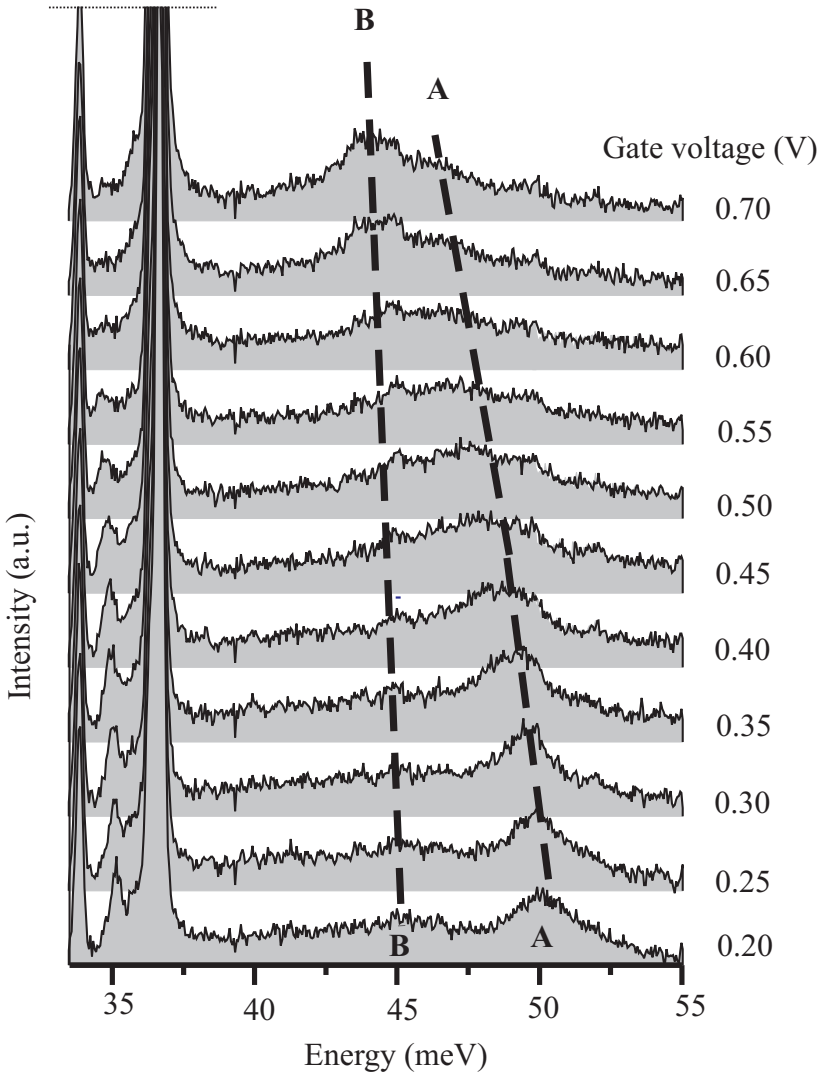

Figure 5.3: Polarized spectrum of InAs quantum dots for different gate voltages. The two bands designated as A and B are electronic excitations. The dashed lines are guides to the eye.

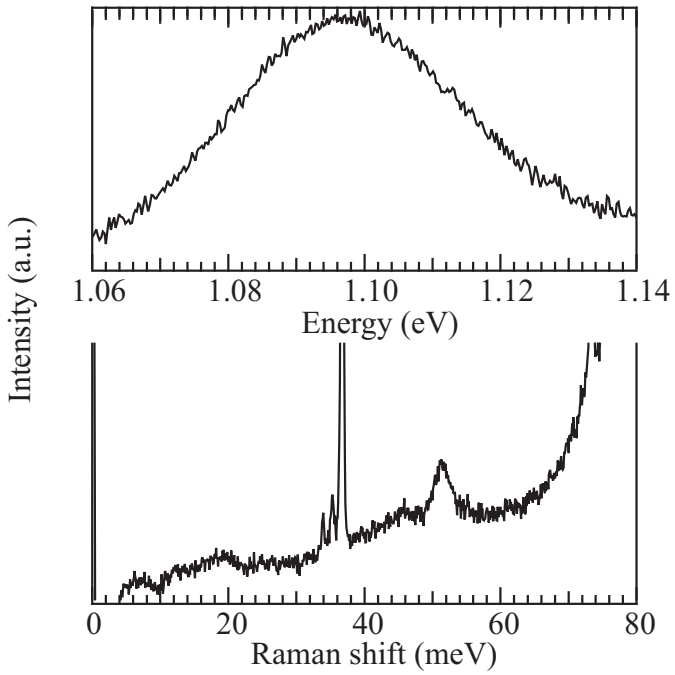

Figure 5.4: Comparison between a photoluminescence (upper part) and the Raman measurement (lower part). The peak width of the Raman signal is one order of magnitude smaller than that of the luminescence.

served transition is from the conduction band to the valence band states and thus also affected by the dot height. It turns out that a variation in the height of the dots has a much larger effect on the quantization energy than a lateral variation of the same amount because of the two-dimensionality of the dots. This phenomenon and similar small peak widths of electronic excitations in quantum dots have been observed previously in far infrared absorption experiments [Dre94].

Remaining for a moment in the single-particle picture, we can explain the intensity behavior of the two peaks A and B in Fig. 5.3 by looking at the capacitance measurement. We deduce that at 0.1 V the dots are loaded with two electrons and at 0.55 V with six electrons. In the Raman measurement we observe that the excitation A from the s to the p shell is heavily suppressed when there are no free states in the p shell, i.e. at 0.55 V and above. The excitation B from the p to the d shell on the other hand appears when the p shell is loaded with electrons and increases in intensity when more electrons are charged into the dot. This is consistent with our explanation. The broadening and red shift of excitation A on the other

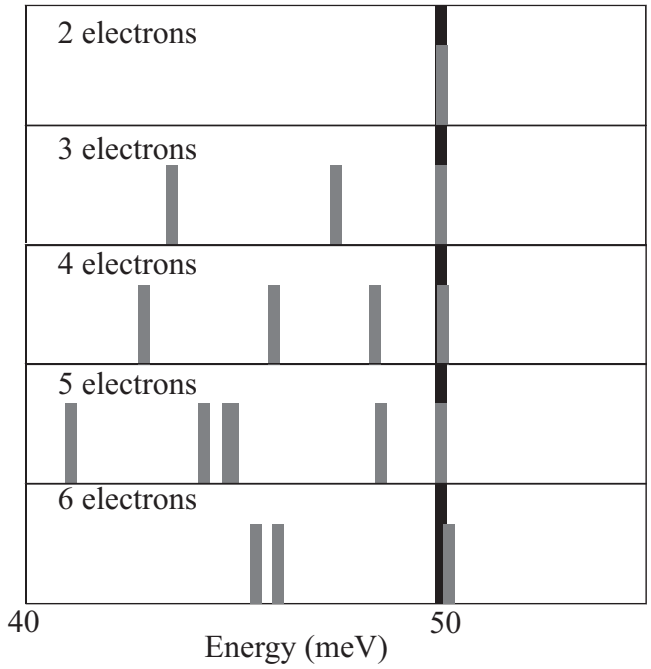

Figure 5.5: Theoretical calculations of the low-energy collective excitations of a two-dimensional parabolic quantum dot for different electron numbers in the dot. The Kohn mode at $\hbar\Omega_0$ =50 meV is shown in black.

hand, cannot be understood in the simple single-particle model. We would rather expect a blue shift of the excitation for more electrons in the p shell because of the Coulomb interaction. Evidently, we need to include the full many-particle interactions in our model to describe the possible excitations theoretically. This has been done by Bernhard Wunsch in the group of Prof. Daniela Pfannkuche, who calculated the possible excitations without spin flip, which are expected in the polarized spectra. The low-energy excitations of a quantum dot with electron number N were calculated by exact diagonalization for $N = 2, ..., 6$ with the bulk InAs value $m^* = 0.024m_0$ for the effective mass and $\epsilon = 15.5$ for the dielectric constant. The result of these calculations is shown in Fig. 5.5. At $\hbar\Omega_0 = 50$ meV there is always an excitation, regardless of the electron number. This is a direct consequence of the generalized Kohn's theorem [Mak90]. Below the Kohn mode we see several other lines appearing for $N = 3, .., 6$ that we account for the broadening and red shift of excitation A, assuming that the different lines cannot be resolved in our experiment. It can be argued that the good *quantitative* agreement that we get is due to the choice of parameters m^* and ϵ, but the

very good *qualitative* agreement is, of course, independent of this choice. For a better understanding of the microscopic origin of the low-energy excitations the different quantum mechanical contributions can be expanded in a series of Slater determinants. We have presented this in [Bro03a] for the situation of three electrons. Warburton *et al.* present in [War98] a perturbative approach to the calculation of the excitation energies that yields the same qualitative result of an excitation-energy reduction because of the reduction in Coulomb energy for higher shells. This can be attributed to the wider spatial distribution of the p shell in comparison to the s shell.

Considering the actual scattering processes involved in our experiment, we find that the two excitations A and B should become resonant at different energies. The first steps of the simple two-step processes for example, are the creation of an s-p (p-d) electron-hole pair for excitation A (B). Hence, we would expect the resonance energies of the two excitations to be approximately 60 meV apart. We were able to show in [Bro03b] that the two excitations do actually exhibit different resonance energies where that of excitation B (1.700 eV) is more than 40 meV larger than that of excitation A (< 1.660 eV). Unfortunately, it was technically impossible to go beyond or even onto the resonance of excitation A. As one would come to expect, the resonance curve of excitation B has the same width as the dot luminescence (30 meV) because it depends on the transition between a hole d state in the split off-band and an electron d state. This is another strong indication that our assignment of the two excitations is indeed correct.

5.2 The backgate wetting–layer system

5.2.1 Voltage-dependent Raman measurements

We have so far neglected the two-dimensional electron systems in our sample, namely the inverted *HEMT* functioning as a backgate in our sample and the InAs wetting layer beneath the dots, although they present a very interesting electronic system in themselves that can show a series of collective excitations. To find out more about this system and to be entirely sure that the previously observed excitations did actually originate in the dots and not in the *2DES*s, we examined another sample that was grown and prepared exactly as the quantum dot sample with the sole exception that there were no dots embedded, only the InAs wetting layer. Most of the experimental work on this sample was carried out by diploma student Arne Stührk in close collaboration with the author. We will start off along the same lines as for the dots, i.e. with a capacitance measurement. As expected, the mea-

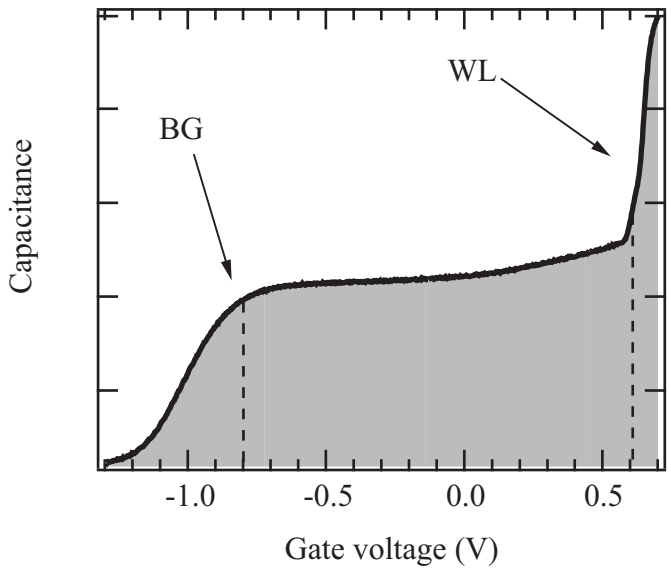

Figure 5.6: Capacitance measurement on the sample with only a wetting layer embedded in the *MIS* structure. *BG* and *WL* mark the onset of the backgate and wetting layer charging, respectively.

surement (Fig. 5.6) shows two steps: one at −0.8 mV where the backgate states start to get filled and one at 0.6 mV where the wetting layer is loaded. Between the two steps the differential capacitance is constant which means that the electronic density of states rises linearly with the gate voltage. We calculated the band structure of the system for different gate voltages with the method presented in Chapter 2.2. Beside the band structure, we also got the electronic ground state energies and wave functions, and the three-dimensional electron densities as a result. These are plotted in Fig. 5.7 for several gate voltages. In the simulation, the electron density in the backgate is 0 up to a voltage of −0.6 V. With further increase of the gate voltage, the electron density rises linearly up to 0.4 V, where the wetting layer starts to be charged and consequently the electron density of the backgate continues to rise linearly but with a considerably smaller slope. This agrees very well qualitatively with our capacitance measurement, although there is a small quantitative deviation in the voltages at which the charging of the *2DES*s sets in. The electron density of the doping layer does not vary noticeably.

There is a very small coupling between the ground states of the backgate and the wetting layer. The wave functions of the two ground states are shown in Fig. 5.8. It is obvious that the lowest state is strongly localized in the backgate while the second state is localized in the wetting layer, but

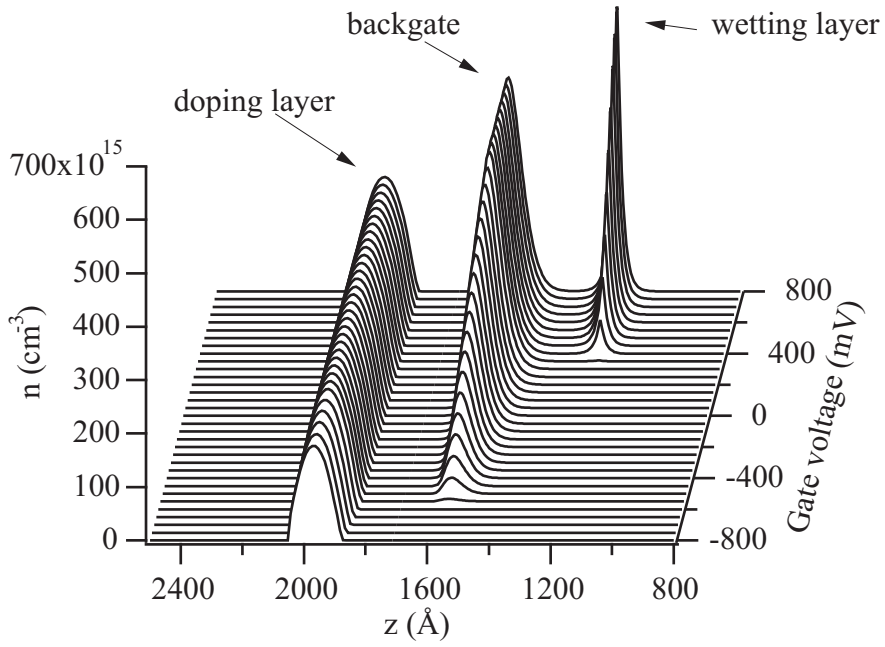

Figure 5.7: Calculated three-dimensional electron densities n plotted against the distance z to the sample surface for different gate voltages. The doping layer, backgate and InAs wetting layer are indicated.

there are small contributions in the respective other *2DES* for both states. However, because of the strong localization we will refer to them as the backgate ground state ψ_0^{BG} and the wetting layer ground state ψ_0^{WL}.

Raman measurements (not shown here) on this sample at the same laser energies as for the measurements presented in the previous chapter did not show any electronic excitations. This was, of course, expected, since the system should have different resonance energies as compared to the dot system. These were found to be in the region of 1.615 eV and below by means of several measurements at varying laser energies shown in Fig. 5.9. The measurements were taken in the polarized configuration with an angle of 25° between the surface normal and the incident laser light. The gate voltage was 0.7 V so that both the backgate and the wetting layer ground state were charged with electrons. Besides the GaAs LO and $2LO$ phonon lines at 36.8 and 73.6 meV as in the quantum dot measurements, we see six peaks that we attribute to electronic excitations in the backgate wetting–layer system. The denomination as shown in Fig. 5.9 may seem a bit arbitrary at this point, but we will provide the reasons for this classification in the course of this chapter. The assignment of the *CDE*s, *SDE*s and *SPE*s has been done according

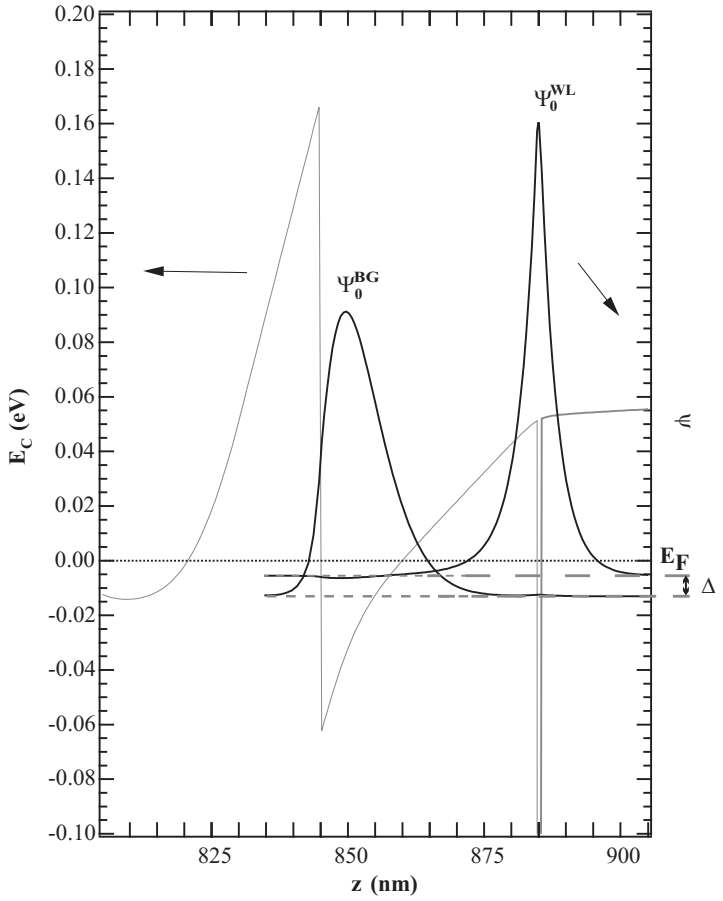

Figure 5.8: Electron wave functions for the backgate and the wetting layer ground state calculated by the 1D Poisson solver described in Chapter 2.2. The states are strongly localized with small contributions to the respective other system.

to the Raman selection rules — *CDE*s are visible in polarized spectra only, *SDE*s are visible in depolarized spectra, and *SPE*s in both. Due to the fact that our polarization selectivity in the spectrometer is not perfect, there is always a small contribution of the *CDE*s (*SDE*s) to the depolarized (polarized) spectra. The excitation marked *ISP* (intersubband plasmon) is attributed to a plasmon where the charges oscillate between the wetting layer ground state and the first excited state in the backgate. Looking at the peak widths of the excitations it stands out that the ${}^{BG}CDE_{01}^{-}$ and ${}^{BG}CDE_{01}^{+}$ are quite narrow. This is because there is a strong interaction between the charge-density excitations and the phonons in a polar crystal like GaAs. We will come back to this later. In Fig. 5.10 the peak intensities of the electronic excitations are

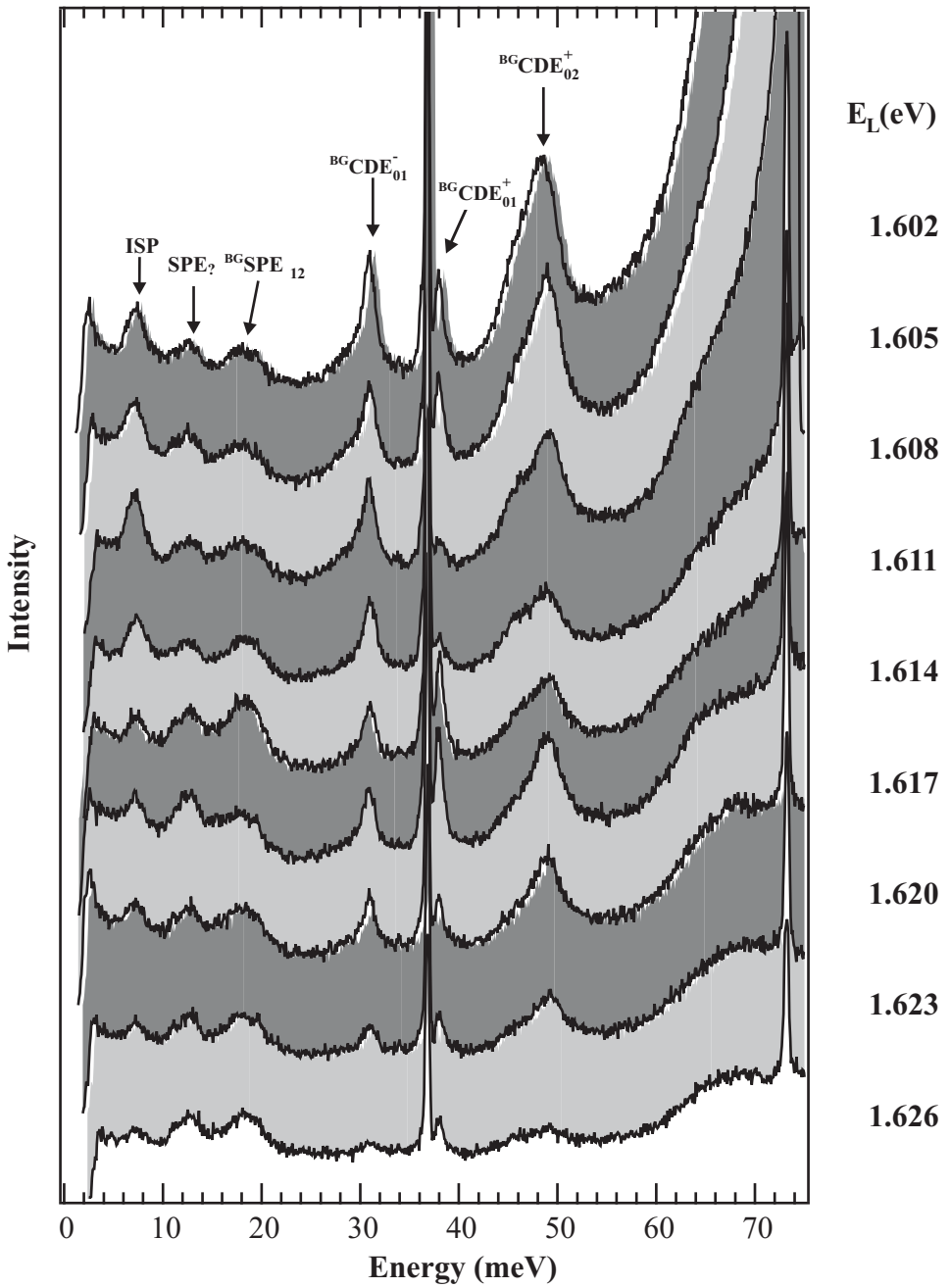

Figure 5.9: Raman resonance measurements on the sample without quantum dots at 0.7 V. The electronic excitations have been denominated forestalling the findings of this chapter.

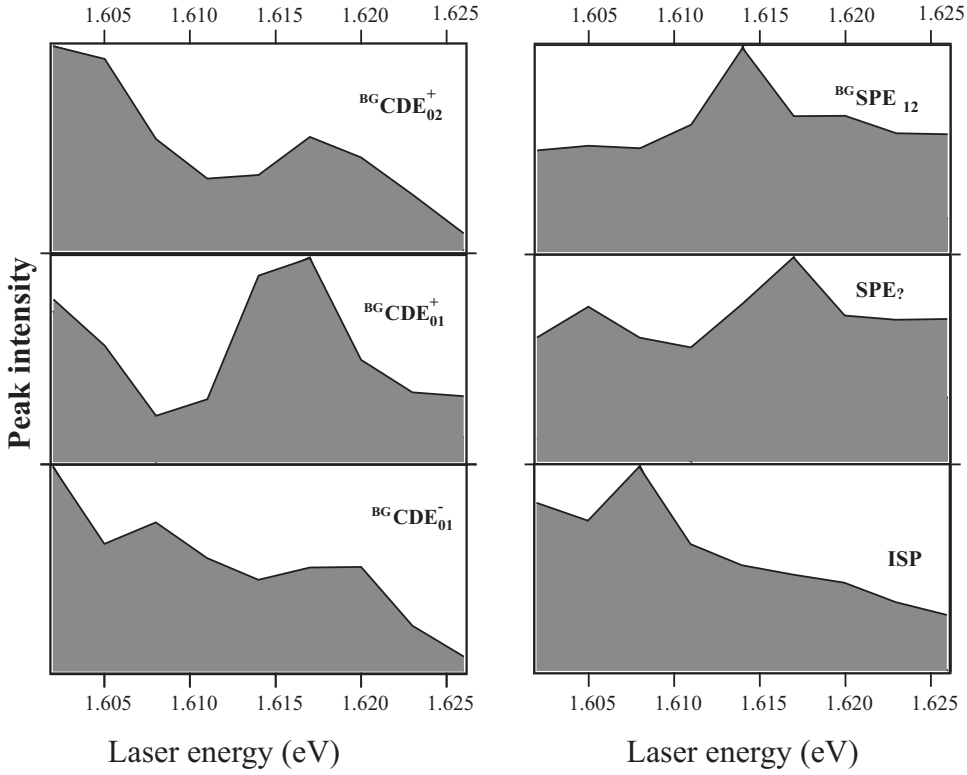

Figure 5.10: Resonant spectroscopy: Peak intensities of the electronic excitations shown in Fig. 5.9 as a function of the laser energy.

plotted against the laser energy. The ${}^{BG}CDE_{01}^{+}$ exhibits the most distinct resonance maximum at 1.615 eV, but for the majority of the excitations the maximum resonance seems to be beneath 1.602 meV. Unfortunately, as in the quantum dot measurement, it was not possible to measure at lower laser energies because of a strong luminescence. We can nevertheless establish that the resonance energies found in this experiment are significantly smaller than those measured in the quantum dot experiment. This leads to the conclusion that the transitions responsible for the resonances in this experiment cannot be within the wetting layer (alone), because the thin wetting layer has higher ground state energies for the electrons and holes than the quantum dots. This argumentation is only valid for the $E_0 + \Delta$ gap of the wetting layer and quantum dots, of course, the E_0 gap of the wetting layer being at 1.4 eV. The observed resonances are hence ascribed to E_0 gap transitions of the backgate.

By varying the gate voltage applied to the sample, we achieve in principle two effects: a change in the charge densities as shown in Fig. 5.7 and a change

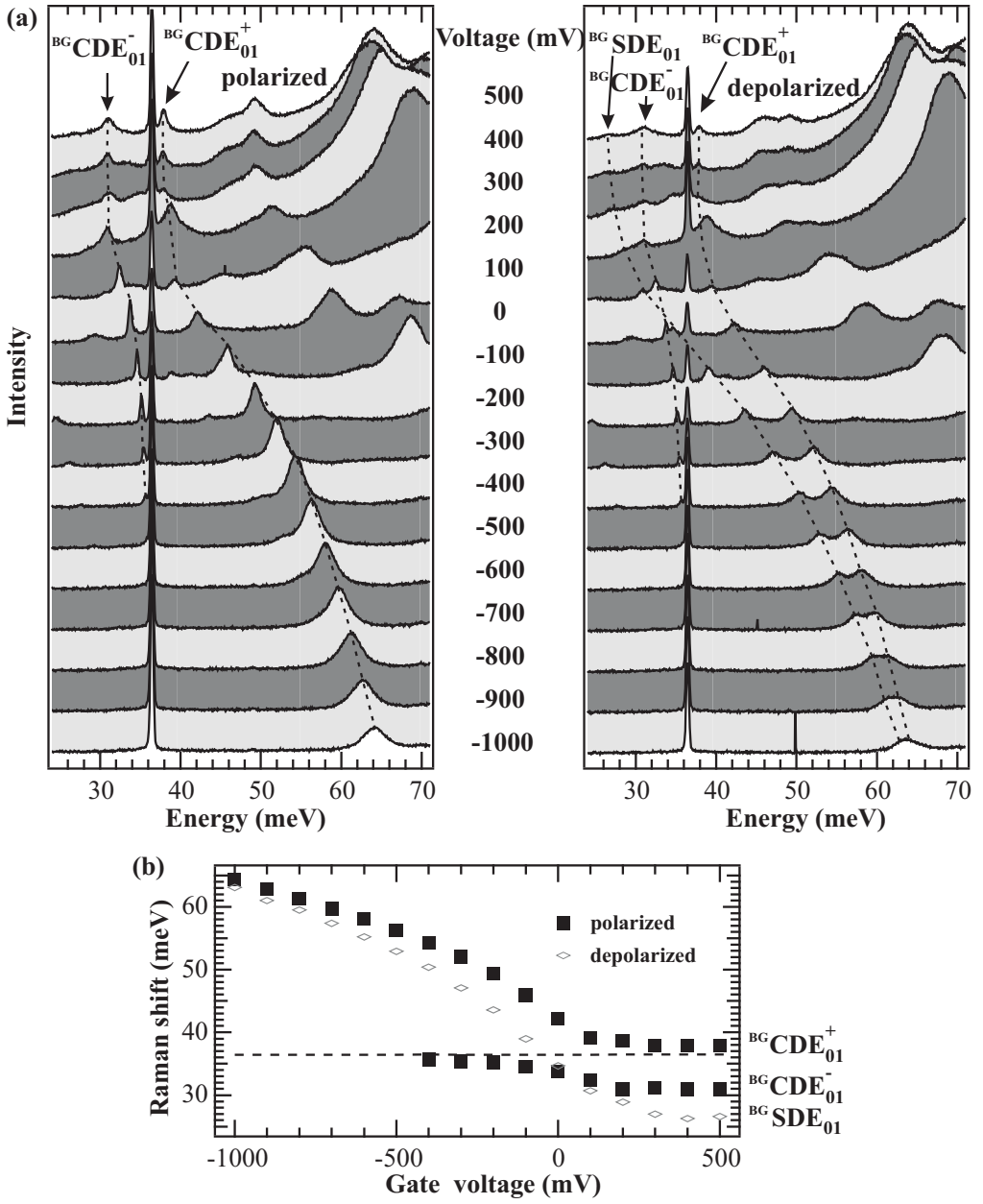

Figure 5.11: (a) Polarized and depolarized Raman measurements of the sample without quantum dots for different gate voltages at a laser energy of 1.617 eV. The dashed lines are guides to the eye. (b) Dispersion relation of ${}^{BG}CDE_{01}^{-}$, ${}^{BG}CDE_{01}^{+}$ and ${}^{BG}SDE_{01}$ energies against the gate voltage. The dashed line marks the position of the GaAs LO phonon.

in the band structure. The latter leads to a diminution of the difference between the backgate and the wetting layer ground state as the wetting layer is affected more strongly by a change in the gate voltage. It also leads to a flattening of the triangular backgate potential and hence to a decrease of the first excited backgate state with respect to the ground state. Therefore, we expect to get further insight into the nature of the observed excitations by measuring their dependency on the applied voltage. Fig. 5.11 (a) shows an excerpt of such a measurement for gate voltages between −1000 and 500 mV and Raman energies between 25 and 70 meV. The laser energy was 1.617 eV and the sample was slightly tilted (5°) in order to reduce stray light from the laser reflection. At the lowest voltages, only one electronic excitation, the ${}^{BG}CDE_{01}^{+}$, can be observed in the polarized spectra that shifts from 64 meV down to 37 meV with increasing gate voltage where it remains near the GaAs LO phonon line. At about −300 mV a second line appears in the spectra just below the GaAs LO phonon, the ${}^{BG}CDE_{01}^{-}$. This line also shifts to lower energies for higher gate voltages. The dispersion relation for these excitations is displayed in Fig. 5.11 (b). They exhibit a typical anti-crossing behavior. Because of the strong Fröhlich interaction between the excitation and the phonon, the *CDE* cannot cross the phonon energetically but rather splits into two excitations — one to higher and one to lower energies than the phonon[2] — that become *phonon-like* when they are in the vicinity of the phonon energy. If there was no interaction between the phonon and the *CDE* it would pass straight through the phonon — as does the ${}^{BG}SDE_{01}$, which can be observed in the depolarized spectra. It parts out of the ${}^{BG}CDE_{01}^{+}$ at about −800 mV, the difference between the two excitations increasing steadily. This can be explained by an increase in the exchange interaction when there are more electrons in the *2DES*. The ${}^{BG}SDE_{01}$ passes through the phonon energy between −100 and 0 mV and finally drops below the ${}^{BG}CDE_{01}^{-}$ at around 100 mV.

Seeing that with increasing gate voltage we reduce the energy differences between the subbands, we would expect all excitations to decrease steadily. Instead, we observe that for higher voltages than 300 mV the excitations remain at the same position. This behavior implies that either there is a leakage current between front and backgate or that the charging of the wetting layer sets in, screening the potential variation. The former could be ruled out by simply measuring the current flow between the gates, which did not increase abnormally before the usual breakthrough of the Schottky barrier at 700 mV. The latter contradicts our capacitance measurement where the wetting layer step was at 600 mV. We have to take into account that during

[2]Hence the denomination CDE^{+} and CDE^{-}.

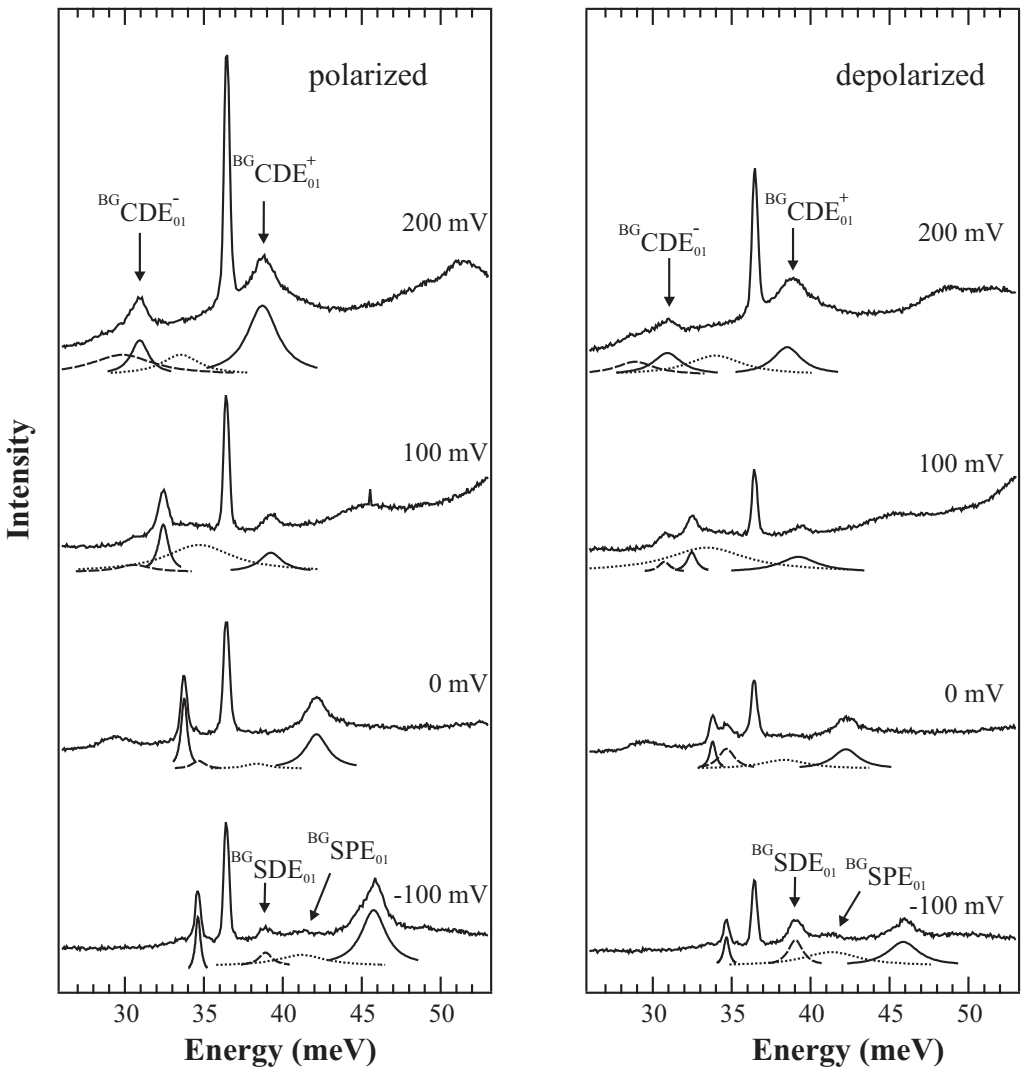

Figure 5.12: Excerpt of Fig. 5.11 (a). Below the measurements fits to the experimental peaks are shown: solid lines are for *CDE*s, dashed lines for the *SDE* and the dotted line for an *SPE*.

the capacitance measurement the sample was not illuminated, so we will assume here that the illumination of the sample leads to additional charges in the system and thus an earlier onset of the wetting layer occupation.

In Fig. 5.12 the measurements between -100 and 200 mV are displayed once more with the respective peak fits for the electronic excitations. These fits reveal that the broad $^{BG}SPE_{01}$ is also visible in the spectra but it often lies beneath some other excitation so that it is difficult to spot with the naked

eye. This representation also shows nicely the polarization dependence of the different excitations and the energetic position of the *SDE* and the *CDE* relative to the *SPE* so that by now the denotations of the ${}^{BG}SPE_{01}$, ${}^{BG}SDE_{01}$, ${}^{BG}CDE^{+}_{01}$ and ${}^{BG}CDE^{-}_{01}$ are well established. The ${}^{BG}SDE_{02}$, ${}^{BG}CDE^{+}_{02}$ denoted in Fig. 5.9 show a very similar behavior and can be assigned in much the same way despite the fact that the corresponding *SPE* cannot be observed.

We want to focus now on the two single-particle excitations that have been denoted in Fig. 5.9 as $SPE_?$ and ${}^{BG}SPE_{12}$. Their behavior for different gate voltages is shown in Fig. 5.13 (a) and (b). The two peaks are equally strong in both polarizations, which is why we labeled them as *SPE*s. The unidentified $SPE_?$ only appears for a small voltage range between −400 and 100 mV but else is not visible in this measurement. Likewise, the intensity of the ${}^{BG}SPE_{12}$ diminishes for higher voltages and could not be fitted above 400 mV. This is not due to the laser energy, because both excitations are in fact strongest around 1.617 eV as can be deduced from Fig. 5.9, where they were well visible at a gate voltage of 700 mV. This can only be explained by a less good adjustment of the optics in this measurement compared with the resonance measurement. The reason for assigning the ${}^{BG}SPE_{12}$ to a transition between the first and second excited states of the backgate is that its energy equals the difference between the ${}^{BG}CDE^{+}_{02}$ and the ${}^{BG}CDE^{-}_{01}$ (i.e. 19 meV) at the same voltages. Since the difference between the subbands does not change significantly for higher voltages, we would expect the ${}^{BG}SPE_{12}$ to be at approximately the same position. This fits well with our resonance measurement, which was taken at 700 mV and shows the excitation at 18 meV. A priori, we expected the first subband of the backgate to be empty so that this excitation should not be visible. It is conceivable, however, that it is populated thermally with electrons that have been excited by the laser light. The provenience of the $SPE_?$ cannot be solved with these measurements. It cannot be excluded that this is the ${}^{BG}SPE_{23}$, which might be expected in this energy range, but further proof is missing.

Finally, in Fig. 5.9 we observed an excitation labeled *ISP* which was only visible at voltages above 700 mV. To examine this excitation in more detail we executed another measurement where we changed the gate voltage in 10 mV steps, shown in Fig. 5.14 (a). The sample was tilted to an angle of 25° with respect to the laser beam which was set to 1.608 eV, because there the *ISP* was strongest in the resonance measurement (see Fig. 5.10). There is another *CDE* appearing at 1.2 meV. Fig. 5.14 (b) shows the peak positions of the two excitations plotted against the gate voltage.

In contrast to the excitations discussed previously, the *ISP* moves to higher energies with increasing gate voltage. The straight-forward explanation for this behavior would be a transition between two subbands whose

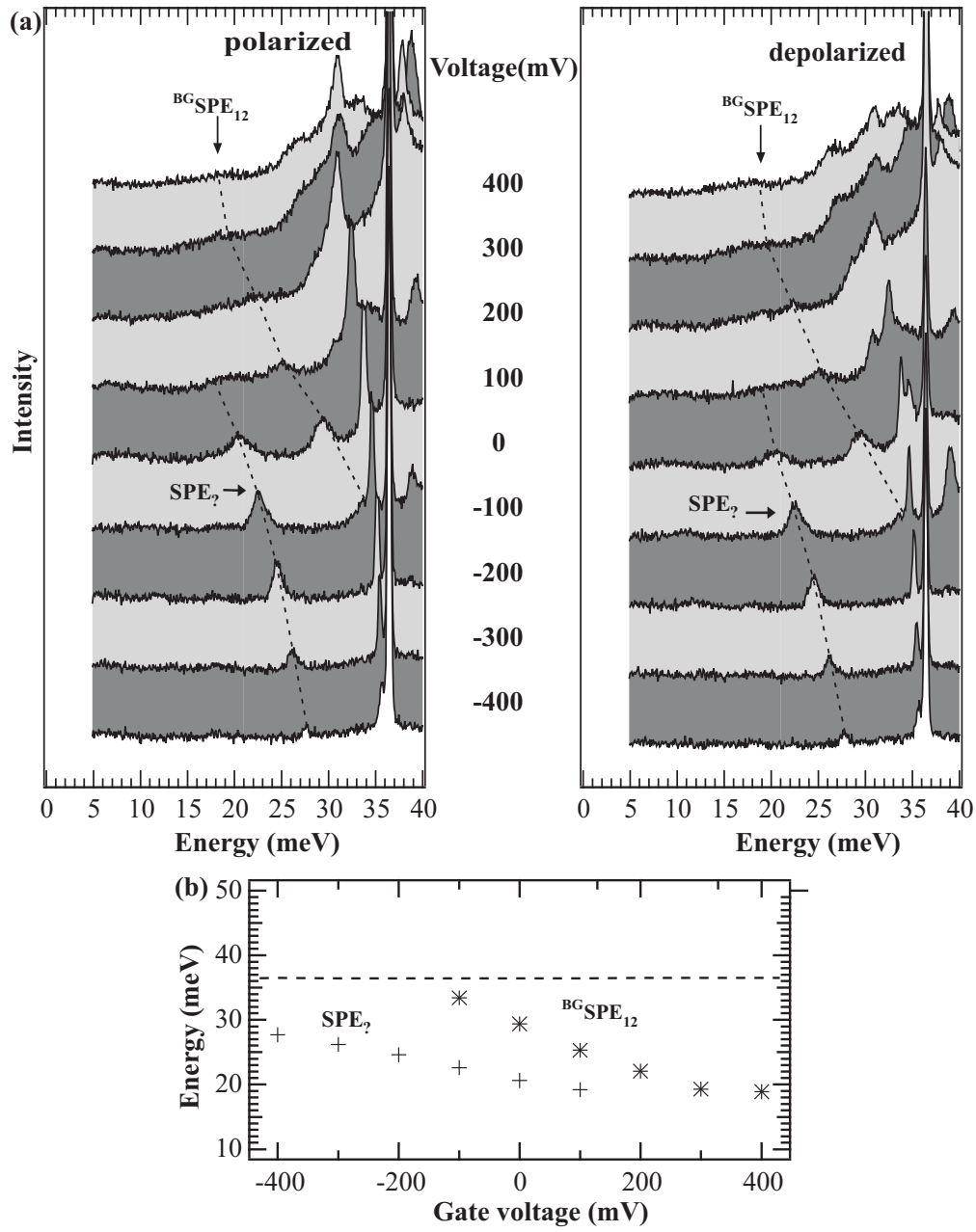

Figure 5.13: (a) Raman measurements on a sample without dots for different gate voltages at a laser energy of 1.617 eV. Two single-particle excitations can be traced. The dashed lines are guides to the eye. (b) Peak positions of the $^{BG}SPE_{12}$ and the unidentified $SPE_?$ represented against the gate voltage.

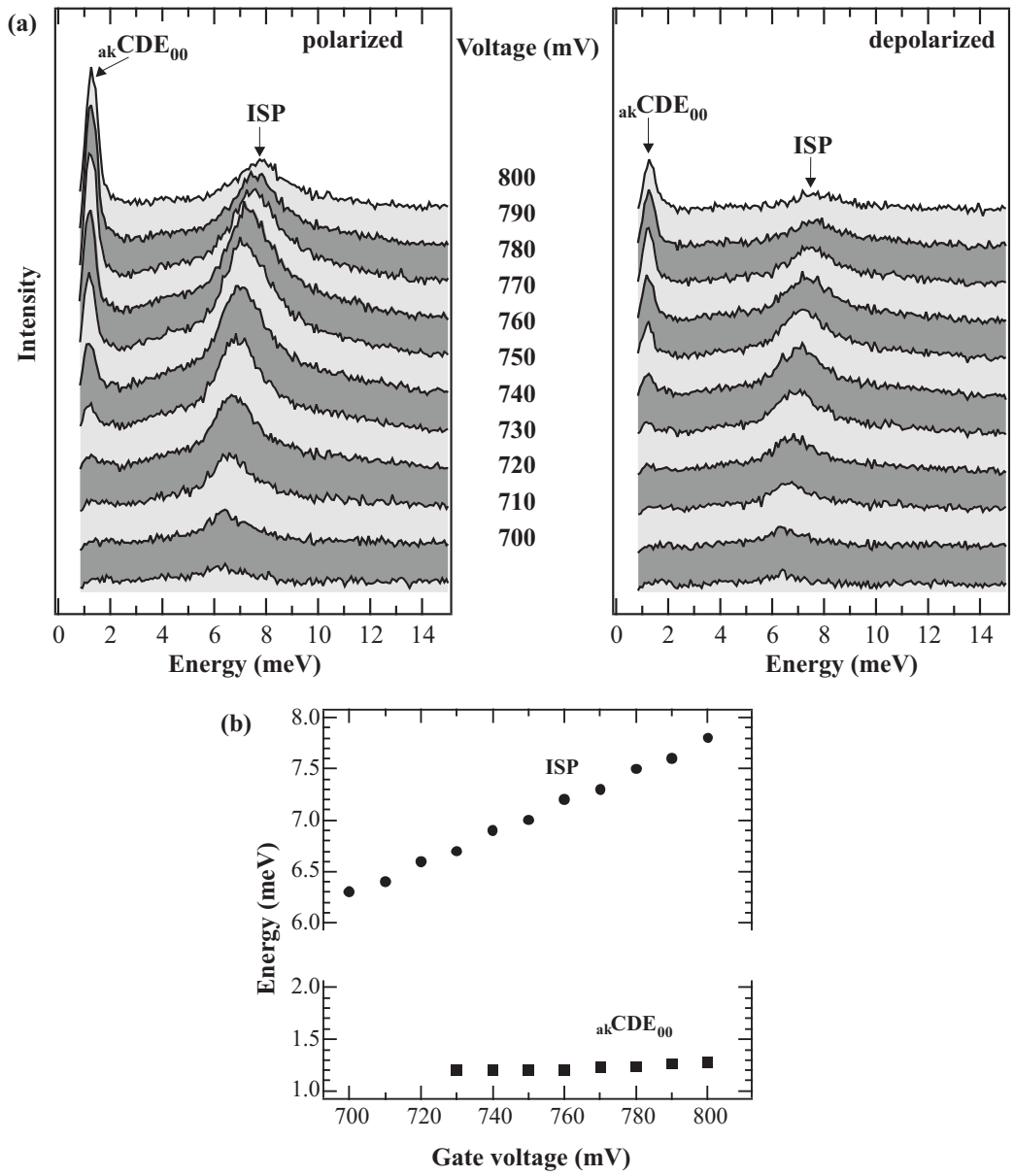

Figure 5.14: (a) Low energy part of the Raman spectra on the sample without quantum dots for gate voltages between 700 and 800 mV at a laser energy of 1.608 eV. (b) Fitted positions of the *ISP* and the $_{ak}CDE_{00}$ against gate voltage.

energy difference grows for increasing voltages. The wetting layer ground state and the first excited state of the backgate present such a system, because the wetting layer states are affected much stronger by the gate voltage than the backgate states. Another argument for this explanation is that in all measurements the *ISP* did not appear until the wetting layer was charged with electrons according to the capacitance measurement. We are aware that this presents an unresolved contradiction: in the previous paragraphs we assumed that the wetting layer would be charged earlier in the Raman experiments, because the backgate excitations almost remain at the same energies for gate voltages higher than 300 mV. Presumably, the *ISP* is just too small to be detected for the lower subband occupations. The further *CDE* is identified as an acoustical plasmon that appears in our measurements because we have an asymmetrical coupled system (backgate–wetting layer) [Ste97]. It does not change significantly with the gate voltage on this scale.

5.2.2 Comparison with simulations

In the previous subsection we already showed some results that we obtained with the 1D Poisson solver by G. Snider, notably the electron densities in the sample and the electron wave functions of the ground states. While we could not extract electron wave functions for the higher states, we did get their energies from the simulation. The results for the energy levels involved in the observed excitations are shown in Fig. 5.15 (a). The energy scale goes from -20 to 220 meV where 0 meV corresponds to the Fermi energy E_F. The figure shows nicely how the wetting layer is affected much stronger by the gate voltage than the backgate states. It is also apparent that there is a sharp bend in the energy curves whenever one of the levels drops under the Fermi energy. Furthermore, the higher the energy level in the backgate, the more these are affected by the gate voltage. We suppose that this effect can be explained by the flattening of the triangular backgate potential which leads to a larger spatial distribution of the higher states.

Next, in Fig. 5.15 (b) we have displayed the energy *differences* between some of the calculated energy levels. These differences represent the energies of the single-particle excitations between two states. As expected, the excitations within the backgate all decrease in energy for higher gate voltages, but nearly stop at 350 mV, when the wetting layer is charged. The excitations between the two ground states (SPE_{00}^{BG-WL}), also shown in Fig. 5.15 (b), drops much faster than the other *SPE*s and still changes significantly for higher voltages, even if not as much as before.

The comparison between the simulation and the measurement yields a

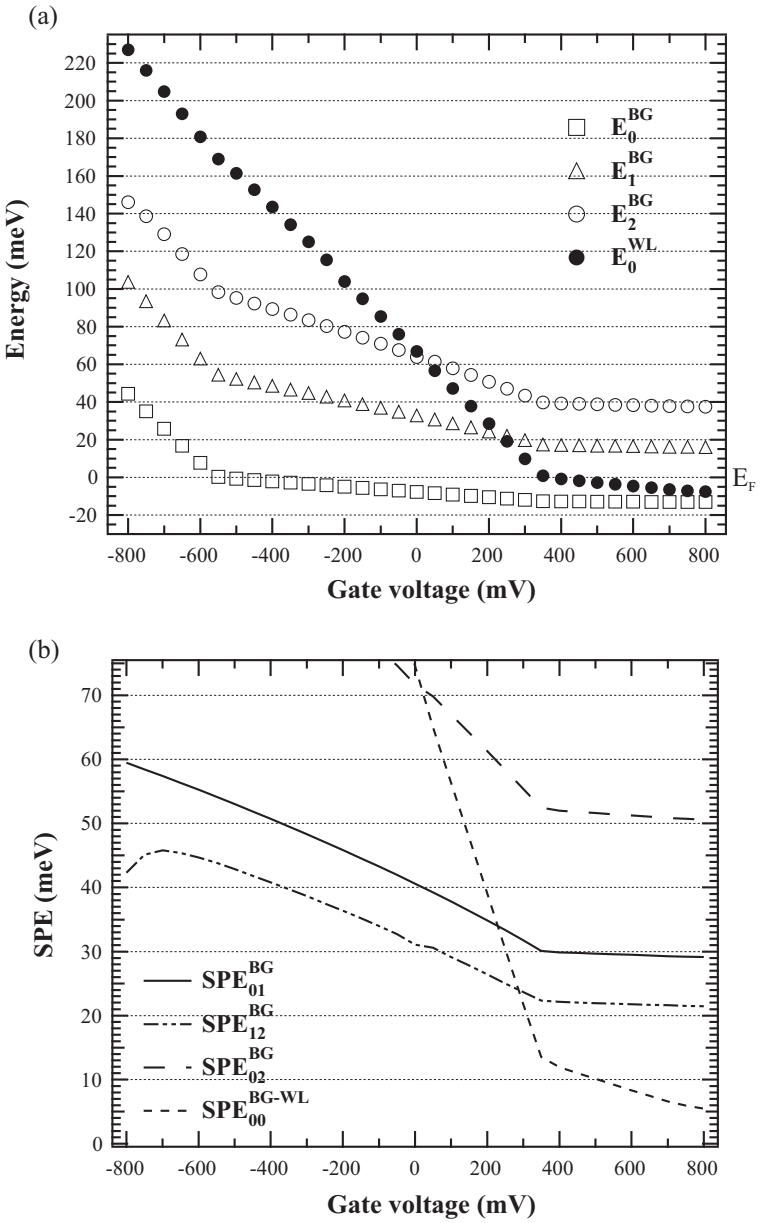

Figure 5.15: (a) Calculated energies of the first three backgate levels and the wetting layer ground state. The black circles represent the ground state energy of the wetting layer and the empty symbols the energy levels of the backgate. (b) The resulting *SPE*s corresponding to the observed peaks in our Raman measurement for different gate voltages.

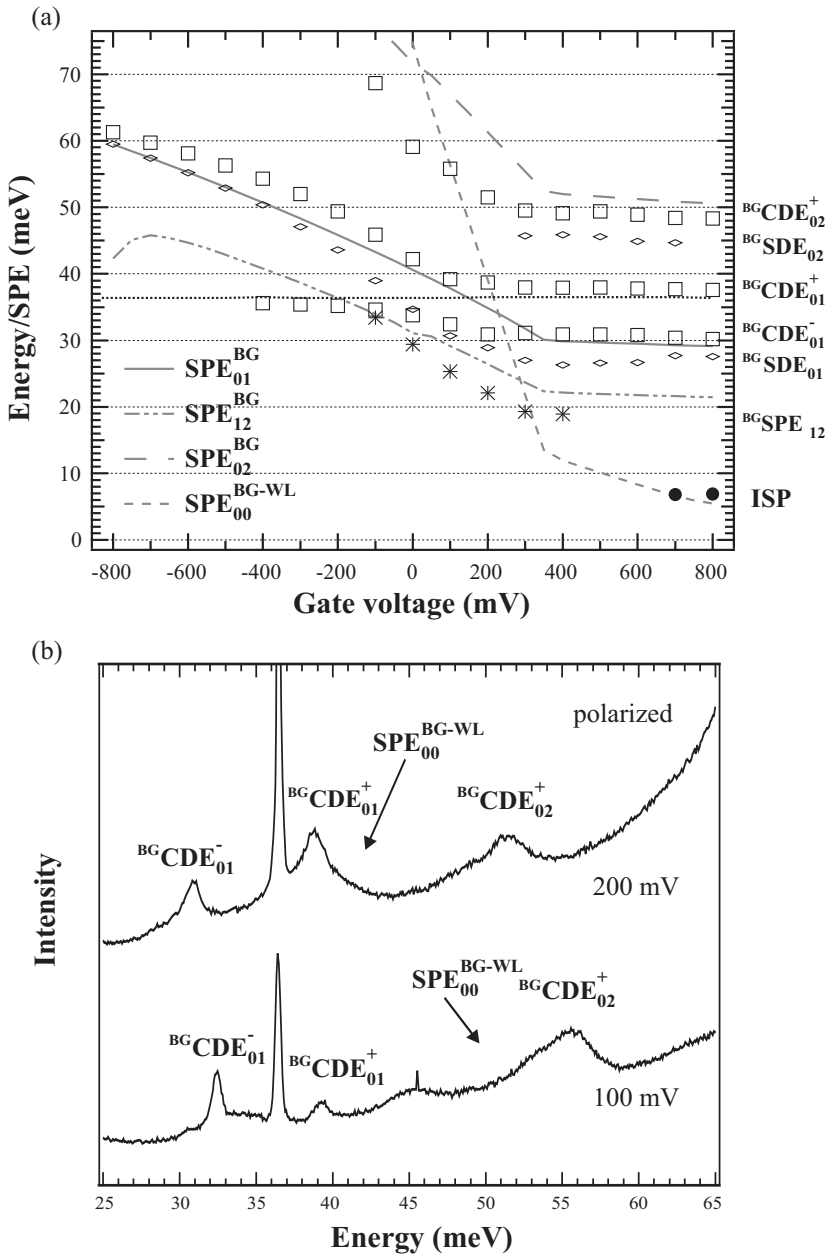

Figure 5.16: (a) Comparison between calculated *SPE* energies(curves) and measured Raman shifts (symbols). (b) Excerpt from Fig. 5.12; the arrows indicate possible positions of the SPE_{00}^{BG-WL}.

good agreement (see Fig. 5.16 (a)). We plotted the calculated *SPE*s from Fig. 5.15 (b) together with the positions of the *CDE*s, *SDE*s and *SPE*s from the experiments. The agreement is especially good for the excitation between the first and second state of the backgate. The calculated SPE_{01}^{BG} lies between the ${}^{BG}SDE_{01}$ and the ${}^{BG}CDE_{01}^{+}$ for all voltages and shifts between the ${}^{BG}SDE_{01}$ and the ${}^{BG}CDE_{01}^{-}$ for voltages higher than 400 mV. This corresponds very well to the behavior as described earlier and which was also confirmed for some voltages in Fig. 5.12, namely that *CDE*s (*SDE*s) are shifted to higher (lower) energies than the corresponding *SPE*. The calculated SPE_{02}^{BG} is a little too high in energy, indicating a slightly smaller energy difference between the second and third backgate level in the real system. This is confirmed by the fact that the simulated SPE_{12}^{BG} also is slightly higher than the measured ${}^{BG}SPE_{12}$. The qualitative agreement, however, is very good if we consider that we did not put much effort into determining the real doping concentrations in the system. It is also rather surprising that our simulation fits so well considering that our capacitance measurement showed a significantly higher voltage for the charging of the wetting layer.

So far we had not been able to account for the SPE_{00}^{BG-WL} in our measurements, but the simulations now yield indications where to look for it. The most prominent features that may be related to this excitation can be found in the measurements at 100 and 200 mV in Fig. 5.11 (a), of which the polarized measurements are shown in Fig. 5.16 (b). In the measurement at 100 mV we can see what seems to be a *SPE* at 45 meV. In the measurement at 200 mV there is a *SPE* at the same energy as the ${}^{BG}CDE_{01}^{+}$ (39 meV), thus making it appear very strong in the polarized spectrum and giving an unusually strong contribution to the depolarized spectrum for a *CDE*. It is also apparent that the ${}^{BG}CDE_{01}^{+}$ has a wide «foot» which it does not have in the other measurements. Looking at our simulations we notice that the SPE_{00}^{BG-WL} is at exactly 39 meV for 200 mV and at 55 meV for 100 mV. These calculated positions are indicated by the arrows in Fig. 5.16 (b), showing that the calculated position of the SPE_{00}^{BG-WL} is in fact underneath the ${}^{BG}CDE_{02}^{+}$ and the ${}^{BG}SDE_{01}$. So either the *SPE* is hidden in the measurement at 100 mV or it does not shift as much as the simulation predicts and is hence detected at 45 meV. In order to clarify this, a measurement with smaller voltage steps would be necessary in the region between 100 and 200 mV.

We have included the *ISP* in Fig. 5.16 (a) for completeness. Its position is not far away from the simulated SPE_{00}^{BG-WL}. However, we had established previously that the *ISP* experiences a red-shift with increasing voltage, contrary to the calculated *SPE*. The difference can not be explained by the involved many-particle interactions (Eq. 2.6) either as these also predict a

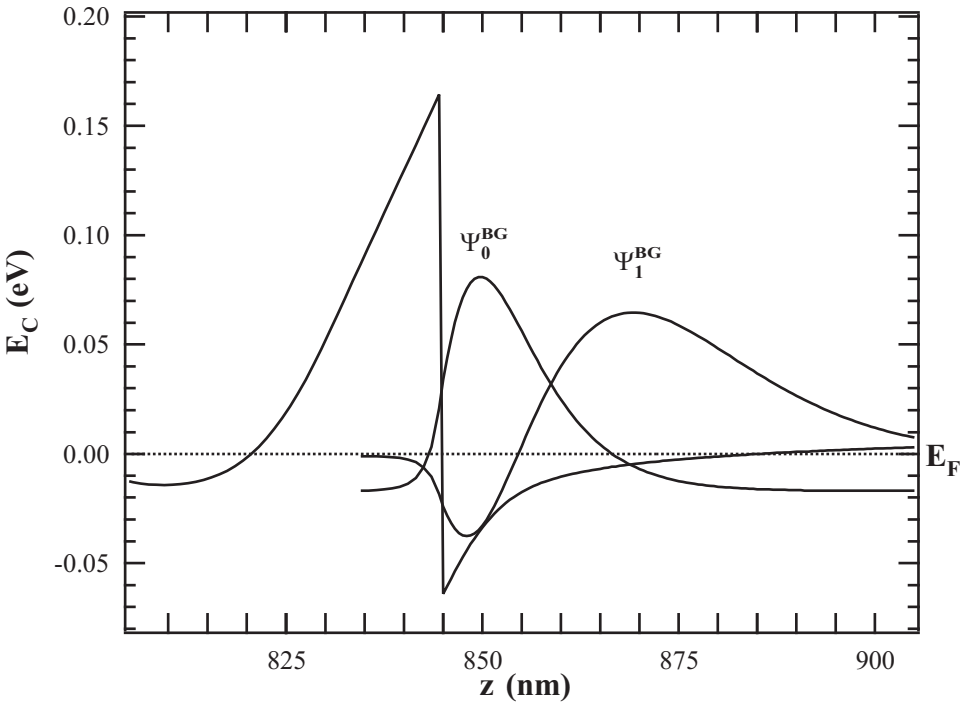

Figure 5.17: Conduction band for the backgate, simulated with the 1D Poisson solver by G. Snider. The parameters given for the calculation were the same as before, but without the wetting layer in order to obtain the wave function of the second electronic state in the backgate.

decrease in energy as the difference between the electron densities decreases. Hence, we hold on to our explanation of the *ISP* as an excitation between the wetting layer ground state and the first excited state of the backgate.

Unfortunately, in our simulation we could not calculate the electron wave function of the second backgate state in our system because the charging of that state would have occurred at unrealistically high voltages. To get an idea of the spatial distribution of electrons in that state nevertheless we calculated the first two backgate states in a system exactly as before but without the wetting layer. The result is represented in Fig. 5.17. The wave function of the ground state does, of course, look very similar to the one presented in Fig. 5.8. The second state has a higher electron density in the direction of the surface and thus toward the wetting layer, if it had been implemented. To make a definite statement about the wave function of the second backgate level, there is evidently no way around a calculation *with* the wetting layer. What we want to show here, however, is that the higher states in the backgate can have electron wave functions that lap into the region of

the wetting layer. It is our considered opinion that these states are likely to exhibit a stronger coupling to the *2DES* in the wetting layer. We therefore believe that an excitation from the wetting layer ground state to the second backgate state is more probable than a transition from the backgate to the wetting layer ground state even if the calculated energies in our simulations do not support this belief.

5.2.3 q-vector dependent Raman measurements

Eventually, we want to examine the dependence of the observed excitations on the q-vector transferred to the system. In order to do so, we did a series of measurements for angles between 10° ($q = 0.248 \cdot 10^7$ m^{-1}) and 80° ($q = 1.608 \cdot 10^7$ m^{-1}) where the angle was changed in 5° steps. We applied a gate voltage of 800 mV and adjusted the laser to an energy of 1.608 eV so that all excitations would be visible in the spectra. The dispersions for the intersubband excitations are shown in Fig. 5.18. The two excitations that show the most conspicuous dispersion are the ${}_{ak}CDE_{00}$ and the ${}^{BG}CDE^{-}_{01}$. The former is linear in the region where the excitation could be observed which is what we would expect from an acoustical plasmon whereas optical plasmons would have a dispersion that goes with the square root of the q-vector. The rather small energies at high q-vectors that we measure for this excitation (around 2.2 meV) are also an indication for an acoustical rather than an optical plasmon. The increase in energy of the ${}^{BG}CDE^{-}_{01}$ with higher q-vectors is what we expect for such an excitation (see Fig. 2.2). Attempts to quantitatively calculate the q-vector dispersions of these plasmons did not yield any good agreement with the measured values [Stü05]. We believe that this is due to the fact that the calculations fail to incorporate the rather unusual characteristics of our system, e.g. the different materials and widths of the two coupled systems.

5.2.4 Summary and comparison to the quantum dot system

We were able to observe charge density, spin density and single particle excitations in the system that consisted of an inverted *HEMT* as a backgate and the InAs wetting layer. We were able to identify and explain these excitations with only few exceptions by measuring their intensities and energy dispersions as a function of the laser energy, the applied gate voltage and the q-vector. At first glance, there are some similarities between the Raman measurements on the quantum dot system and the system without the quantum dots. These are mainly the energetic positions of some of the excitations

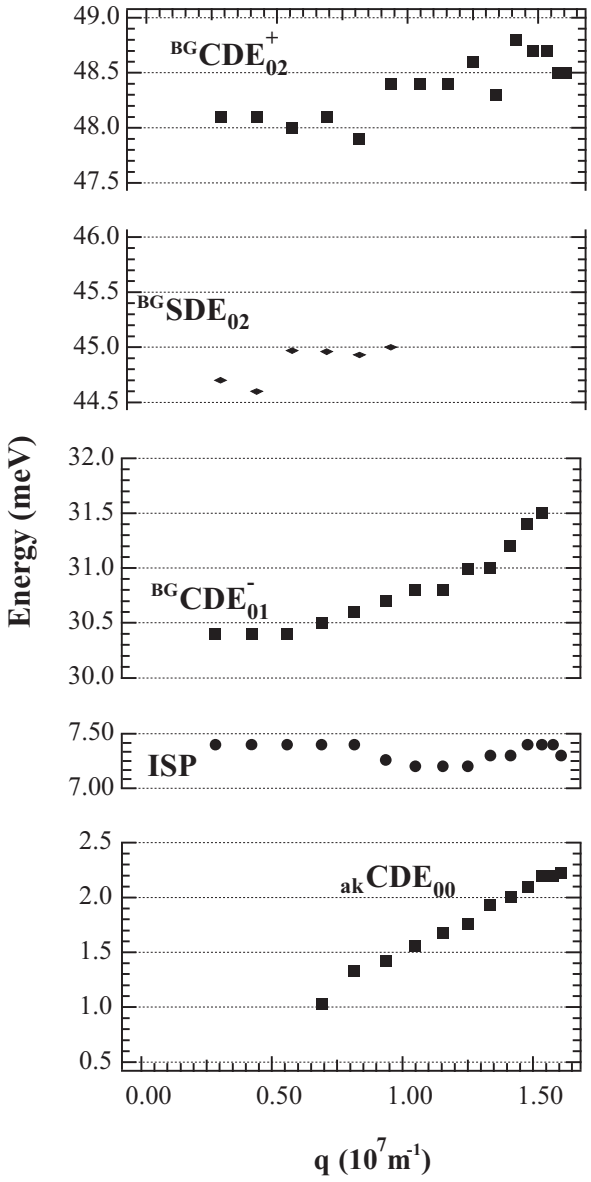

Figure 5.18: Dispersions of the intersubband excitations in the sample with a backgate and wetting layer at a laser energy of 1.608 eV and a gate voltage of 800 mV.

and, quite generally, the decrease in energy of the excitations with higher gate voltages. However, by our extensive analysis, we are able to distinguish between excitations in the quantum dot system and in the backgate–wetting layer system.

Firstly, the resonance energies found in the two systems are different. In the quantum dot system we have found one excitation to be resonant at 1.69 eV and the other is expected to be at 1.64 eV, although this could not be measured. However, the backgate–wetting layer system does not show any excitations when the laser is tuned to these energies, but the observed excitations in this system have considerably lower resonance energies of 1.617 eV and below.

Secondly, the energy dispersion for the applied gate voltage is quite different for the two systems, despite the qualitative similarities. In the quantum dot system, it is mainly one excitation that exhibits a red shift in the small voltage interval that is assigned to the charging of the p shell. In the backgate–wetting layer system we observe the strongest shifts of the excitations for the comparably large band of voltages where the wetting layer is not yet charged. Besides, the excitations in the second system are manifold and subject to strong changes in energy with varying gate voltage so that it is not that surprising to find excitations at the same energies as in the quantum dot samples in some measurements.

Finally, the backgate–wetting layer system clearly shows *SDE*s that were not present in the quantum dot sample and some excitations have a noticeable q-vector dispersion that is neither expected nor found for the excitations in the quantum dot spectra. We are therefore very confident that the excitations discussed in Chapter 5.1 originate from electrons excited within the quantum dots.

5.3 Measurements on self-assembled InAs double quantum dots

In our previous work we have performed measurements on double quantum dots that were fabricated by holographic lithography and deep-mesa etching on a double quantum well [Bro03b]. These quantum dots were fairly large (200 nm in diameter) and we assumed them to contain about 100 electrons each. In order to gain more control over the system we wished for a sample with fewer electrons per dot that would also be charge tunable, just like the InAs single quantum dot system we had used. As we have already mentioned in Chapter 3.2.2 it is (in principle) possible to produce ensembles of self-

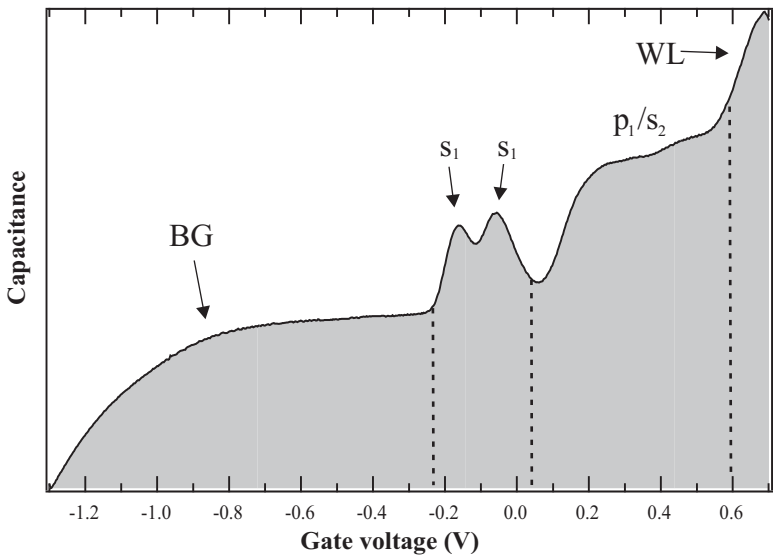

Figure 5.19: Capacitance measurement on a sample with two layers of *SAQD*s. The two instances of s_1 mark the charging of the s shell of the first dot layer, the second broader band is believed to contain the charging of the p shell of the first layer as well as the s shell of the second quantum dot layer or the antisymmetric states respectively. The charging of the backgate (*BG*) and wetting layer (*WL*) are also marked.

assembled InAs double quantum dots. Such a sample with two layers of quantum dots was grown in the group of Prof. W. Hansen. The thickness of the GaAs layer between the two quantum dot layers was 7 nm in order to obtain a level splitting between the symmetric and antisymmetric states of the order of 15 meV or smaller (we used the results of [Hin01] as a reference) so that we could well observe transitions between the symmetric and the antisymmetric state and distinguish them from the excitations within one of the dots.

As a first characterization we performed a *C*-*V* measurement on the sample, shown in Fig. 5.19. As for the other samples, the charging of the inverted *HEMT* (backgate) and the wetting layer appear as steps around -1 and 0.6 V respectively. The first two states in the s shell of the double quantum dots are neatly separated and at nearly the same position as in the sample with one layer of quantum dots (-0.16 and -0.06 V). At 0.2 V a broad almost step-like maximum sets in before the wetting layer gets charged, that contains another smaller structure at 0.5 V. We assign this broad maximum to

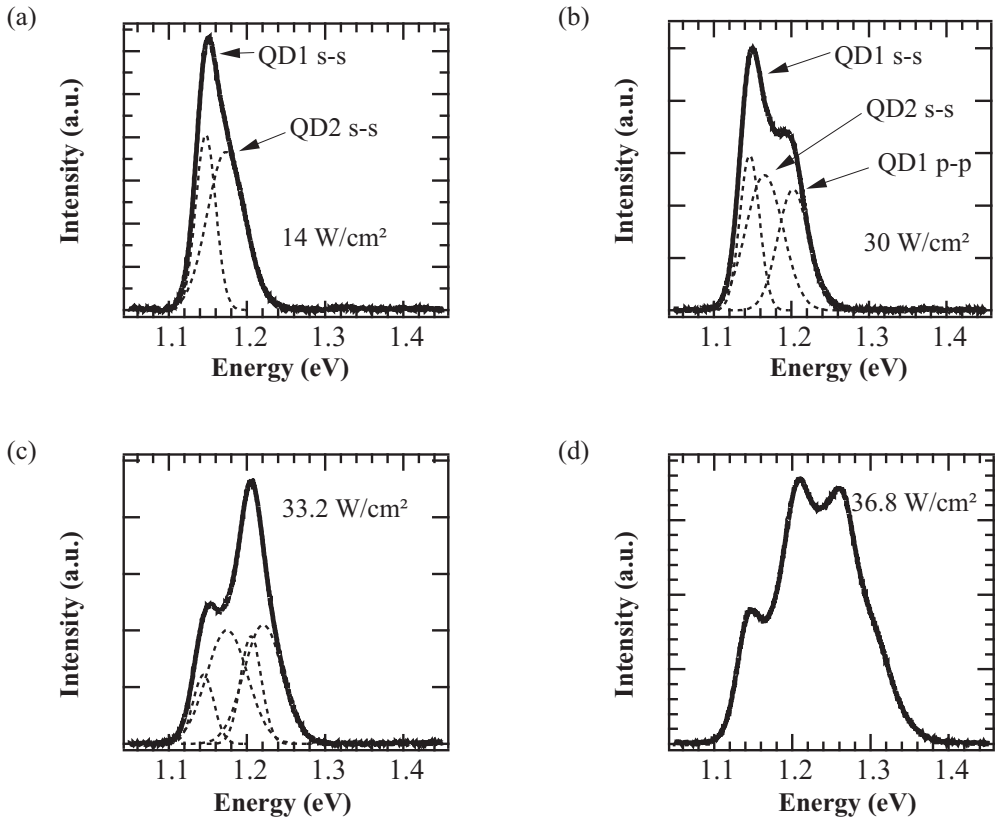

Figure 5.20: Photoluminescence measurements on a sample with two layers of *SAQD*s separated by a 7 nm GaAs layer at different power densities and a gate voltage of 0 V. For measurements (a), (b) and (c) the dashed lines represent Gauss fits of the peaks. The peak fits in (c) are merely shown for demonstrational purposes, they are not necessarily the physically correct ones.

the charging of electrons into the p-state and the second s shell[3]. The order in which these are charged cannot be determined from the spectrum since no individual peaks can be resolved.

For further characterization we measured the photoluminescence signal of the sample with an Ar^+ laser emitting at 514 nm for different laser intensities and gate voltages. Four measurements for laser intensities of 35, 75, 83 and 92 mW (corresponding to power densities of approximately 14, 30, 33.2 and 36.8 W/cm^2) are shown in Fig. 5.20. All measurements shown

[3]We cannot yet say for sure if the two layers are actually tunnel-coupled to one another, i.e. if the second s shell is the energy level with the asymmetric states or simply the s shell of a second layer of quantum dots that gets charged at higher voltages because it is farther away from the backgate.

were performed at a gate voltage of 0 V. In Fig. 5.20 (a), which was taken at a considerably lower laser intensity than the other three measurements, we observe two peaks — one at 1.147 eV and one at 1.173 eV — that are too close together to be resolved individually. Nevertheless, the observed peak is clearly asymmetric and the best fit results are obtained by fitting two peaks as indicated by the dashed lines. At this point, we can still not tell for sure whether the electrons can in fact tunnel between the two dot layers or not. In any case, the rather small energy difference between the two peaks of 26 meV indicates that the second peak is not the transition of an electron in the p shell to a p state in the valence band. At a laser intensity higher than twice the original value, we see a third peak evolving (Fig. 5.20 (b)) that eventually gets stronger than the s-s transition for even higher intensity values (Fig. 5.20 (c)). This peak has an energy of 1.202 eV, which is where we would expect the p-p transition for a single quantum-dot layer. It appears in the spectra when the laser intensity is so high that more electron-hole pairs are created than fit into the s shells of the quantum dots. Therefore, some electron-hole pairs cannot relax completely before recombination. As the intensity is further raised, the higher shells get filled up, too, so that more transitions become visible (Fig. 5.20 (d)). The measurements on our double quantum dot system seems to show this behavior very clearly, although a more detailed investigation reveals a few particularities. From measurement (a) we derived that there is a second transition at 1.173 eV. In measurement (b) this excitation is barely visible, as the p-p transition becomes prominent. There is only a slight kink in the high energy flank of the s-s transition that reveals this feature and there is a good agreement of our fit with three peaks with the measured spectrum. As we further increase the intensity in (c), the slight kink is no longer visible. With the naked eye, we can only make out two peaks in this spectrum. Physically though, there is no reason why with increasing intensity one of the peaks would vanish and if we assume that the three previous peaks are still there and at approximately the same position as in (a) and (b), we can fit the spectrum very well by adding a new peak at 1.221 eV, i.e. at about 20 meV from the p-p transition. While it is tempting to accept these fits (which we have displayed in Fig. 5.20 (c) as dashed lines) as the correct ones since they can be easily explained, we want to point out that there are numerous other ways to get a good agreement with the spectrum by multiple peak fitting. As long as we lack further evidence for the physical correctness of our peak fits and the explanation, they have to be viewed as exemplary.

Further evidence for a coupling between the two quantum dot layers comes from photoluminescence measurements at different gate voltages shown in Fig. 5.21. At a laser intensity of 35 mW we increased the voltage in 100 mV

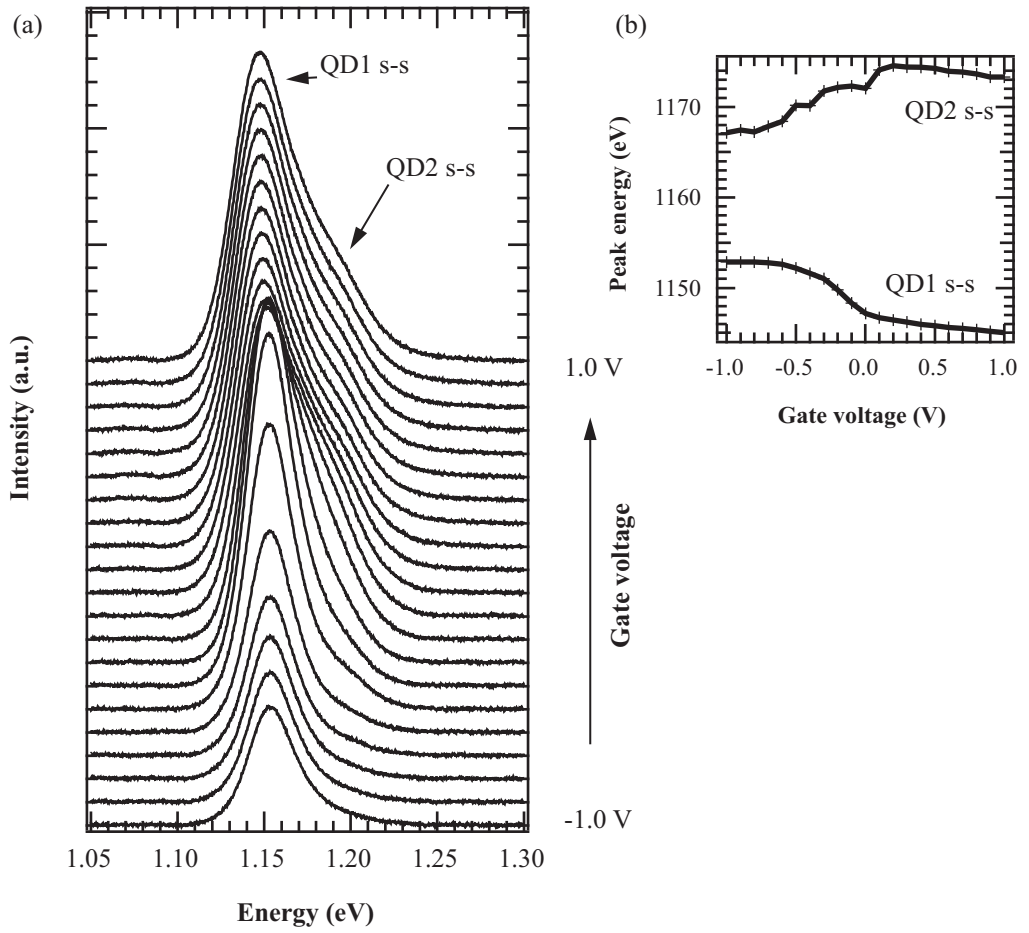

Figure 5.21: (a) Photoluminescence measurements on the sample with two layers of *SAQD*s at different gate voltages from −1.0 to +1.0 V at a laser intensity of 35 mW. (b) Energy dispersion of the two peaks with the gate voltage.

steps from −1.0 V to 1.0 V. As can be seen in Fig. 5.21 (a) the intensities of the two peaks increase up to a voltage of about −0.2 V, which is where the charging of the s shell sets in in the unilluminated capacitance spectrum. With increasing voltage we see the second peak emerging a little more distinctly. Looking at the energy dispersion of the peaks in Fig. 5.21 (b) we deduce that this is because the two peaks show a quite different behavior. The first peak shows a nearly step-like decrease in energy between −0.2 and 0 V, whereas the second peak increases in energy up to a voltage of about 0.2 V before its energy slowly decreases with the same slope as the first peak. If the two dot layers were not coupled at all and the two peaks were just due to two independent layers of dots, we would have expected the two peaks to

exhibit similar dispersions with a voltage offset because one layer is closer to the backgate than the other. A step-like behavior of the photoluminescence signal like that of the first peak has also been observed by Bertram Su in [Su03] on the samples with single quantum dots we discussed earlier. It can be explained by a simple model for the Coulomb interaction of the electrons and holes in the quantum dots as proposed by Warburton *et al.* [War98]. The increase in energy of the second peak could possibly be explained by the growing asymmetry of the double quantum dot system, thereby increasing the Δ_{SAS}, if we do in fact have a coupled system. Again, this is not enough to prove the coupling of the two quantum dot layers but another indication for it.

The Raman measurements performed on this system showed the same excitations as those performed on the backgate-wetting layer system, when the laser was tuned to the same energies [Stü05]. The only difference was in the energy dispersion for different gate voltages. The energy shift for the excitations in the system with quantum dots was much smaller than that of the system without dots. This might be explained by a screening effect from the quantum dot layers, changing the electron densities in the *2DES*s. Measurements at energies where the $E_0 + \Delta$ gap of the double dot system was expected did not yield any electronic excitations. The most simple explanation for this would be that the gap is not in the energy region where we expected it to be.

5.4 *PLE* spectroscopy on InAs quantum dots at the $E_0 + \Delta$ gap

To investigate the exact position of the $E_0+\Delta$ gap in our different samples we tried using photoluminescence excitation spectroscopy. Using the method in this context is not standard, since most of the electron-hole pairs are created in the GaAs bulk material before recombining within the dots. Taking into account also that we looked at a large ensemble of quantum dots we did not expect to see an on-off-behavior of our luminescence signal with varying laser energy. We were looking for variations in the intensity and shape of the signal instead. The measurement itself confronted us with quite a few problems that the reader should be aware of when looking at our results. We will discuss these by explaining our data collection and analysis processes in detail.

We have mentioned before that we used a method that we call *multi-channel PLE* in this work. This means that we did not just measure the

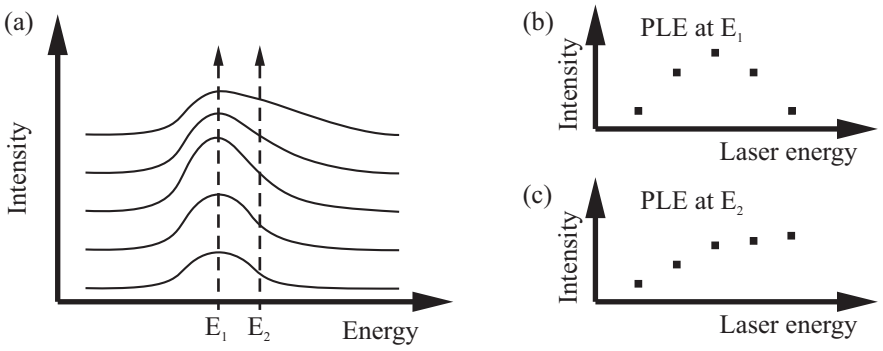

Figure 5.22: Exemplary illustration of the multichannel *PLE* technique (with fictional data for illustrational purposes): (a) *PL* measurements are taken at different energies of the exciting laser. Plotting the measured intensities at a given energy (dashed lines) against the laser energy we obtain the *PLE* representations shown in (b) and (c).

intensity dependence of one luminescence wavelength on the laser energy but the dependence of the whole luminescence spectrum. In practice this meant taking a *PL* spectrum for each laser energy we measured at. We have illustrated this in Fig. 5.22 (a) for five different laser energies. Taking, for example, the energy of the photoluminescence maximum E_1 and plotting its intensity against the laser energy, we obtain a *PLE* curve as shown in Fig. 5.22 (b). If the shape of the *PL* signal changed with variation of the laser energy we would obtain a quite different *PLE* curve at another *PL* energy E_2 as illustrated in Fig. 5.22 (c).

To erase the effects of the laser power variation on the luminescence intensity we measured and readjusted the laser power before each measurement. However, it was impracticable to fully erase the wavelength dependence of our powermeter. This might lead to small effects that would be the same in all of the measurements and could thus be distinguished from those that are of interest for us. Typically, we would collect more than 200 photoluminescence spectra for varying laser energies in order to compensate for the signal noise and to cover a large laser energy range. It would take several hours to convert the 200 *PL* spectra into 200-point *PLE* spectra so that we could not judge whether we had enough data or not during the measurement. During the time of the data collection (about seven hours) some interruptions were inevitable including laser breakdown and necessary readjustments which is why not all measurements resulted in presentable data. Likewise, the data presented may include features that are not necessarily due to physical processes within the sample.

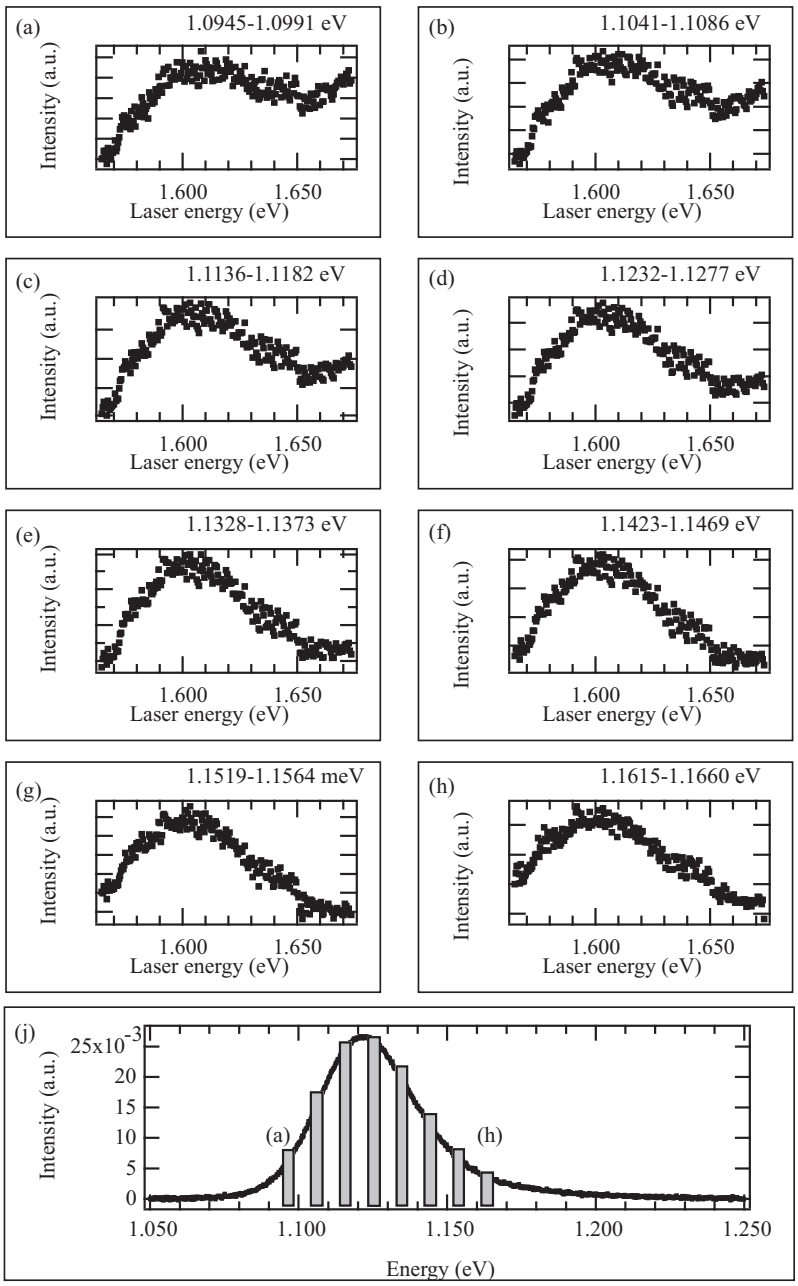

Figure 5.23: (a)-(h) *PLE* curves measured by multichannel *PLE* on uncharged InAs quantum dots. The energy region of the summed up pixels is indicated in the upper part of the figures. The intensity axes do not start at zero and are each on a different scale. (j) Example of a *PL* measurement from which the *PLE* curves were extracted. The gray bars mark the energy bands for which the *PLE* curves in (a)-(h) are taken.

Nevertheless, we wish to present some of the measurements here to show the potentials and flaws of the method when used above the $E_0 + \Delta$ gap of the dots. The first measurement we want to show was realized on the same sample that we had used for charge-dependent Raman spectroscopy. The gate voltage was set to -0.5 V so that there were no electrons in the dots without illumination. For our *PLE* representation we took small energy bands out of the *PL* spectrum and summed up the intensities of the data points in this band. The width of the bands was chosen in a way that the signal to noise ratio was enhanced at an acceptable loss of resolution. In Fig. 5.23 we show several such spectra. The energy band width was chosen to be 4.5 meV which corresponds to summing up 20 points and we show every second spectrum obtained in this way. The curves are each shown on different intensity scales, the variation in intensity was typically of the order of 15 %. Note that the intensity axes of the *PLE* curves do not start at zero but at the minimum intensity of that spectrum. Fig. 5.23 (j) shows one of the approximately 200 *PL* measurements that we extracted the points for the *PLE* curves from. The gray bars indicate the energy bands for which the *PLE* spectra are shown in Fig. 5.23 (a)-(h).

All spectra show a maximum at 1.6 eV which fits well with our resonant Raman measurement where we found the s-p and the p-d resonance at < 1.66 and 1.70 eV. The maximum at 1.6 eV could then be assigned to the s-s($+\Delta$) absorption, although it is not clear why this peak is the same in all *PLE* spectra. We have argued before that the statistical size distribution of the dots leads to a broad *PL* signal. By reducing the evaluated energy to a small band instead of looking at the whole spectrum we expected to selectively evaluate an ensemble of dots with a limited size distribution. For example, the spectrum displayed in Fig. 5.23 (a) originates from the lower-energy part of the *PL* spectra and should therefore contain information about the larger dots, while the spectrum in Fig. 5.23 (h) should come from small dots. Since the s-s absorption energy depends on the dot size the position of the *PLE* maximum should depend on the evaluated energy. It is likely that the absorption of the bulk material is somehow enhanced at 1.6 eV and therefore the *PL* signal increases for all quantum dots alike. There is, however, a difference in the spectra from larger to smaller dots on the high energy side: while the *PL* signal of the larger dots increases in intensity at energies above 1.65 eV, the *PL* signal of the smaller dots decreases steadily for energies larger than 1.60 eV. This indicates that we do in fact measure effects of the quantum dot absorption and not only of the bulk material. Nevertheless, a satisfactory explanation for the observed behavior has not yet been found. Following the assumption that the maximum at 1.60 eV corresponds to the s-s$+\Delta$ absorption we expect the next maximum at about 1.66 eV, based on

the energies measured in *PL* experiments. The experimental results, on the contrary, show a minimum in intensity at this laser energy. Assuming that the peak at 1.60 eV is entirely explained by bulk effects, we could assign the second maximum to the s-s+Δ absorption — expectedly setting in earlier for the larger dots — but this would not agree with our resonant Raman measurements.

In order to affirm our ability of measuring quantum dot absorption effects in our experiments we measured another sample that consisted of similar quantum dots but without the inverted *HEMT* structure. There was no doping layer in the vicinity of the quantum dots so that they were nominally uncharged. The results are displayed in Fig. 5.24. Here we summed up only 5 pixels of the *PL* measurements, resulting in an energy resolution of 1 meV as noted in the individual diagrams. Comparing the result with the previous representations, we observe some qualitative similarities. As before there is a maximum in all curves that is the same for all *PL* energies evaluated[4] although here the maximum is at 1.69 eV instead of 1.60 eV. The curves also show features that depend on the evaluated *PL* energy, namely two smaller peaks at 1.62 eV and 1.665 eV, both being visible in the spectra of the lower *PL* energies and disappearing into the broad slope of the fixed peak for the higher *PL* energy spectra. We would have hoped for these two smaller peaks to shift with the evaluated energy if they were really to be explained by quantum dot absorption. Detailed analysis of the curves actually reveals that the peaks disappear without shifting. This does effectively not support our assumption that these peaks result from a sub-ensemble of large dots.

Further measurements on these samples and samples with the two layers of quantum dots did not yield presentable data, eventually leaving the reproducibility of the measurements questionable. Therefore, we did not pursue these experiments any further.

We come to the conclusion that the *PLE* experiments neither supported nor disproved our resonant Raman measurements. We were able to distinguish bulk effects from other effects by selectively looking at the *PLE* curves from small energy bands within the dot luminescence. The exact provenience of these effects, however, remains unsolved. Especially, the method could not be utilized to identify the $E_0 + \Delta$ gap of the quantum dots or the double quantum dots.

[4] The curves belonging to the energies between the shown ones do not reveal any abrupt changes or new features and are hence not included here for the sake of clarity.

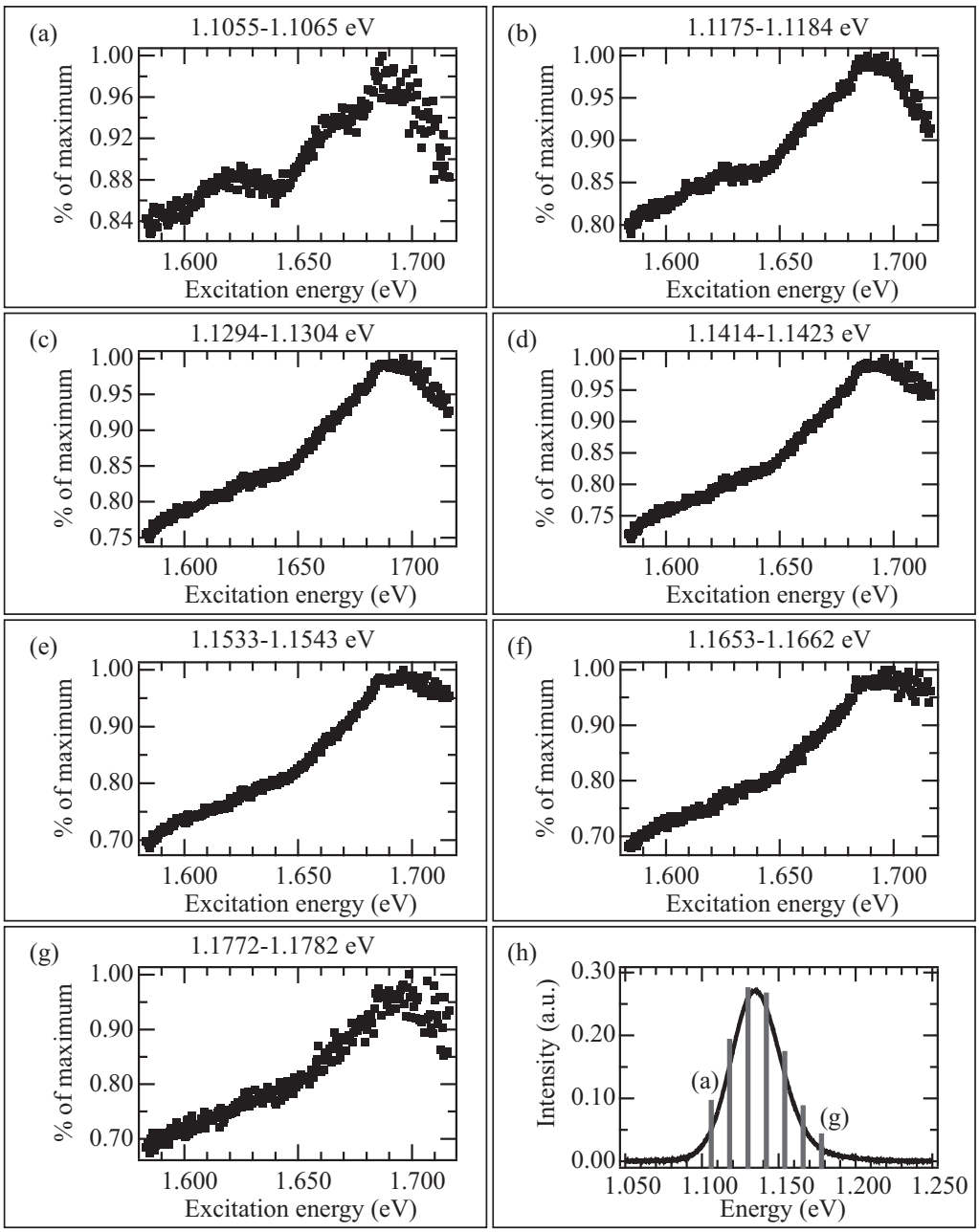

Figure 5.24: (a)-(g) Multichannel *PLE* curves of a nominally uncharged quantum dot ensemble without gate and backgate. The curves are the result of adding up 5 pixels, corresponding to about 1 meV as indicated in the graphs. (h) Example of a *PL* measurement from which the *PLE* curves were extracted. The gray bars mark the energy bands for which the *PLE* curves in (a)-(g) are taken.

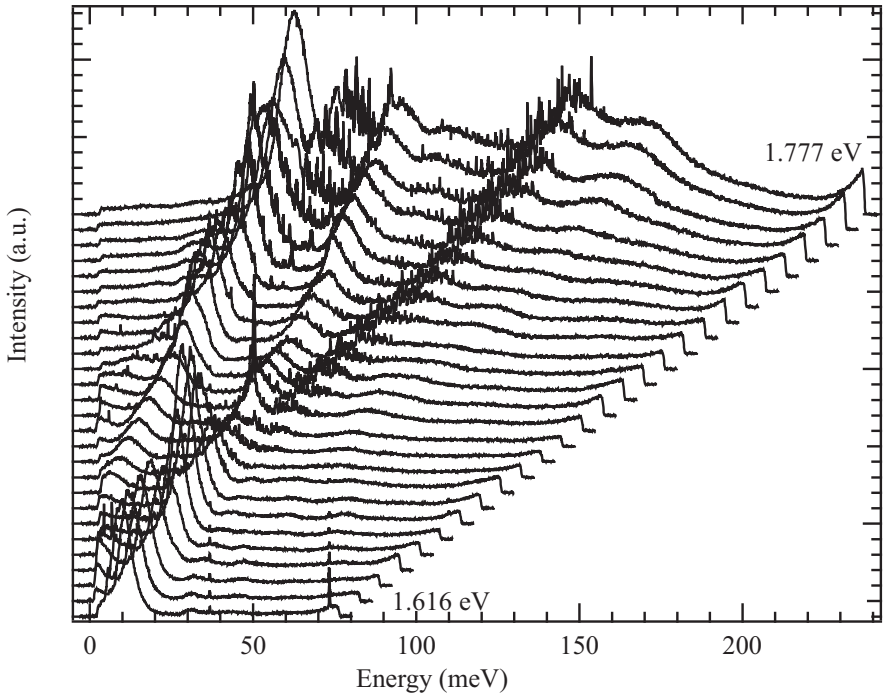

Figure 5.25: Resonant Raman spectroscopy on an ensemble of InAs quantum dots on AlAs. The laser energy was varied from 1.616 eV to 1.777 eV. Only the polarized spectra are shown.

5.5 Spectroscopy on InAs/AlAs quantum dots

As we said previously, performing Raman measurements at the E_0 gap instead of the $E_0 + \Delta$ gap is favorable because of the much stronger resonance effects. The obvious ways to achieve such measurements are to enhance the E_0 gap by one of the methods described in Chapter 3.2.3 and/or to adapt the setup for larger wavelengths. In a first attempt, we performed Raman experiments on InAs dots grown on AlAs, where the E_0 gap would be in the visible range so that no changes to the experimental setup were required. The sample was also grown in the group of Prof. W. Hansen at our institute. We had some experience on this system as Dr. Lars Karsten had performed photoluminescence and photoluminescence excitation spectroscopy on the same samples as a part of his PhD thesis in our group [Kar04]. Hence we expected the E_0 gap to be at an energy of about $1.65 - 1.70$ eV, with possible size (and thus energy) variations depending on the original position of the sample on the wafer.

We performed a resonant Raman experiment on the sample by varying the

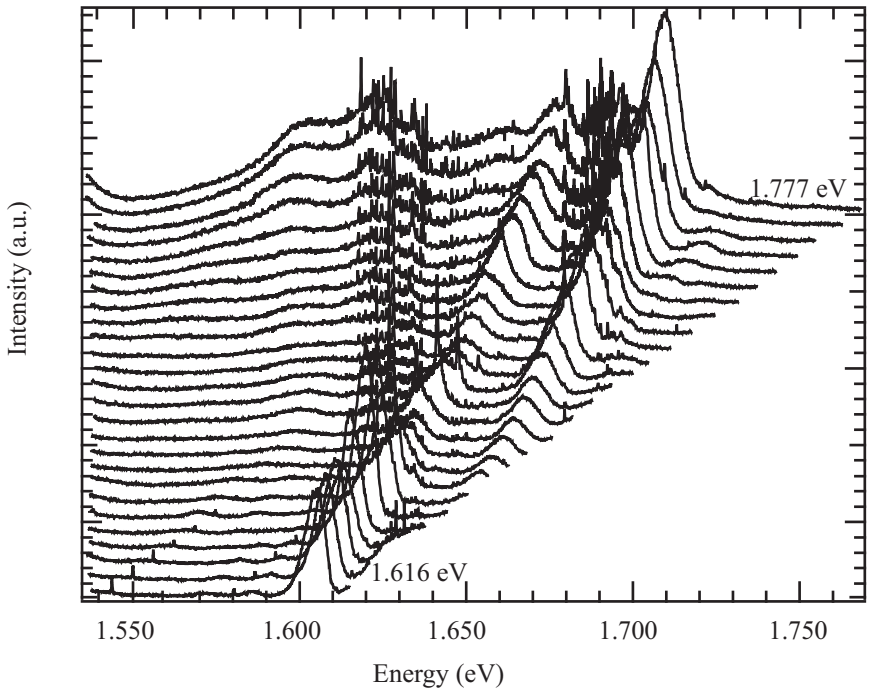

Figure 5.26: Same measurement as Fig. 5.25 but plotted on an absolute energy scale, showing clearly that the fine lines remain at the same absolute energy while the large peaks shift in energy in this representation as well as in the Raman representation.

laser energy E_{Laser} between 1.616 eV and 1.777 eV in steps of approximately 6.2 meV. In Fig. 5.25 we display the results in the Raman representation, i.e. Raman excitations are found at the same energy for all laser energies. At 36.6 meV and 73.2 meV we can identify the GaAs LO and $2LO$ phonon lines. This is not unexpected as the AlAs and dot layers were grown on a GaAs substrate and we excite above the GaAs band gap. At energies above 1.65 eV we observe an AlAs-like LO phonon at 50.5 meV while the GaAs phonons can hardly be detected anymore. At a laser energy of 1.69 eV the phonon is strongly enhanced. This could be explained by the laser being at an energy equal to the energy of a photoluminescence recombination plus a phonon. This would imply that there is a photoluminescence at about 1.64 eV, which we should detect in our experiment as well as the Raman signals. To make the distinction between the two types of signal easier, we show the same measurements again on an absolute energy scale in Fig. 5.26.

This second representation should make clear that a resonant Raman experiment can also be seen as a multichannel PLE experiment if a photolu-

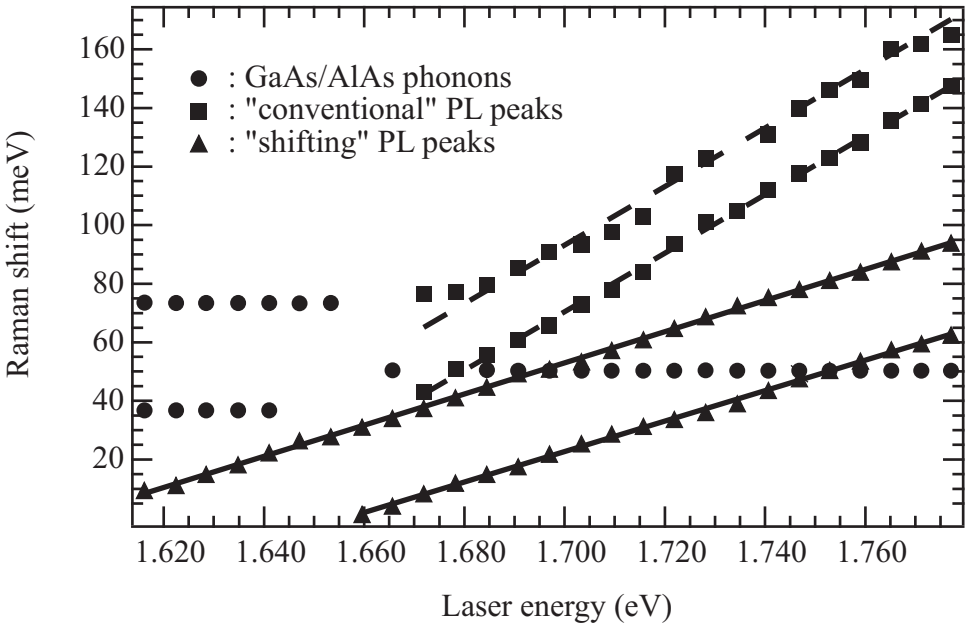

Figure 5.27: Raman energy dispersions of some of the peaks shown in Fig. 5.25. We have plotted the GaAs and AlAs phonons as circles, two exemplary photoluminescence signals as squares and the two «shifting» photoluminescence signals as triangles. Also shown are line fits for both kinds of photoluminescence peaks.

minescence signal is present in the spectra. On the absolute energy scale the photoluminescence peaks would be on a vertical line while the Raman signals should move as the distance to the laser is constant. In Fig. 5.26 we observe many sharp lines in the energy range between 1.62 and 1.70 eV that are at the same absolute energy independent of the laser energy. It would be rather optimistic at this point to claim that each line is a photoluminescence of a single quantum dot — we still discuss measurements on large ensembles of dots with the macroscopic Raman setup. Measuring single dot luminescence in this experimental setup could only be explained by resonant absorption in dots of a specific size. However, the recombination energy of the resonantly excited dots would be a function of the absorption energy, because the two energies are related to one another. This is clearly not the case for the lines in our spectra. Thus, there would have to be a continuum of states in the vicinity of some of the dots, leading to a higher signal from these dots.

Up to this point we assumed that all peaks are nearly independent of the laser energy either on an absolute scale (*PL* peaks) or on a relative scale (Raman peaks). There are two peaks in the spectra that obviously contradict this assumption as they show the same dependence on the laser energy on

both scales, i.e. their energy shift equals almost exactly half the difference in laser energy between two measurements. This exact relation can be deduced from Fig. 5.27 where we show the Raman peak positions of the observed phonons, two photoluminescence signals that do not shift on the absolute scale and the two peaks that exhibit a shift in energy. In this representation, the phonons remain at the same energy as long as they are detectable. The dashed lines represent the «conventional» photoluminescence behavior, i.e. they have a slope of 1 in the Raman representation. The solid lines are line fits to the data points of the two peaks that shift in both representations. The slopes of these line fits are 0.53 and 0.52 for the upper and lower line, respectively. We want to propose a model here that would explain the two excitations as photoluminescence signals that shift because we resonantly excite dots with different sizes.

Let us first consider the situation of an ensemble of dots where all the dots have the same height but varying lateral dimensions. By resonantly exciting only the dots that have a p-p transition at E_{Laser} we also detect only these dots. So a higher laser energy will obviously lead to a higher photoluminescence energy. To understand why the photoluminescence will not shift as much as the laser we have to recall Equation 2.9:

$$E_{nm} = \hbar\Omega_0(2n + |m| + 1) = N\hbar\Omega_0,$$

where $N = 1, 2, ...$ We can directly deduce that the ground state with $N = 1$ of a smaller dot with the quantization energy $\hbar(\Omega_0 + \omega)$ will have a ground state energy enhanced by $\Delta E = \hbar\omega$ and a p state with $N = 2$ enhanced by $2\Delta E$. The same argument is valid for the hole states which we do not discuss here but which are part of the luminescence process. Consequently, if we enhance the laser energy by $2\Delta E$, and thus excite smaller dots, these will exhibit a luminescence energy enhanced only by ΔE. The fact that in our experiment the dots are not all of the same height does not change this argumentation. It merely leads to a broadening of the signal, as there are now some dots that are smaller in height but larger in lateral dimensions and vice versa. This does not lead to the full width of the ensemble *PL* signal as measured when exciting in the wetting layer or the bulk material, because the large effect of the height distribution always results in dots that will not meet the resonance condition because the smaller effect of the lateral confinement cannot compensate for the energy difference. Note that this argumentation only holds for uncharged dots as the existence of many-particle states in between the single-particle states would allow for a resonant absorption in a much broader energy band so that dots of many different sizes would be excited resonantly disregarding the excitation energy.

Following the same line of argumentation we can also deduce why we do not observe such an effect for Raman signals. In the first step we would expect the Raman signal to shift just like the luminescence signal does, but here the height distribution nullifies this argumentation because now we can find dots that fulfill the resonance condition with every possible lateral size by choosing an appropriate dot height. We always have the full peak from the lateral size distribution so that an energy shift is not possible, assuming that dot height and width are not correlated. The *PL* signal, on the other hand, can still shift because it is affected by the height distribution and not all dots are excited resonantly at once.

So, in short, when tuning the laser through the resonance of an ensemble of quantum dots, the Raman signal *always* shows the full peak width of the lateral size distribution because for every dot width, a dot height can be found so that the dot resonance coincides with the laser energy. On the other hand, the *PL* signal will not show the full width of the height distribution because the extent of the lateral size variation is not large enough. The fact that the observed ensemble Raman signals in Chapter 5.1 did not shift can therefore be understood as evidence that dot height and dot width distributions are not correlated.

Assigning the two observed signals to photoluminescence processes also explains the enhanced signal when the relaxation energy coincides with the energy of an AlAs *LO* phonon. For the other spectra, the relaxation process is still not resolved because of the phonon bottleneck. The origin of two photoluminescence signals with a separation of only 30 meV is also uncertain, as well as the sharp lines and the luminescence signals that do not shift with variation of the laser energy. These uncertainties, combined with the fact that we did not see any electronic Raman excitations in these experiments and some important experimental challenges related to the AlAs barriers, discouraged us to continue these experiments.

5.6 Raman Spectroscopy on InAs/GaAs quantum dots at the E_0 gap

In the experiments described in the previous sections we used the Ti:Sa laser in the visible range. By exchanging the high reflection mirrors of the cavity with a different set it was possible to operate the laser in the near infrared range between 850 and 990 nm ($1.25 - 1.46$ eV), the laser operation becoming increasingly difficult for lower energies. The quantum efficiency of the *CCD* camera installed in the Raman setup was still over 20 % for

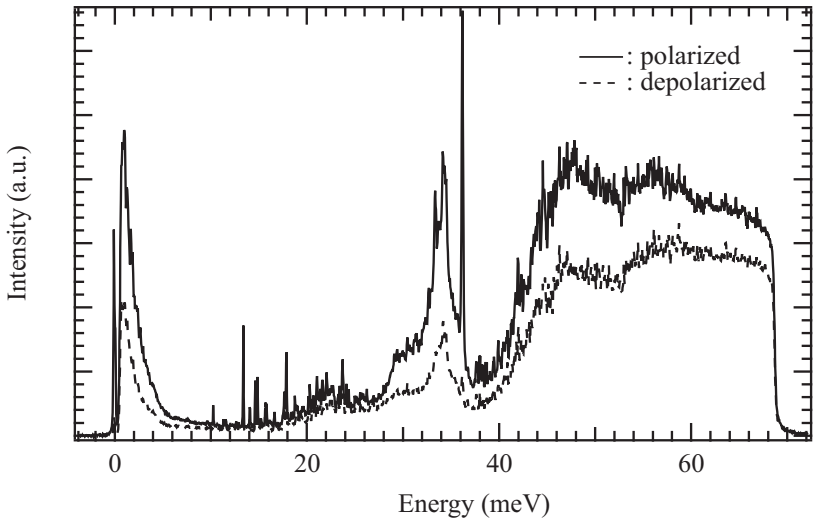

Figure 5.28: Polarized (solid line) and depolarized (dashed line) Raman spectrum of a sample with InAs/GaAs quantum dots taken at a laser energy of 1.251 eV.

energies down to 1.27 meV but decreased rapidly for smaller energies. The self-organized InAs/GaAs dots we discussed in the previous sections had the E_0 gap at approximately 1.1 eV so that the first energy that we could excite and detect with our setup was the f-f transition, given an energy spacing of about 50 meV. This inevitably led to difficulties in the evaluation because we were only able to calculate electronic states in the quantum dots up to six electrons per dot. It was also uncertain if the f states still existed when a high voltage was applied to the sample because of the change in band structure. The fact that we only observed the charging of electrons up to the p shell in capacitance spectroscopy implied that even the existence of d states was doubtable at high voltages.

Despite these difficulties we want to show a few results that we obtained with this configuration. Fig. 5.28 shows exemplary polarized and depolarized spectra taken with the laser at 1.251 eV. The chosen spectra show two Raman peaks at 45 and 55 meV, not unlike the spectra shown in Chapter 5.1 in spite of the completely different resonance conditions. As we will see in Chapter 5.7.2, we probably do not have the best resonance conditions yet, as the GaAs LO phonon is still stronger in intensity than the electronic Raman excitations. We could not determine the number of electrons in the dots in this experiment, so that for now we want to focus on some qualitative results we obtained by limiting the region from which the scattered light was collected in our macroscopic setup.

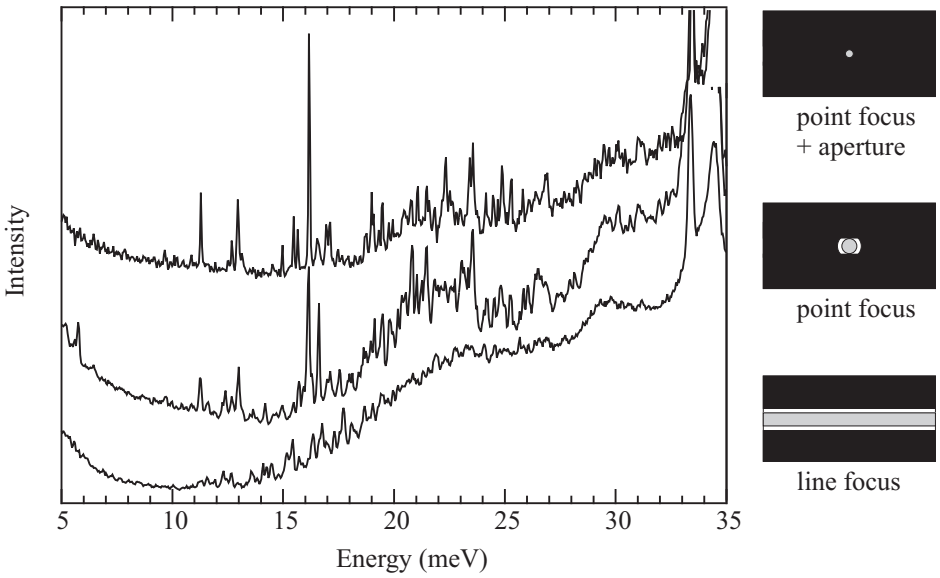

Figure 5.29: Raman spectra of a sample with InAs/GaAs quantum dots taken at a laser energy of 1.251 eV. From bottom to top: spectrum taken with laser in line focus, in point focus, and with point focus and an aperture introduced in the image plane within the spectrometer. The observed image is sketched on the right hand side. The intensities of the spectra are not comparable.

In Fig. 5.29 we show three polarized Raman spectra that were all taken at the same laser energy as before. We show only a small excerpt of the whole spectrum. The bottom spectrum was taken with the laser focused by a cylindrical lens into a narrow line (about 50 µm wide). We used this focusing method often in our ensemble measurements because it would increase the amount of dots measured because of the larger focal area. This resulted in a stronger signal from the quantum dots compared to the point focus without increasing the bulk signal because the overall laser intensity would remain the same. In the middle spectrum the laser was focused on the sample by a spherical lens, thus reducing the illuminated area to a spot of about 100 µm in diameter, resulting in a factor 10 decrease in the area with respect to the line focus. A further reduction of the illuminated area was not possible in the macroscopic setup so we used an iris aperture in the image plane of the focusing lens within the spectrometer to reduce the observed area by a factor of 10 with respect to the middle spectrum. A simple digital camera that could be introduced in the image plane allowed us to observe the area from which light was collected. Schematic pictures of the images on the camera for the respective spectra are shown on the right hand side

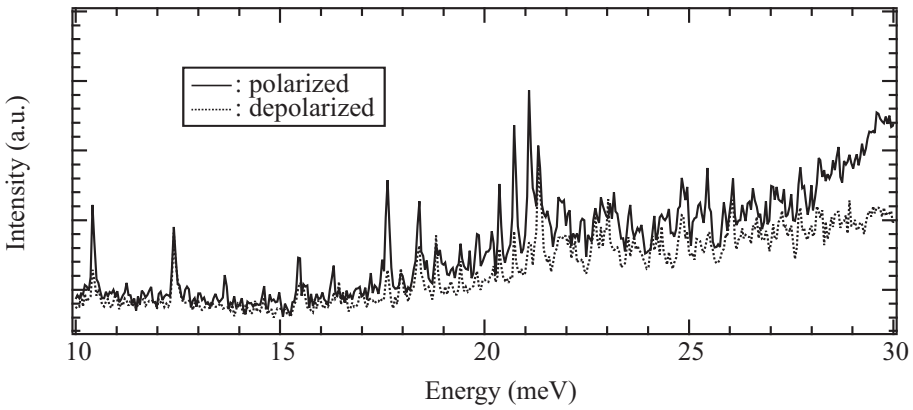

Figure 5.30: Excerpt from the polarized and depolarized spectra taken with point focus and the aperture in the image plane. Several of the lines are strongly dependent on the polarization while others are not at all. This explains the slight dependence on polarization we sometimes observe in ensemble spectra.

of Fig. 5.29. As the area from which the signal is collected is reduced, the broad signal as seen in the bottommost spectrum splits up into narrow lines. Note that the measurement parameters were different for each measurement so that the intensities in Fig. 5.29 cannot be compared. We were able to identify the broad signal as a Raman signal by varying the laser energy, although we could not determine the electronic origin of the signal because of the aforementioned difficulties. By narrowing down the observed area we progressively investigate fewer quantum dots, which are excited resonantly so that even in comparably large area of approximately 800 µm^2, where we still expect several ten thousand quantum dots, only few contribute to the measured signal.

In Fig. 5.30 we display an excerpt from the polarized and depolarized spectra taken with the laser in point focus and with the aperture to reduce the measured area. It is still impossible to assign the observed lines to any specific electronic excitation as we still observe many quantum dots. However, it is interesting to note that among the many narrow lines there are some that show an on/off behavior when switching between the polarized and depolarized configuration (although incomplete because of the less than 100 % polarization selection of the spectrometer gratings) while other lines show no polarization dependence at all. This is especially interesting because these lines are relatively close together and there is no correlation between energy and polarization dependence. We conclude that the broader ensemble peaks do not necessarily consist of only one kind of excitation (*SDE*, *CDE* or

SPE) but may also contain different excitations that can not be resolved in the ensemble measurement. These ensemble peaks may show a weak polarization dependence. We will show ensemble measurements with such peaks later in the next chapter.

5.7 Spectroscopy on *SAQD*s grown with the In-flush technique

5.7.1 Macroscopic photoluminescence experiments

In order to avoid the difficulties in determining the electronic origin of our Raman signal from the conventional dots, we had to alter the dots so that their fundamental s-s transition would be of the order of 1.2 eV and above, the experimental setup already being used at its lowest energy limits. We found that the In-flush technique suits our goals best as it considerably enhances the s-s transition energy while theoretically leaving the lateral confinement — and hence the energies affecting our Raman shift — nearly unchanged (see Chapter 3.2.3). Such samples were grown for us by Holger Welsch and Andreas Schramm in the group of Prof. Wolfgang Hansen. The quantum dots were embedded in a *MIS* structure like the conventional dots in our previous experiments, but unfortunately the density of defects in the sample and on the sample surface was too high to allow any capacitance spectroscopy experiments. We measured a resistance of 1.4 kΩ between the Ti gate and the back contact, which is far too small for our experiments. We therefore could not determine or control the number of electrons in the quantum dots during our measurements.

As a first characterization and to prove that the In-flush technique did indeed result in quantum dots with a higher E_0 gap we performed macroscopic photoluminescence measurements with the Fourier transform setup and the Ar^+ laser at intensities between 100 mW and 1.3 W. The results are shown in Fig. 5.31. In all spectra we see at least two peaks at 1.207 and 1.270 eV that we assign to the s-s and the p-p transition of the quantum dots. At higher intensities, more peaks appear as the recombination rate of the lower state electrons becomes smaller than the absorption rate. At the highest intensity the presumed d-d and f-f peaks are visible at 1.330 and 1.378 eV. The appearance of the higher transition in the spectra has been observed in all quantum dot photoluminescence experiments. We would expect the high energy peaks to surpass the s-s transition at high laser intensities, though, because the higher electronic states progressively contain more electrons and holes that can recombine. We have observed this expected behavior, for

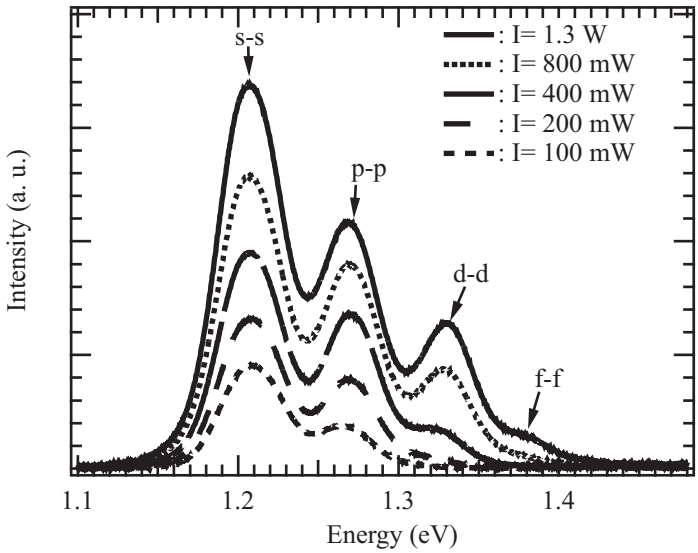

Figure 5.31: Photoluminescence measurements at different laser intensities on a sample with InAs/GaAs quantum dots grown with the In-flush technique. The observed transitions are denoted in the spectrum as well as the laser intensities.

example in the double quantum dot measurements shown in Chapter 5.3.

Taking a different sample from the same wafer we have obtained the spectrum shown in Fig. 5.32. The measurement was taken at a laser intensity of 1.2 W. The dashed lines show Gauß fits performed on the spectrum to determine the peak energies and widths. The s-s transition of the quantum dots in this sample is at 1.236 eV, giving an offset of nearly 30 meV as compared to the other sample. We assume that this offset as well as the smaller PL intensities can be explained by a considerable variation of dot size and density over the wafer. In another measurement on a different sample we were able to show a variation of the s-s transition of several meV even within the sample[5]. The peak widths in the measurements shown in Figures 5.31 and 5.32 are between 24 and 29 meV. In PL measurements on conventional InAs dots on GaAs grown in Prof. Hansen's group, the peak widths are of the order of 30 to 35 meV. We have previously claimed that the peak width in any ensemble measurement can be assigned to the size distribution of the dots and that in PL peaks the predominant effect comes from the height distribution of the dots. Since the In-flush technique supposedly assimilates the dot heights we could have expected PL peak widths of 5 meV on the In-flush

[5]The samples were all rectangular in shape with dimensions of 4.9 x 5.4 mm.

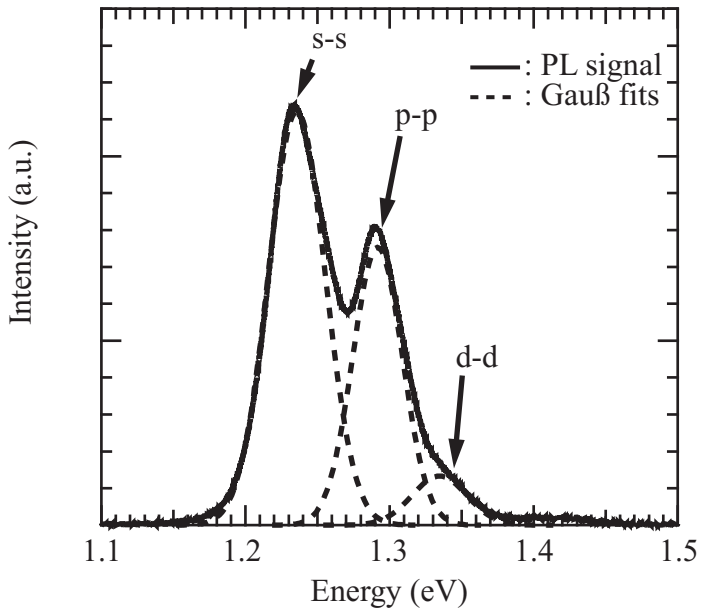

Figure 5.32: Photoluminescence measurement taken on a different sample of the same wafer, showing that there is a considerable size distribution across the wafer. Gauß fits to the observed peaks are shown as dashed lines.

dots, as now the lateral size distribution is supposed to be the dominating factor. In this context, the measured peak widths appear to be rather large. Since we do not have any cross-section measurements of the In-flush dots we cannot say for sure whether the growth procedure did result in the disk-like structures reported in [Was99][6]. We assume that either we still have a considerable height distribution of our quantum dots or that the peak widths of the In-flush dots can be attributed to GaAs intermixing effects during the heating procedure. The latter should also affect ensemble Raman measurements while the former would lead to similar Raman peak widths as for the conventional quantum dots.

5.7.2 Resonant Raman experiments

We used the second sample with the higher ground state energies for resonant Raman scattering. The laser energy was tuned from 1.245 to 1.379 eV in 2.48 meV steps at a laser intensity of 10 mW in line focus and at an angle of

[6] In [Was99] the *PL* measurements shown were performed on multi-layered quantum dot samples. The reported widths of 37.5 meV cannot be compared to our measurements because there is an additional effect from increasing dot size in the upper layers.

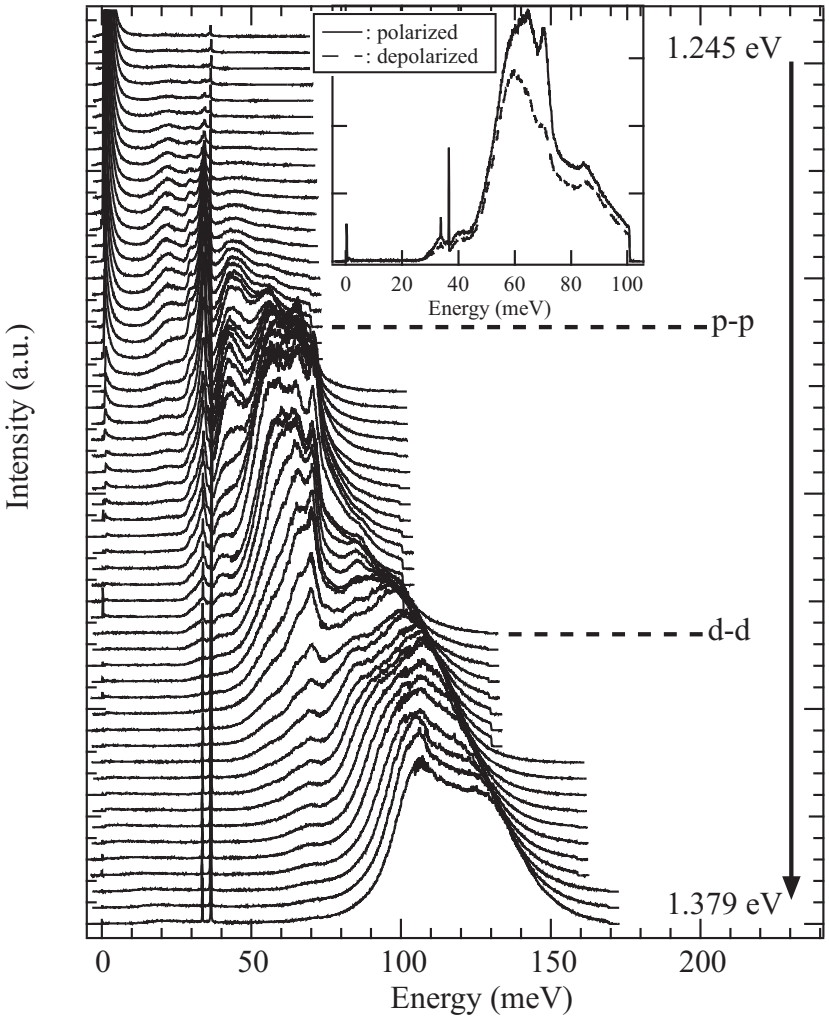

Figure 5.33: Resonant Raman spectroscopy on quantum dots grown with the In-flush technique. The laser energy has been varied in 2.48 meV steps from 1.245 to 1.379 eV. The p-p and d-d transition as determined from the measurement shown in Fig. 5.32 are indicated. The inset shows a typical polarized and depolarized spectrum for comparison. In the main frame only the polarized spectra are shown.

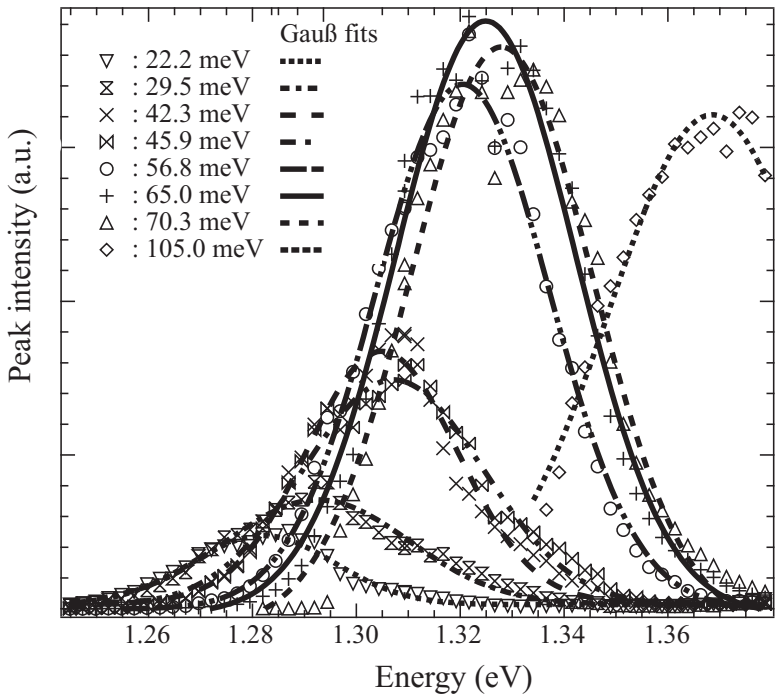

Figure 5.34: Peak amplitudes of eight different electronic Raman excitations versus the laser energy. The curves were approximated by Gauß fits shown as different solid and dashed lines.

70° so that we had very similar conditions to the other Raman spectra. The resulting polarized spectra are shown in Fig. 5.33. The depolarized spectra were very similar to the polarized spectra except for the intensity. In the inset of Fig. 5.33 we show a typical comparison of a polarized and a depolarized spectrum. The slight intensity dependence on polarization of the peaks can be explained by them consisting of *SPE*s, *SDE*s and *CDE*s as shown in the previous chapter. The depolarized spectra should contain *SPE*s and *SDE*s while the polarized spectra should consist of *SPE*s and *CDE*s. Assuming that for each *CDE* there is an *SDE* at a slightly lower energy, we would expect the peak in the depolarized spectrum to be at a lower energy than the peak in the polarized spectrum. This is indeed the case for the laser energy shown in the inset, but at other energies this could not always be affirmed.

In the polarized spectra we can clearly make out several Raman excitations. At 33.6, 34.2 and 36.5 meV we detect narrow Raman signals that we assigned to the GaAs-like *TO* (33.6 meV) and *LO* phonons (36.5 meV), as well as an interface phonon (34.2 meV) similar to the one we observed in

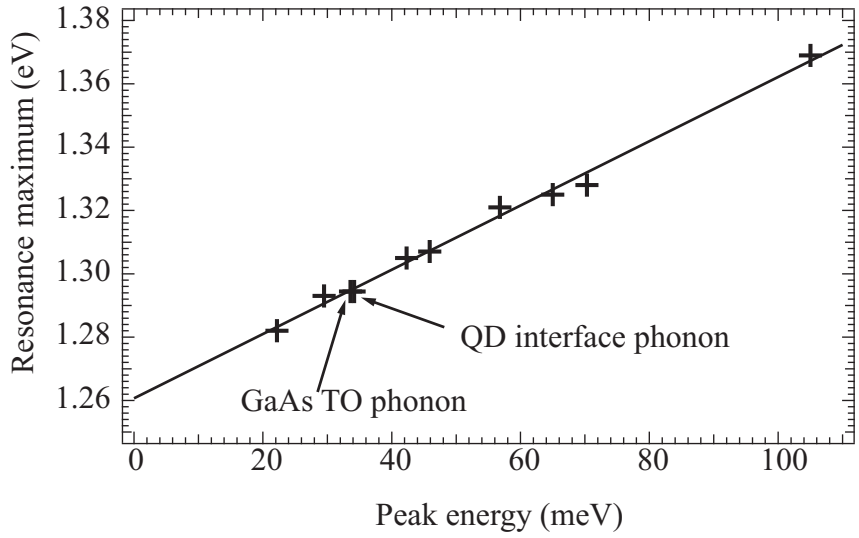

Figure 5.35: Resonance maxima of the observed electronic Raman excitations displayed versus their Raman energy. In addition, the GaAs-like TO phonon and the quantum dot interface phonon resonance maxima are displayed. The solid line is a linear fit through the displayed data.

Chapter 5.1. The energies at which Raman peaks were detected that can be assigned to electronic excitations are 22.2, 29.5, 42.3, 45.9, 56.8, 65.0, 70.3 and 105.0 meV. It is immediately apparent that excitations with higher Raman energies become resonant at higher laser energies than the low-energy excitations. The peak widths of the Raman excitations are of the order of 7−10 meV, which is slightly larger than the Raman peak widths measured in Chapter 5.1. As mentioned before, this may be a result of intermixing effects taking place during heating phase of the In-flush procedure. Compared to the photoluminescence peak widths this is still rather small, indicating that there is still an important effect of the dot height distribution in the PL transition energy.

In Fig. 5.34 we have plotted the resonance curves of the electronic Raman excitations shown in Fig. 5.33. The curves have been approximated by Gauß fits, displayed as various dashed and dotted lines in the graph. The peak widths of the fitted resonance peaks were between 19 and 28 meV and thus comparable to the peak widths we measured in the photoluminescence experiment. This is as expected, as the first step in the scattering process is always an absorption, where the size distribution enters in the same way as in the recombination. For a better understanding of the scattering processes taking place we plotted the resonance maxima of the electronic excitations,

the TO phonon and the interface phonon against their Raman energies in Fig. 5.35. We did not include the LO phonon as this did not show a resonance maximum in the measured laser energy range. The scattering processes for the creation of a LO phonon probably take place mostly within the bulk material so that the electron states of the quantum dots do not contribute much to the phonon resonances. The TO phonon, on the other hand, can theoretically not be detected in the backscattering configuration we used in our experiments [Yu99]. We assume that the processes for the creation of a TO phonon take place within the quantum dots. Fig. 5.35 reveals that in this representation all the plotted excitations lie on a straight line described by

$$E_{res} = 1.260\,eV + E_{exc}$$

where E_{res} and E_{exc} are the resonance and excitation energies. This indicates that, assuming a two-step Raman process because the three-step process is considered to have a smaller resonance width, the second step would always be a recombination with the energy 1.260 eV. In the photoluminescence measurement shown in Fig. 5.32, however there is no recombination at that energy. In his diploma thesis, Tim Köppen shows that the difference of 24 meV between the two measurements can be attributed to the rapidly decreasing sensibility of the CCD camera used in the Raman setup (see [Köp06] for details). By comparing a photoluminescence measurement of the dots taken with the Raman setup with the signal of a reference that emitted white light, he showed that the s-s transition that we observed at 1.236 eV in the Fourier transform setup would appear to be at 1.260 eV in the Raman setup. We therefore suggest that all observed Raman processes involve the s-s transition as the recombination step, or in other words that the observed excitations are all excitations of electrons from the s shell. This implies that there are probably one or two electrons in the quantum dots. We cannot exclude that there are up to three electrons in the p shell as well, but we did not detect any excitations of these electrons.

In Fig. 5.36 we have sketched the two-step scattering mechanisms that we believe to take place in our experiment. Fig. 5.36 (a) shows a scattering process for a single particle excitation as described in Chapter 2.5.1. Fig. 5.36 (b) shows the same process for a collective excitation, or a many-particle excitation as the electron does not receive the single particle energy of the Kohn mode but — in this case — the smaller energy needed to occupy a many-particle state. The excitation we observe at 22.2 meV, for example, could be explained by such a process. In the schematic representation we assume the dot to be occupied by three electrons. Note that in order to comply with our measurements it is always the first step that is forbidden in a photolu-

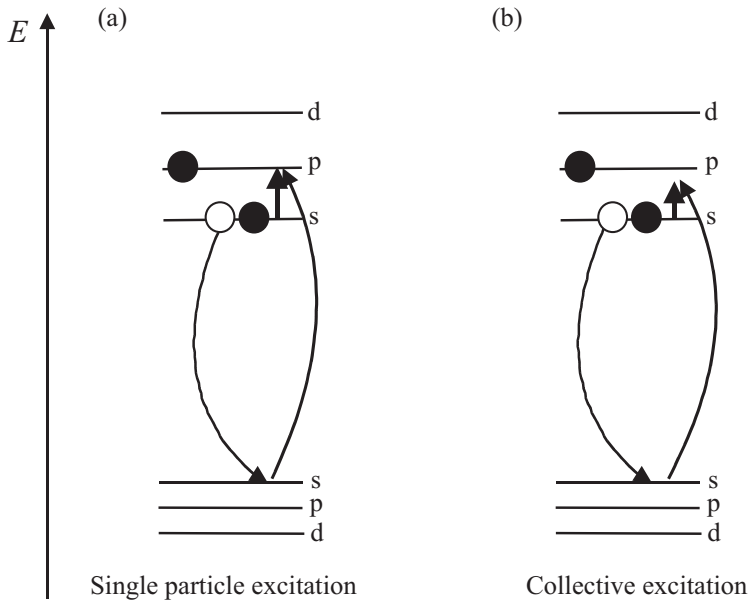

Figure 5.36: Examples for possible two-step scattering mechanisms leading to the observed behavior of the In-flush quantum dots: (a) Scattering process for a single particle excitation. (b) Scattering process for a collective excitation.

minescence process because of the selection rule that $\Delta N = 0, 2, 4, ...$ while the recombination step is a real transition. Other processes, where the first step is a p-p transition and the second step a s-p recombination would have been conceivable as well but are not observed in our experiments.

Another interesting phenomenon is that the resonance position of the TO and the interface phonon indicate that they are created by the same processes as the electronic excitations or at least that there are electronic excitations at exactly the same energy as the phonons so that a three-step process would be possible. Oulton *et al.* have shown in [Oul03] that there is a coupling between the GaAs LO phonons and the quantum dot electrons but not for the TO phonon. In our experiment, however, we observe electronic resonance effects for the TO and interface phonons and not for the GaAs LO phonon.

It could be argued that we do not detect several Raman excitations but that we resonantly excite electrons to different states in the quantum dots and always detect the s-s photoluminescence transition. The distinction between these two processes is in fact not easy. The width of the peak alone cannot be taken as the distinguishing mark. We have shown before, when discussing the InAs dots on AlAs, that a resonantly excited ensemble photo-

luminescence peak is not necessarily as broad as an ensemble *PL* peak where the excitation takes place in the surrounding bulk material. But we have also shown in Chapter 5.5 that resonantly excited *PL* peaks would shift with half the difference in laser energy in an ensemble resonance experiment. This is not the case for the observed peaks in our measurements, but we had only argued with single particle states, not many-particle states. As we assume our dots to be charged with electrons we would expect an ensemble photoluminescence peak to be broader than the observed peaks. We have also mentioned above that the first step involved in the processes is a forbidden transition. The selection rules might be broken more easily in the Raman scattering process, where the first step is only a virtual one, than in the luminescence process, where the first step is a real transition.

5.8 Measurements with the microscope setup

Comparing the Raman measurements excited resonantly at the E_0 gap to those of our first Raman experiments at the $E_0 + \Delta$ gap we see an important increase in intensity which is due to a few changes in the setup, namely the installation of a new *CCD* camera, as well as the larger densities of states and hence the stronger resonance effects. As we had already detected an array of peaks that we attributed to the Raman signals of few quantum dots in earlier measurements it was conceivable to further decrease the number of quantum dots measured with the ultimate goal to perform resonant Raman scattering measurements on a single quantum dot. We chose to gradually decrease the number of dots by working with the microscope Raman setup and collecting measurements on an unstructured sample, using first an objective with 20× magnification, then an objective with 80× magnification and finally by focusing the laser on a hole in an aluminum mask, prepared as described in Chapter 3.4. In the microscope measurements, the angle between the incident laser light, the sample surface and the scattered light cannot be changed. Neglecting the laser focus through the objective, incident and scattered light are always parallel to each other and perpendicular to the sample surface. This implies that there is no momentum transfer to the sample in the lateral direction and hence we would expect to see only the Raman allowed excitations with even parity. Especially with the 80× objective we expect a certain q-vector distribution though, because of the focused laser.

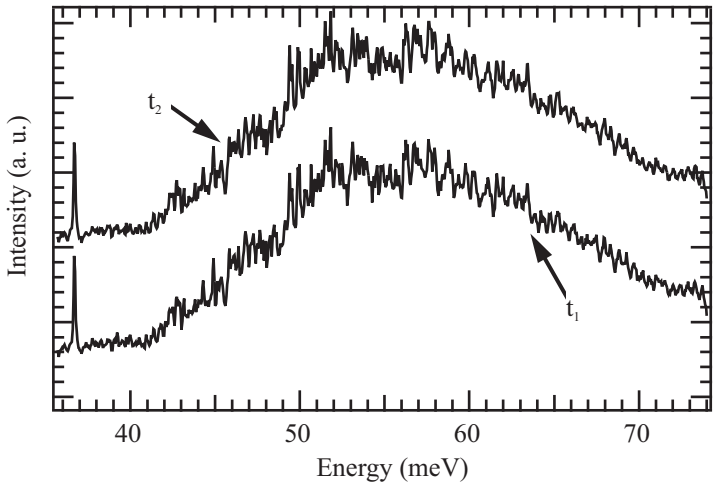

Figure 5.37: Polarized microscope Raman measurements on the unstructured part of the sample with the 20× objective. The two measurements were taken at different times with several minutes between them.

5.8.1 Measurements on the unstructured part of the sample with the 20× objective

Our first measurements were taken with the smallest magnification in order to verify that the ensemble signal in the microscope setup resembled the macroscopic measurements. By focusing and collecting light through the 20× objective of the microscope setup we reduced the size of the laser spot to a diameter of 5.4 µm. Considering that the dot density on our sample was of the order of 10^{10} cm^{-2} the number of dots excited by the laser was reduced to about 2300 (compared to about 80000 in the macroscopic measurements). At this number we still expected to see a rather large ensemble signal. In Fig. 5.37 we show two measurements taken at a laser energy of 1.2938 eV. The laser intensity, measured between the objective and the cryostat, was 8.75 µW which corresponds to an excitation density of A =38 W/cm^2. Within the large signal around 56.8 meV, which we also detected in the macroscopic measurements, small peaks appear that we assign to single quantum dots. The two measurements were taken separately within several minutes to exclude the possibility that the peaks were only due to statistical signal noise. The peak is still rather large, considering that we expected only those dots among the 2300 to contribute to the spectrum that were excited resonantly.

By changing the excitation energy from 1.2938 eV to 1.2944 eV we ob-

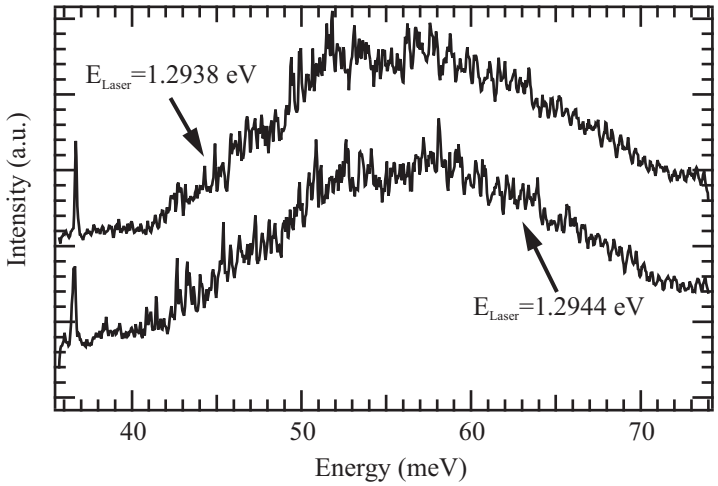

Figure 5.38: Polarized microscope Raman measurements at different laser energies. As above, the 20× objective was used to focus the laser onto the unstructured part of the sample.

tained the bottom spectrum of Fig. 5.38. As there are still so many small peaks it is difficult to say whether any of them are Raman or photoluminescence peaks. Nevertheless, we do clearly observe quite a different spectrum, indicating that different dots are excited resonantly when the excitation energy is changed as little as 0.6 meV. In both spectra we detect an excitation at 36.7 meV that we assign to the LO phonon of the GaAs bulk material.

Fig. 5.39 shows a polarized and a depolarized spectrum at the excitation energy of 1.2938 eV. Contrary to what we saw in our previous macroscopic measurements the intensity of the depolarized spectrum is much smaller than that of the polarized spectrum. This can mainly be explained by the presence of two additional beam splitters in the optical path which have different properties depending on the polarization of the incident light. We determined a 30 % loss in intensity of the incident laser light for the depolarized configuration. Despite this much smaller excitation intensity there is a peak at 42.3 meV in the depolarized spectrum that does not appear in the polarized spectrum at all. We therefore assume that this is a spin density excitation. As with any of the observed peaks in these measurements we can not verify this assumption and it is still conceivable that the peak is a photoluminescence which we would also expect to see in this energy range. These may show a polarization dependence as well.

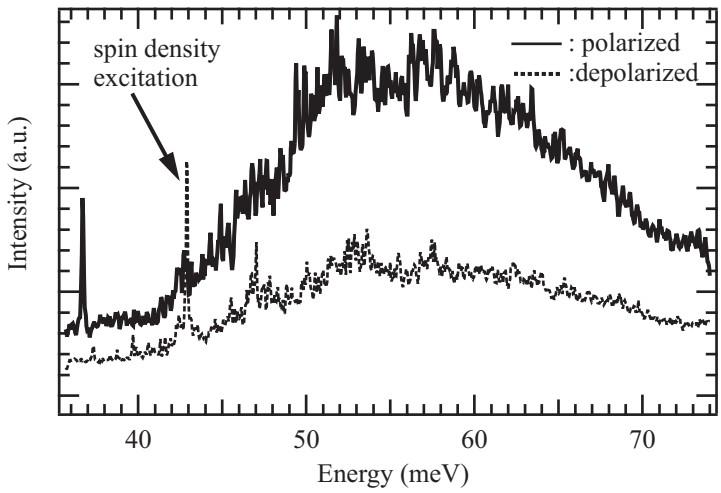

Figure 5.39: Polarized (solid line) and depolarized (dashed line) microscope Raman measurements on the unstructured part of the sample with the 20× objective. The excitation marked with an arrow can be detected only in the depolarized spectrum.

5.8.2 Measurements on the unstructured part of the sample with the 80× objective

Changing to the 80× objective we reduced the number of dots in the laser focus to about 200. In this configuration the broad ensemble signal has almost entirely vanished, as can be seen in Fig. 5.40. We show four measurements where the laser energy was varied between 1.298 and 1.306 eV in 2.48 meV steps. The laser intensity was 3.5 µW (A =137 W/cm^2). It is still impossible to tell which of the small peaks is a Raman signal and which is a photoluminescence peak, but overall the peaks appear in the same energy range between 35 and 65 meV for every laser energy so that it seems that the signal of a larger ensemble would unambiguously be identified as a Raman excitation. We hence assume that at least an important part of the peaks are Raman excitations. In order to tell exactly which excitations are actually Raman excitations, we further decreased the number of observed dots again by means of the iris aperture within the spectrometer as shown before in the macroscopic measurements. The parameters were otherwise unchanged except that the laser intensity was also reduced to 2 µW (A =79 W/cm^2). We show two such measurements on different sample positions in Fig. 5.41. It is apparent that we now have reduced the number of observed quantum dots enough to see only single peaks in the spectra. The two measurements are

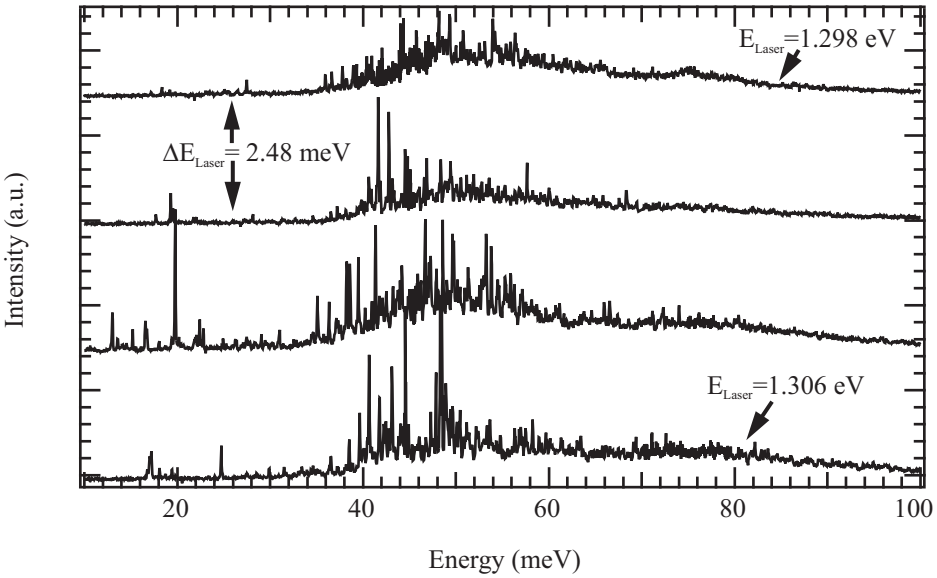

Figure 5.40: Polarized microscope Raman measurements with the 80× objective on the unstructured part of the sample at four different laser energies between 1.298 eV and 1.306 eV.

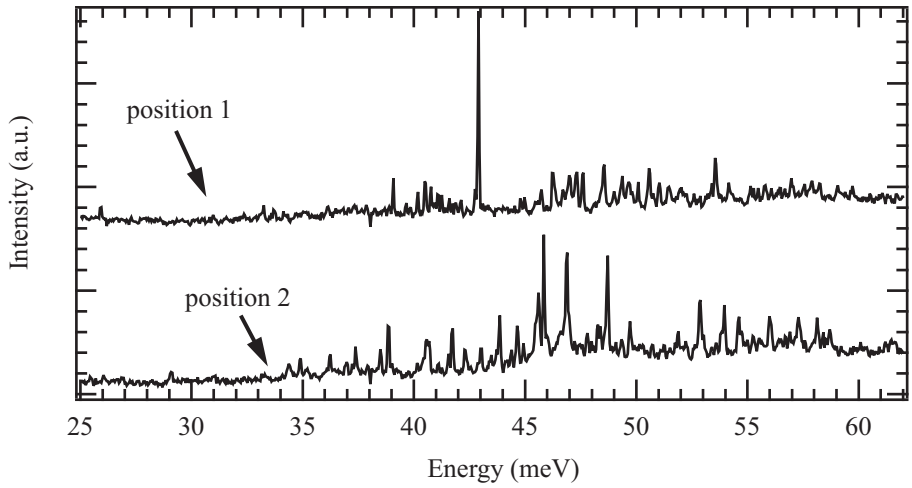

Figure 5.41: Polarized microscope Raman measurements with the 80× objective and the iris aperture in the spectrometer nearly closed to selectively detect only very few quantum dots. The two spectra were taken on different sample positions on the unstructured part of the sample.

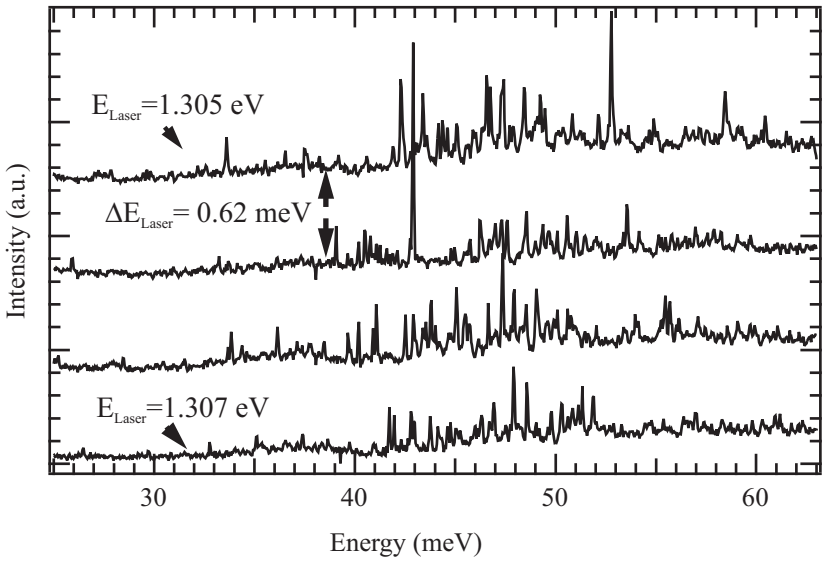

Figure 5.42: Polarized microscope Raman measurements with the 80× objective and the iris aperture in the spectrometer nearly closed to selectively detect only very few quantum dots. The laser energy was varied in 0.62 meV steps between 1.305 eV and 1.307 eV.

also completely different because the dot sizes and hence their luminescence and Raman energies differ at the two different sample positions.

With this measurement setup we took another resonance measurement, this time with small 0.62 meV steps between the measurements. These measurements are shown in Fig. 5.42. Looking at the individual peaks throughout the different measurements we observe that there are some peaks that appear in more than one of the measurements. These peaks seem to exhibit a resonance behavior at certain energies. For a more exact evaluation of these peaks we show an excerpt of the measurements in Fig. 5.43. In this representation we can see several peaks with a resonance behavior. Some of these remain at the same energy relative to the laser and some have the same absolute energy. The former are easily made out and can be identified as Raman excitations. The latter shift by 0.62 meV from measurement to measurement in our Raman representation and can be assigned to photoluminescence signals. We have pointed out two Raman and two photoluminescence peaks in Fig. 5.43.

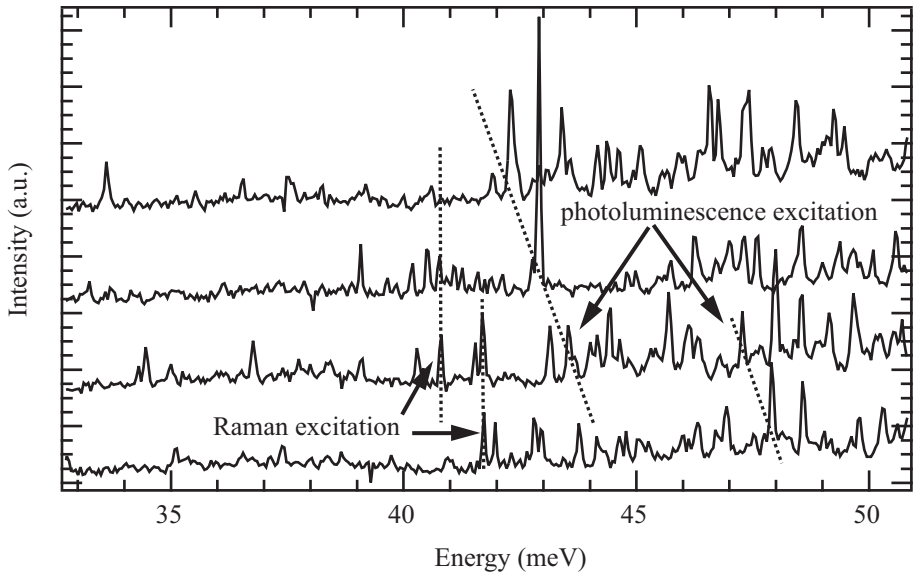

Figure 5.43: Excerpt from Fig. 5.42. Two Raman and two photoluminescence excitations are assigned corresponding to their resonance behavior.

5.8.3 Measurements with the 80× objective through nanoapertures

Finally, in order to detect the signal of even fewer or single quantum dots, we took a few measurements by focusing the laser through a hole in the aluminum mask. This was done with the aid of a *CCD* camera on the microscope that enabled us to see the nanoapertures on the sample as well as the infrared laser. It turned out that we could only detect photoluminescence signals but no Raman signals in this configuration. A possible explanation is that the aluminum on the sample surface led to a band distortion resulting in the electrons being dispelled from the quantum dots. Since it is crucial that there are electrons in the quantum dots in order to enable Raman scattering processes, we were not able to detect any Raman signals. We therefore present the following measurements on an absolute energy scale rather than a Raman representation.

In Fig. 5.44 we show eight measurements taken at laser energies between 1.305 and 1.307 meV with an energy spacing of 0.25 meV. The laser intensity was 4.75 µW ($A = 187$ W/cm^2). The most prominent peak is detected at 1.2605 eV. Its intensity first increases and then diminishes with increasing laser energy. We have plotted its resonance curve as a Lorentz fit through the measured intensities in Fig. 5.45. The maximum was determined to be at

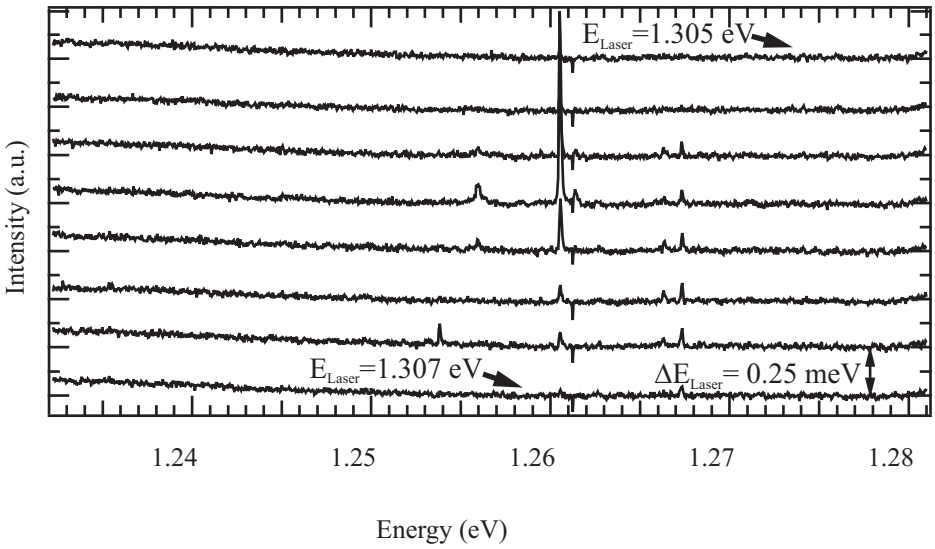

Figure 5.44: Microscope measurements with the 80× objective through a nanoaperture on an absolute energy scale. The laser energy was varied in 0.25 meV steps between 1.305 eV and 1.307 eV.

1.3057 eV with a full width at half maximum (FWHM) of 0.26 meV. Comparing this data to the macroscopic measurements on this sample where we found the s-s, p-p and d-d transitions to be at 1.207, 1.267 and 1.313 eV, we can assign the observed peak to a p-p transition of a single quantum dot excited resonantly at the d-d gap. The observed dot exhibits energies that are both about 7 meV smaller than the mean value found in the macroscopic measurement, indicating that it is larger than the average. The width of the luminescence signal has been determined to be 0.14 meV and is thus similar to the resonance width. We were not able to detect any peaks in the region of the s-s transition. The reason for this may be the rapidly decreasing sensibility of the *CCD* camera in this energy range.

There is a second, smaller signal at 1.267 eV that is at exactly the same energy as the macroscopic p-p transition peak. We assume that this peak has the same origin as the previously discussed peak but that it originates from a different dot. This dot would be a little smaller because of the higher transition energy. It is also probably not situated as much in the center of the nanoaperture as the other dot, resulting in the considerably smaller luminescence intensity.

In Fig. 5.46 we show a series of measurements on a different nanoaperture. The energy was varied in 0.062 meV steps between 1.2745 and 1.2747 eV at an intensity of 5 µW (A = 196 W/cm^2). Note that not only the excitation

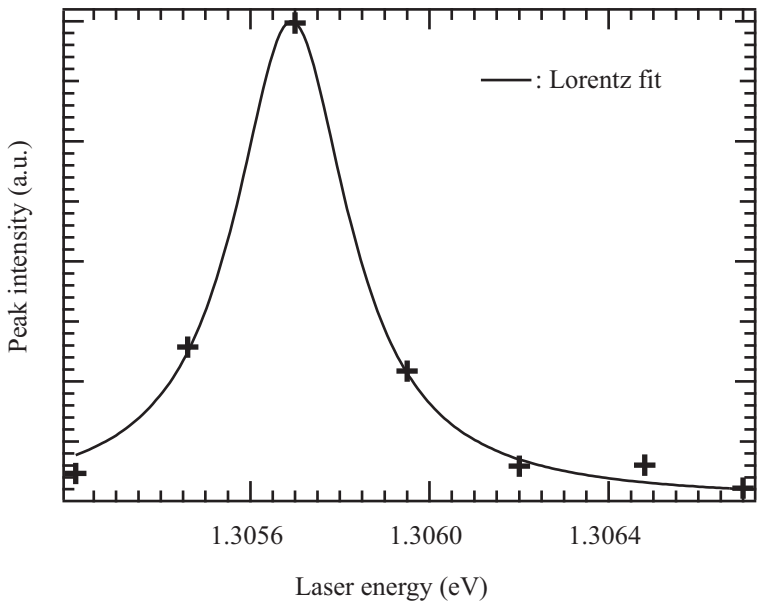

Figure 5.45: Resonance curve of the photoluminescence signal at 1.2605 eV from Fig. 5.44. The shown line is a Lorentz fit through the measured points.

energies are smaller in this measurement but also the detected signal is nearer to the s-s transition of the quantum dots compared to the previous measurement. We observe two peaks at 1.2281 and 1.2286 eV that both have their peak intensity at a laser energy of 1.2746 eV as can be seen from Fig. 5.47. The energy difference of about 47 meV between resonance energy and transition energy suggests that the observed peaks involve the s-s transition while the resonance occurs at the p-p transition. From the information we have it is impossible to say whether the two lines originate from two different dots or whether the energetically lower peak is in fact the recombination of a biexciton, i.e. a quasi-particle consisting of two electrons and two holes. The distinction between biexciton and exciton photoluminescence could be made by a series of measurements at varying intensities. However, we do not want to go into further detail as the investigation of single dot photoluminescence was not the focus of this work and has been discussed previously to great extent in the work of other groups (see, e.g., [Bay00] or [Fin01] as a reference).

Finally, we want to show a series of intensity-dependent measurements on a different nanoaperture and at a laser energy of 1.425 eV that we performed as a further characterization of the sample. The energy was deliberately chosen high enough to create electron-hole pairs in the wetting layer that

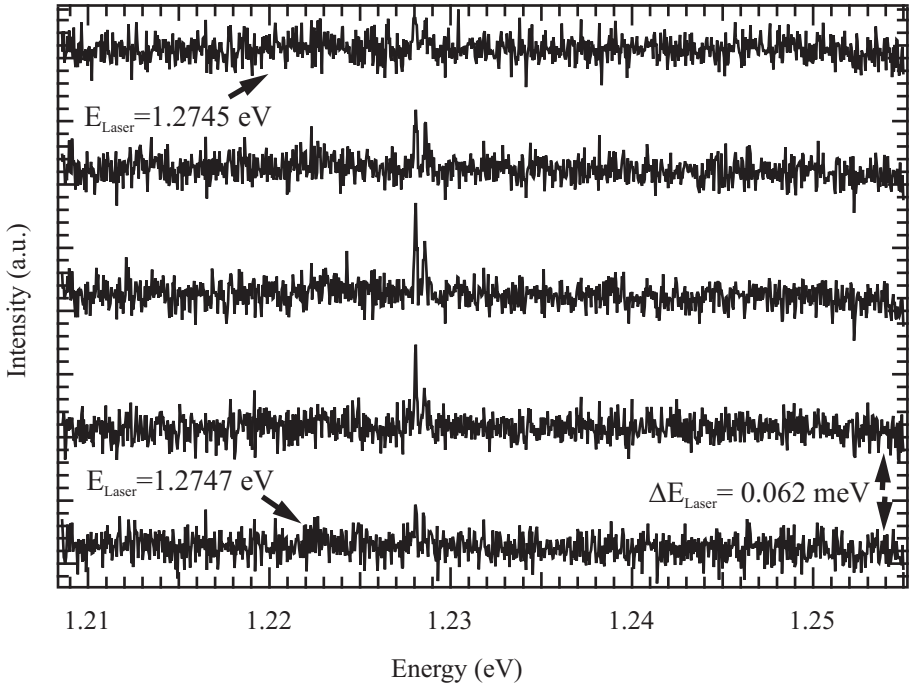

Figure 5.46: Further microscope measurements on a second nanoaperture at different laser energies. This time, the laser energy was varied in even smaller steps of 0.062 meV.

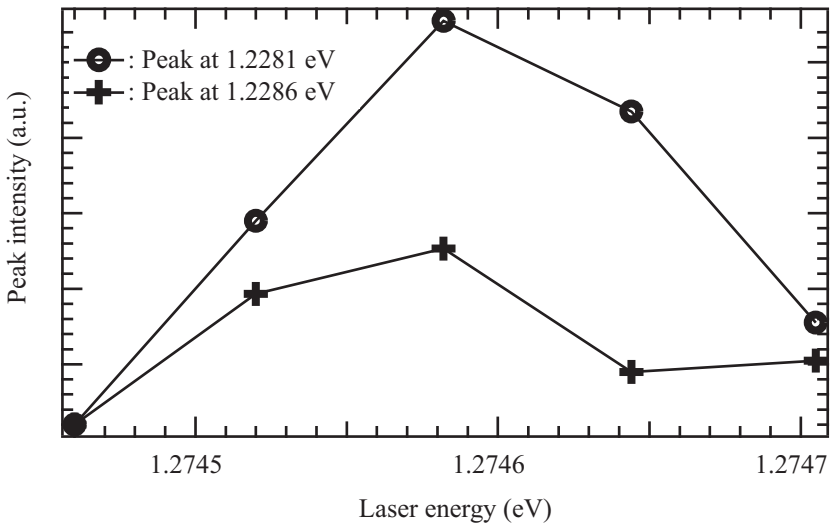

Figure 5.47: Resonance curves of the photoluminescence signals at 1.2281 and 1.2286 eV from Fig. 5.46.

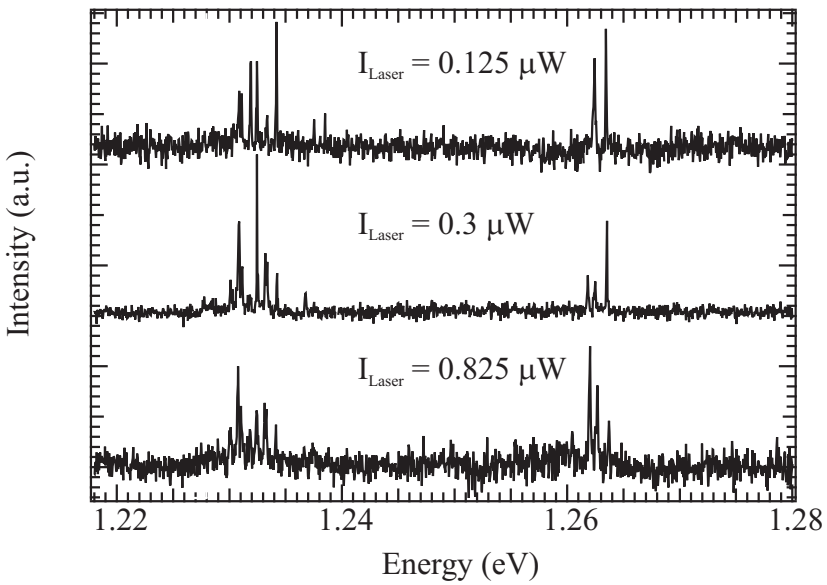

Figure 5.48: Microscope measurements through another nanoaperture taken at three different laser intensities of 0.125, 0.3 and 0.825 µW.

would relax into the quantum dots before recombination. This would allow us to collect signals from all the dots present underneath the nanoaperture, not just those that were excited resonantly. The chosen laser intensities were 0.125 µW ($A = 5\,\mathrm{W/cm^2}$), 0.3 µW ($A = 12\,\mathrm{W/cm^2}$) and 0.825 µW ($A = 32\,\mathrm{W/cm^2}$). Note that the intensities of the measurements cannot be compared as they were taken at different camera settings, namely with different times for the data collection. The observed peaks are concentrated around 1.232 eV and 1.262 eV. In the previous measurements we observed peaks at very similar energies that we attributed to s-s and p-p transitions. We are inclined to make the same assignment here although it is impossible to say how many dots contribute to the overall signal. It is very likely that it is more than one dot since Bayer *et al.* have reported in [Bay00] that a maximum of four *PL* lines can be detected from a single quantum dot at a given laser intensity. It is also interesting to note that the number of observed lines changes with varying laser intensity as well as the relative intensities within the spectrum. The additional lines at higher intensities probably originate in biexcitons or charged excitons that emerge when a second electron-hole pair or an additional electron or hole falls into a quantum dot already occupied by an electron-hole pair.

Chapter 6

Summary

In this work we investigated, by means of optical spectroscopic methods, on electrons in self-organized InAs quantum dots and related low-dimensional systems grown on GaAs or AlAs with different techniques. Whereas Raman spectroscopy was the focus of this work, we also took advantage of other methods such as photoluminescence (PL), photoluminescence excitation (PLE) and capacitance spectroscopy for a better understanding of the systems. All our samples were grown by molecular beam epitaxy.

In Chapter 5.1 we showed results of resonant Raman spectroscopy on self-assembled InAs quantum dots on GaAs, grown in the conventional way. In these experiments, the laser was tuned to the energy of the $E_0 + \Delta$ gap. The number of electrons could be tuned by applying a bias voltage between a Ti front gate and an in-grown backgate, which could be shown by capacitance spectroscopy. We measured the dependence of mainly two electronic Raman signals on the number of electrons that could be explained by s-p and p-d transition of electrons within the charged dots. A red shift of the s-p excitation could be explained by a comparison with exact many-particle calculations for the possible excitations in a quantum dot at a given number of electrons between two and six.

Additionally, we examined the weakly coupled, highly asymmetrical double quantum well that consists of our backgate and the InAs wetting layer. A sample where the growth process was intentionally aborted before the formation of quantum dots, was examined with resonant Raman spectroscopy, dependent on the applied gate voltage, laser energy and q-vector. We compared the energy dispersions of the observed spin density, charge density and single particle excitations to self-consistent calculations of the Poisson and Schrödinger equations of the system. The qualitative agreement between theory and experiment was good and showed evidence for the coupling of the two systems. We were also able to establish properties of the observed

excitations that allowed the identification as quantum dot or quantum well excitations despite the similarity in energy and line width.

Another sample was grown where a 7 nm thick layer of GaAs was grown on top of the quantum dots and subsequently a second layer of InAs quantum dots was formed, allegedly mirroring the positions of the first layer of quantum dots. We found several indications to verify this assumption via capacitance spectroscopy and intensity- and gate voltage-dependent photoluminescence spectroscopy. The presence of a second layer of quantum dots could be proved by the appearance of additional peaks in the spectra, whereas the strongest indication to the coupling of the two quantum dot layers is possibly the increasing Δ_{SAS} as the number of electrons and the asymmetry of the system was increased. We were not able to observe any electronic Raman signals from this sample that we could have assigned to the quantum dot layers.

Furthermore, we presented the results of *PLE* experiments carried out at the $E_0+\Delta$ gap of an ensemble of InAs quantum dots on GaAs. By selectively choosing small energy bands out of the *PL* spectra and thus creating *PLE* spectra for different dot sizes, we were able to distinguish quantum dot effects in the spectra from what seemed to be bulk material effects. However, the method proved to be too complicated and not repeatable enough to yield any usable results.

Measurements on InAs dots grown on AlAs were shown in Chapter 5.5 where the laser could be tuned to the E_0 gap of the dots because of the highly increased dot transition energy. Whereas we did not observe electronic Raman excitations, the GaAs and AlAs *LO* phonons in the spectra varied strongly with the laser energy, indicating a strong coupling between the electronic states in the quantum dots and the phonons of their surrounding material. We also observed very narrow lines that can be identified as photoluminescence lines as they do not exhibit any energy shift when the laser energy is varied. While they do look similar to what in later chapters have been identified as single dot luminescence lines, they behave differently and could only be explained as such if there was a continuum of states in the vicinity of only few dots. The spectra further featured two broad energy bands that exhibited the same energy dispersion on the relative Raman scale as on the absolute *PL* scale. We explained this previously unknown behavior by the resonant absorption of a sub-ensemble of dots with a smaller size distribution than the whole ensemble, much like the selection of small energy bands out of the *PL* spectra in the *PLE* experiments.

Changing the experimental setup so as to operate in the near infrared regime enabled us to perform Raman measurements on the InAs dots grown on GaAs exciting resonantly at the E_0 gap, more specifically the f-f transition.

By modifying the laser focus and introducing an iris aperture into the optical path we were able to split up a broad ensemble Raman signal into a series of narrow lines that we consequently attribute to the Raman spectra of many single quantum dots.

Using the In-flush technique, quantum dots were grown whose E_0 gap energy matched the detectable energies of our experimental setup much better than the conventionally grown InAs/GaAs dots. An extensive study of the resonance effects in this sample revealed that all observed Raman scattering processes included the s-s transition as the last step. Interestingly, the TO phonon resonance suggests a similar scattering process although we would expect a coupling of the electrons to the LO phonon rather than the TO phonon.

Measuring with the microscope setup and two different objectives we were able to break down the broad Raman signal into even fewer single dot lines, revealing that within the broad signal there were Raman lines as well as photoluminescence lines. Measuring through nanoapertures in an Al mask the Raman lines vanished, possibly because of a band deformation induced by the Al on top of the sample, but we were able to study the photoluminescence of very few and even single quantum dots.

Bibliography

[Abs79] G. Abstreiter and K. Ploog. *Inelastic light scattering from a quasi-two-dimensional electron system in GaAs-$Al_xGa_{1-x}As$ heterojunctions.* Phys. Rev. Lett. **42**, 1308 (1979).

[Bal01] P. Ballet, J. B. Smathers, H. Yang, C. L. Workman, and G. J. Salamo. *Control of size and density of InAs/(Al,Ga)As self-organized islands.* J. Appl. Phys. **90**, 481 (2001).

[Bay00] M. Bayer, O. Stern, P. Havrylak, S. Fafard, and A. Forchel. *Hidden symmetries in the energy levels of excitonic 'artificial atoms'.* Nature **405**, 923 (2000).

[Bit04] Karsten Bittkau. *Einfluss von selbstkonsistenten Umverteilungen und Elektron-Phonon Wechselwirkung auf kollektive Anregungen in niedrigdimensionalen Elektronensystemen.* Phd thesis, Universität Hamburg, 2004.

[Boo03] Maik-Thomas Bootsmann. *Elektronische Raman-Spektroskopie an Quantenpunkten, Doppelquantenfilmen und Doppelquantenpunkten.* Phd thesis, Universität Hamburg, 2003.

[Bro03a] T. Brocke, M.-T. Bootsmann, M. Tews, B. Wunsch, D. Pfannkuche, Ch. Heyn, W. Hansen, D. Heitmann, and C. Schüller. *Spectroscopy of few-electron collective excitations in charge-tunable artificial atoms.* Phys. Rev. Lett. **91**, 257401 (2003).

[Bro03b] Thomas Brocke. *Elektronische Ramanspektroskopie an Halbleiter-Quantenpunkten.* Diploma thesis, Universität Hamburg, 2003.

[Bur80] E. Burstein, A. Pinczuk, and D. L. Mills. *Inelastic light scattering by charge carrier excitations of two-dimensional plasmas: theoretical considerations.* Surface Science **2**, 451 (1980).

[Chu99] L. Chu, M. Arzberger, G. Böhm, and G. Abstreiter. *Influence of growth conditions on the photoluminescence of self-assembled InAs/GaAs quantum dots.* J. Appl. Phys. **85**, 2355 (1999).

[Chu00] L. Chu, A. Zrenner, M. Bichler, G. Böhm, and G. Abstreiter. *Raman spectroscopy of In(Ga)As/GaAs quantum dots.* Appl. Phys. Lett. **77**, 3944 (2000).

[Dan89] G. Danan, A. Pinczuk, J. P. Valladaresand, L. N. Pfeiffer, K. W. West, and C. W. Tu. *Coupling of excitons with free electrons in light scattering from GaAs quantum wells.* Phys. Rev. B **39**, 5512 (1989).

[Dec94] R. Decca, A. Pinczuk, S. Das Sarma, B. S. Dennis, L. N. Pfeiffer, and K. W. West. *Absence of spin-density excitations in quasi-two-dimensional electron systems.* Phys. Rev. Lett. **72**, 1506 (1994).

[Dre94] H. Drexler, D. Leonard, W. Hansen, J. P. Kotthaus, and P. M. Petroff. *Spectroscopy of quantum levels in charge-tunable InGaAs quantum dots.* Phys. Rev. Lett. **73**, 2252 (1994).

[Faf99] S. Fafard, Z. R. Wasilewski, C. Ni. Allen, D. Picard, M. Spanner, J. P. McCaffrey, and P. G. Piva. *Manipulating the energy levels of semiconductor quantum dots.* Phys. Rev. B **59**, 15368 (1999).

[Fin01] F. Findeis, M. Baier, A. Zrenner, M. Bichler, and G. Abstreiter. *Optical excitations of a self-assembled artificial ion.* Phys. Rev. B **63**, 121309 (2001).

[Foc28] V. Fock. *Bemerkung zur Quantelung des harmonischen Oszillators im Magnetfeld.* Z Phys **47**, 446 (1928).

[Gar98] J. M. Garcia, T. Mankad, P. O. Holtz, P. J. Wellman, and P. M. Petroff. *Electronic states tuning of InAs self-assembled quantum dots.* Appl. Phys. Lett. **72**, 3172 (1998).

[Gar05] C. P. García, V. Pellegrini, A. Pinczuk, M. Rontani, G. Goldoni, E. Molinari, B. S. Dennis, L. N. Pfeiffer, and K. W. West. *Evidence of correlation in spin excitations of few-electron quantum dots.* Phys. Rev. Lett. **95**, 266806 (2005).

[Gov97] A. O. Govorov. *Resonant light scattering induced by Coulomb interaction in semiconductor microstructures.* J. Phys. Condens. Matter **9**, 4681 (1997).

[Ham69] D. Hamilton and A. L. McWhorter. *Light Scattering Spectra of Solids.* Springer, New York, 1969.

[Hey07] Ch. Heyn, A. Schramm, T. Kipp, and W. Hansen. *Kinetic model of intermixing during self-assembled InAs quantum dot formation.* J. Crys. Growth **301**, 692 (2007).

[Hin01] K. Hinzer, M. Bayer, J. P. McCaffrey, P. Hawrylak, M. Korkusinski, O. Stern, Z. R. Wasilewski, S. Fafard, and A. Forchel. *Optical spectroscopy of electronic states in a single pair of vertically coupled self-assembled quantum dots.* Phys. Stat. Sol. **224**, 385 (2001).

[Hu01] C.-M. Hu, C. Schüller, and D. Heitmann. *Space-asymmetry-induced plasmon mode mixing and anticrossing in coupled bilayer structures.* Phys. Rev. B **64**, 073303 (2001).

[Kar04] Lars Karsten. *Photolumineszenzspektroskopie an Halbleiterquantenpunkten.* Phd thesis, Universität Hamburg, 2004.

[Köp06] Tim Köppen. *Elektronische Raman- und Photolumineszenzspektroskopie an InAs-Quantenpunkten.* Diploma thesis, Universität Hamburg, 2006.

[Leo93] D. Leonard, M. Krishnamurthy, C. M. Reaves, S. P. Denbaars, and P. M. Petroff. *Direct formation of quantum-sized dots from uniform coherent islands of InGaAs on GaAs surfaces.* Appl. Phys. Lett. **63**, 3203 (1993).

[Leo94] D. Leonard, K. Pond, and P. M. Petroff. *Critical layer thickness for self-assembled InAs islands on GaAs.* Phys. Rev. B **50**, 11687 (1994).

[Leo95] R. Leon, S. Fafard, D. Leonard, J. L. Merz, and P. M. Petroff. *Visible luminescence from semiconductor quantum dots in large ensembles.* Appl. Phys. Lett. **67**, 521 (1995).

[Mak90] P. A. Maksym and Tapash Chakraborty. *Qauntum dots in a magnetic field: role of electron-electron interactions.* Phys. Rev. Lett. **65**, 108 (1990).

[Mal97] S. Malik, C. Roberts, R. Murray, and M. Pate. *Tuning self-assembled InAs quantum dots by rapid thermal annealing.* Appl. Phys. Lett. **71**, 1987 (1997).

[Meu92] B. Meurer, D. Heitmann, and K. Ploog. *Single-electron charging of quantum-dot atoms.* Phys. Rev. Lett. **68**, 1371 (1992).

[Mil97] B. T. Miller, W. Hansen, S. Manus, R. J. Luyken, A. Lorke, and J. P. Kotthaus. *Few-electron ground states of charge-tunable self-assembled quantum dots.* Phys. Rev. B **56**, 6764 (1997).

[Nar06] G. A. Narvaez, G. Bester, and A. Zunger. *Carrier relaxation mechanisms in self-assembled (In, Ga)As/GaAs quantum dots: Efficient $p \rightarrow s$ auger relaxation of electrons.* Phys. Rev. B **74**, 075403 (2006).

[Oul03] R. Oulton, J. J. Finley, A. I. Tartakovskii, D. J. Mowbray, M. S. Skolnick, M. Hopkinson, A. Vasanelli, R. Ferreira, and G. Bastard. *Continuum transitions and phonon coupling in single self-assembled Stranski-Krastanow quantum dots.* Phys. Rev. B **68**, 235301 (2003).

[Pin79] A. Pinczuk, H. L. Störmer, R. Dingle, J. M. Worlock, W. Wiegmann, and A. C. Gossard. *Observation of intersubband excitations in a multilayer two dimensional electron gas.* Solid State Commun. **32**, 1001 (1979).

[Pin82] A. Pinczuk and J. B. Worlock. *Light scattering by two-dimensional electron systems in semiconductors.* Surf. Sci **113**, 69 (1982).

[Pin89] A. Pinczuk, S. Schmitt-Rink, G. Danan, J. P. Valladares, L. N. Pfeiffer, and K. W. West. *Large exchange interactions in the electron gas of GaAs quantum wells.* Phys. Rev. Lett. **63**, 1633 (1989).

[Pol99] A. Polimeni, A. Patanè, M. Henini, L. Eaves, and P. C. Main. *Temperature dependence of the optical properties of $InAs/Al_yGa_{1-y}As$ self-organized quantum dots.* Phys. Rev. B **59**, 5064 (1999).

[Pus97] Y. A. Pusep, S. W. da Silva, J. C. Galzerani, D. I. Lubyshev, P. P. Gonzalez-Borrero, E. Marega Jr., E. Petitprez, N. La Scala Jr., and P. Basmaji. *Photoluminescence of excitons in differently oriented self-assembled InAs quantum dots.* Phys. Stat. Sol. **164**, 455 (1997).

[Pus98] Yu. A. Pusep, G. Zanelatto, S. W. da Silva, J. C. Galzerani, P. P. Gonzalez-Borrero, A. I. Toropov, and P. Basmaji. *Raman study of interface modes subjected to strain in InAs/GaAs self-assembled quantum dots.* Phys. Rev. B **58**, R1770 (1998).

[Sar81] S. Das Sarma and A. Madhukar. *Collective modes of spatially separated, two-component, two-dimensional plasma in solids.* Phys. Rev. B **23**, 805 (1981).

[Sch99] Christian Schüller. *Festkörperprobleme, Advances in Solid State Physics 38.* Springer, 1999.

[She74] Y. R. Shen. *Distinction between resonance Raman scattering and hot luminescence.* Phys. Rev. B **9**, 622 (1974).

[Sme23] A. Smekal. *Eine neue Erscheinung bei der Lichtzerstreuung in Krystallen.* Naturwiss. **11**, 873 (1923).

[Stü05] Arne Stührk. *Elektronische Raman-Spektroskopie an niedrigdimensionalen Elektronensystemen.* Diploma thesis, Universität Hamburg, 2005.

[Ste97] C. Steinebach, D. Heitmann, and V. Gudmundsson. *Far-infrared absorption of acoustic and optical magnetoplasmons in double-layered quantem wires.* Phys. Rev. B **56**, 6742 (1997).

[Str94] R. Strenz, U. Bockelmann, F. Hirler, G. Abstreiter, G. Böhm, and G. Weimann. *Single-particle excitations in quasi-zero- and quasi-one-dimensional electron systems.* Phys. Rev. Lett. **73**, 3022 (1994).

[Su03] Bertram Su. *Photolumineszenzspektroskopie an Quantenpunkten.* Diploma thesis, Universität Hamburg, 2003.

[Tan90] I-H. Tan, G. L. Snider, L. D. Chang, and E. L. Hu. *A self-consistent solution of Schrödinger-Poisson equations using a nonuniform mesh.* J. Appl. Phys. **68**, 4071 (1990).

[Ura01] J. Urayama, T. B. Norris, J. Singh, and P. Bhattacharya. *Observation of phonon bottleneck in quantum dot electronic relaxation.* Phys. Rev. Lett. **86**, 4930 (2001).

[War98] R. J. Warburton, B. T. Miller, C. S. Dürr, C. Bödefeld, K. Karrai, J. P. Kotthaus, G. Medeiros-Ribeiro, P. M. Petroff, and S. Huant. *Coulomb interactions in small charge-tunable quantum dots: a simple model.* Phys. Rev. B **58**, 16221 (1998).

[Was99] Z. R. Wasilewski, S. Fafard, and J. P. McCaffrey. *Size and shape engineering of vertically stacked self-assembled quantum dots.* J. Crys. Growth **101-102**, 1131 (1999).

[Woj96] A. Wojs, P. Hawrylak, S. Fafard, and L. Jacak. *Electronic structure and magneto-optics of self-assembled quantum dots.* Phys. Rev. B **54**, 5604 (1996).

[Xie95] Q. Xie, A. Madhukar, P. Chen, and N. P. Kobayashi. *Vertically self-organized InAs qauntum box islands on GaAs(100).* Phys. Rev. Lett. **75**, 2542 (1995).

[Yu99] Peter Y. Yu and Manuel Cardona. *Fundamentals of Semiconductors.* Springer Verlag Berlin Heidelberg New York, 2. Auflage, 1999.

[Zie87] M. Ziesmann, D. Heitmann, and L. L. Chang. *Interaction of optical phonons with electrons in an InAs quantum well.* Phys. Rev. B **54**, 5604 (1987).

Acknowledgments

I wish to thank the following people and organizations:

- Prof. Dr. Detlef Heitmann for the opportunity to work in his group and for many interesting discussions.
- Prof. Dr. Daniela Pfannkuche for the fruitful cooperation and for being the referee of this thesis.
- Prof. Dr. Wolfgang Hansen for supplying me with samples to measure and for being the referee of the defense.
- Dr. Tobias Kipp for his continuing support and discussions throughout the thesis.
- Prof. Dr. Christian Schüller for luring me into the field of electronic Raman spectroscopy and for the support especially during the first part of the thesis.
- Dr. Christian Heyn, Dr. Andreas Schramm and Dr. Holger Welsch for growing the samples and for the help and advice in growth-related questions.
- Arne Stührk and Tim Köppen for the very productive and enjoyable team work.
- Gerwin Chilla for many discussions and great company in and out of the laboratories.
- André Wirthmann, Bertram Su, Steffen Holland, Gerwin Chilla, Arne Stührk, Christian Strelow and Tim Köppen for enduring my presence and — more often than not — my music in the office and in the labs.
- Groups H and W, especially the optics group, for the good atmosphere and interesting discussions about anything that came to mind.

- Herr Hatje and Herr Ahrens for the liquid Helium supply and technical support, Thomas Finger and co-workers for the cleanroom maintenance and the feinmechanische and elektronische Werkstatt for their help.
- The Deutsche Forschungsgemeinschaft for the financial support of this work via SFB 508.
- My new bosses Neil Fox and Dr. Axel Giese at Bosch for giving me enough free time to finish this thesis on a reasonable time scale.
- My friends and my family for brightening up my life outside of the dark optics labs and for always believing in me.